

Addenda and Corrigenda

Page 15, last line should read

'symmetric under all rotations about their major axes and belong to the'

Page 74, insert after the end of the sentence in line 7

'The pig-tails and fuseclips shown mounted on the aluminium tube are connected to the flashlamps in such a manner that current is able to flow through both flashlamps in the same direction, and in the reverse direction in the coaxial tube. This arrangement minimizes the magnetic field between the two flashlamps where the laser rod is mounted, thus avoiding any further splitting of the laser transitions due to the Zeeman effect (see §2.6, page 24). Due to space limitations, a coaxial diffuse reflector of the type shown in fig. 5.2.1 could not be used ...'

Page 126, insert after the end of the paragraph

'Under these circumstances, each part of the oscillating line is coupled closely enough through the wings of the homogeneous line to help keep the pulses in synchronisation, but draws on sufficiently different populations of ions as an energy source to avoid the growth of some parts of the line at the expense of the rest.'

Page 164, insert after the end of the paragraph

'There are several experiments which logically follow on from the work described here. In the first place, it is clear that the measurements to determine the cross relaxation rate by observing the drop in the fluorescence as a function of wavelength after

Addenda and Corrigenda (continued)

Q-spoiling must be repeated, with great care to ensure that a very narrow-band ($< 1 \text{ \AA}$) probe pulse is used, and that all extraneous light such as flashlamp radiation and superfluorescence is excluded from fluorescent measurements. The narrow-band probe experiments described in this thesis should be repeated using a longer flashlamp pulse (but maintaining control of the pulse shape) and studying a greater variety of glasses and doping levels. Perhaps an additional cavity resonator could be included to force single (longitudinal) mode oscillations and further narrow the linewidth. Some experiment should be designed to determine the actual lifetimes of the cascade from the pump bands to the metastable level. Finally, an experiment should be performed on a variety of glasses using an extremely short pump pulse to determine if the saturation observed in our experiments is a general phenomenon, and if it is time dependent (fast solarization) or dependent on which pump band is excited.'

THE INFLUENCE OF ENERGY TRANSFER MECHANISMS ON THE
SPECTRAL PROPERTIES OF THE NEODYMIUM:GLASS LASER

by

George W. Gerrity

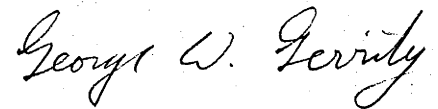
Thesis submitted for the
Degree of Doctor of Philosophy
in the Australian National University.

February 1971



STATEMENT OF AUTHORSHIP

Except where otherwise indicated by references,
the contents of this thesis are entirely my own
work.

A handwritten signature in cursive script that reads "George W. Gerrity". The signature is written in dark ink and is positioned above the printed name.

(George W. Gerrity)

ACKNOWLEDGEMENTS

Experimental research is always a co-operative project involving the talents of many, and to those who have escaped my notice here, I am nevertheless grateful. I am especially indebted to my supervisor Dr. C.E. Dahlstrom for advice, criticism and discussion, and to Dr. L.O. Brown for many helpful suggestions. The careful workmanship of Mr. F. Parchi and others in the workshop has kept technical difficulties to a minimum. I thank Mr. D. Davies for proof-reading the final copy with me, and Miss N. Chin, my typist, for an excellent job.

The financial assistance of a Commonwealth Scholarship and Fellowship Plan Award and a short term Australian National University Award are gratefully acknowledged.

ABSTRACT

Some problems are investigated relating to the spiking behaviour observed in the Nd^{3+} glass laser and the energy transfer within the broadened line of the lasing transition. It is shown by means of group theory that the fluorescence at $1.06 \mu\text{m}$ must be a composite of twelve unresolved lines and a review of the various possible line broadening mechanisms is undertaken to clarify their behaviour when electronic transitions are involved. Two sets of experiments are described: in the first, time-resolved spectrograms are obtained from two different glasses under normal lasing conditions, and when lasing is delayed either by a bleachable thin film absorber or an electronic shutter (Q-spoiled); in the second set of experiments, the laser output as a function of wavelength is studied when it is forced to oscillate in a narrow band by using a diffraction grating as one of the reflectors. On the basis of theory and hole burning observed in the first set of experiments, the fluorescent line is shown to be a composite of a number of lines with a common source, each of them inhomogeneously broadened. Both sets of measurements give estimates of the broadening of the lines to be $\sim 70 \text{ cm}^{-1}$. Cross relaxation between the ground state and excited ions is shown to be slow and is estimated to be $< 10^4 \text{ sec}^{-1}$. The discrepancy between these results and those of Michon (1966) and Boyden and Clark (1966) is resolved. A computer simulation of the rate equations shows that neither relaxation nor the finite lifetime of the terminal level can account for the observed random spiking. However, certain giant pulsations observed in some of the time-resolved experiments appear to be correctly described by these equations. Finally, evidence is produced to show that if the source of the instability arises from mode interactions, then it is not a strong function of the number or type of cavity modes.

TABLE OF CONTENTS

	PAGE
ACKNOWLEDGEMENTS -----	iii
ABSTRACT -----	iv
LIST OF TABLES -----	ix
LIST OF FIGURES -----	x
§1. INTRODUCTION	
1.1. Problems Investigated -----	1
1.2. Methods of Investigation -----	4
1.3. Conclusions -----	7
§2. SPECTROSCOPY OF Nd ³⁺ IN GLASS	
2.1. Introduction -----	9
2.2. Spectral Properties of Nd ³⁺ -----	10
2.3. The Glass Matrix -----	10
2.4. Rare-Earth Ions in Silica-Based Glasses -----	12
2.5. Aspects of Symmetry -----	15
2.6. Discussion of Observations as Compared with Theory -	21
§3. LINEWIDTH	
3.1. Introduction -----	27
3.2. Interaction with the Radiation Field -----	28
3.3. Interactions between Elements of the Ion System ----	29
3.4. Interactions between the System and the Host Material -----	35
3.5. Inhomogeneous Broadening -----	36
3.6. Cross Relaxation -----	39
§4. LASER RATE EQUATIONS	
4.1. Introduction -----	42

TABLE OF CONTENTS (CONTINUED)

	PAGE
4.2. Three Level Approximation	
4.2.1. Model Adopted and Basis for Assumptions -----	42
4.2.2. Relationship between Absorption Coefficient and Stimulated Emission Cross Section -----	46
4.2.3. The Cross Relaxation Term in the Rate Equations -----	48
4.2.4. The Stimulated Emission Term in the Rate Equations -----	53
4.2.5. Two Level Approximation -----	55
4.2.6. Relationship between Internal and External Photon Flux Density -----	56
4.2.7. Threshold -----	57
4.3. Equilibrium Equations	
4.3.1. Introduction -----	58
4.3.2. Single Frequency Operation -----	60
4.3.3. Case I: $\sigma_n \epsilon < 1$ -----	62
4.3.4. Case II: $\sigma_n \epsilon > 1$ -----	65
§5. EXPERIMENTAL ARRANGEMENT	
5.1. Introduction -----	71
5.2. Laser Head	
5.2.1. Choice of Laser Rods -----	71
5.2.2. Pumplight Cavity and Flashlamps -----	72
5.2.3. Flashlamp Triggering Circuit -----	74
5.3. Flashlamp Energy Storage Bank and Power Supply	
5.3.1. Design of the Energy Storage Bank -----	76
5.3.2. Power Supply -----	83
5.3.3. Calibration of the Power Supply -----	88

TABLE OF CONTENTS (CONTINUED)

	PAGE
5.4. Five Metre Spectrograph	
5.4.1. Introduction -----	88
5.4.2. Spectrograph Design and Construction -----	91
5.4.3. Energy Collection and Image Brightness -----	93
5.4.4. Calibration of the Spectrograph -----	96
5.5. Detectors	
5.5.1. Ballistic Thermopile -----	98
5.5.2. PIN Photodiode -----	98
5.6. Optical Bench -----	104
5.7. Streak Camera -----	105
§6. TIME-RESOLVED SPECTROSCOPY	
6.1. Introduction -----	110
6.2. Infra-Red Plate Processing -----	110
6.3. Experiments -----	111
6.4. Results -----	113
6.5. Discussion	
6.5.1. Cross-Relaxation Rate -----	120
6.5.2. Q-Spoiled Pulse Spectral Width -----	121
6.5.3. Pulse Period -----	124
6.5.4. Comparison between Glasses -----	126
§7. TUNABLE NARROW BAND LASER	
7.1. Introduction -----	127
7.2. Method -----	127
7.3. Procedure -----	131
7.4. Results and Discussion -----	132

TABLE OF CONTENTS (CONTINUED)

	PAGE
§8. COMPUTER SIMULATION OF LASER RATE EQUATIONS	
8.1. Introduction -----	140
8.2. Computer Simulation	
8.2.1. Numerical Integrator -----	142
8.2.2. Method of Computation -----	143
8.3. Results and Discussions -----	145
§9. DISCUSSION AND CONCLUSIONS	
9.1. Line Broadening and Energy Transport within the Line -----	156
9.2. Spiking Behaviour -----	159
9.3. Implications of Results -----	163
APPENDIX I -----	165
APPENDIX II -----	175
REFERENCES -----	178

LIST OF TABLES

	PAGE
5.1. Optical and Physical Properties of Two Laser Glasses ---	73
5.2. Oscilloscope Control Settings -----	108
6.1. Breakdown of Streak Photographs into Wide and Narrow Band Pulses -----	124

LIST OF FIGURES

	PAGE
2.6.1 Energy level diagram of Nd^{3+} , indicating the experimentally resolved sublevels, after Snitzer and Young (1968). -----	23
2.6.2 Energy level diagram of the ${}^4\text{F}_{3/2}$, ${}^4\text{I}_{11/2}$ and ${}^4\text{I}_{9/2}$ levels, showing how the terms split as the symmetry is lowered by distortion, from O (octahedral) to D_4 (tetragonal) and D_3 (trigonal), and from T (tetrahedral) to D_2 (orthorhombic) and C_3 (trigonal). -----	26
4.2.1 Energy level diagram of model for three level approximation. -----	43
4.2.2 Energy level diagrams of possible cross relaxation processes. -----	49
5.2.1 Photograph of the single flashlamp pumping cavity. ---	75
5.2.2 Photograph of the double flashlamp pumping cavity. ---	75
5.2.3 Schematic diagram of the flashlamp pulser and its power supply. -----	77
5.3.1 Oscillogram of current versus time for the single flashlamp circuit: vertical scale - 860 A/div.; horizontal scale - 100 $\mu\text{sec}/\text{div}$. -----	79
5.3.2 Emission intensity versus pump energy at the wavelength of the Nd^{3+} absorption bands, for the single flashlamp. -----	81
5.3.3 Emission intensity versus pump energy at the wavelength of the Nd^{3+} absorption bands, for two flashlamps in series. -----	82
5.3.4 Oscillogram of current versus time for the double flashlamp circuit: vertical scale - 172 A/div.; horizontal scale - 100 $\mu\text{sec}/\text{div}$. -----	83
5.3.5 Simplified circuit of the constant current power supply. -----	84
5.3.6 Logic diagram of the relay switching in the power supply. -----	87
5.3.7 Schematic diagram of the capacitor bank charging power supply. -----	89
5.4.1 Photograph illustrating the arrangement of the grating mount and the slits. -----	94

LIST OF FIGURES (CONTINUED)

	PAGE
5.4.2 Photograph of the water-cooled argon lamp. -----	97
5.5.1 Schematic diagram of circuit for calibrating the chart recorder to read energy directly in joules. -----	99
5.5.2 Equivalent circuit for the HPA4205 photodiode. -----	100
5.5.3 Schematic diagram of the oscilloscope connections to the photodiode. -----	100
5.5.4 Diagram of the arrangements used to sample the beam for the photodiode: (a) with light pipe, (b) with ground glass screens. -----	101
5.5.5 Graph of photodiode output voltage versus density (circles) of the neutral density filters, and equivalent density (triangles) for the inverse square data, referenced to zero density. -----	103
5.6.1 Plan of the laboratory illustrating the arrangement of the optical bench and the spectrograph. -----	106
5.6.2 Photograph of the laboratory showing the optical bench and the spectrograph. -----	107
5.7.1 Electrical connections between the streak camera and the oscilloscopes. -----	109
6.4.1 Plate #1-1 of 15-2-69: time scale - 49 μ sec/in; wavelength scale - 26 \AA /in; Kodak ND-11 glass rod in 60 cm Fabry-Perot cavity, Q-spoiled with gold film, $D = 0.63$; $E_{in} = 900$ J ($5.6 \times$ threshold); $E_{out} = 1.5$ J. -----	114
6.4.2 Plate #1-2 of 15-2-69: same parameters as fig. 6.4.1.	114
6.4.3 Plate #2-4 of 16-3-69: time scale - 59 μ sec/in; wavelength scale - 32 \AA /in; Kodak ND-11 glass rod in 251 cm ring cavity, Q-spoiled with gold film, $D = 0.50$; $E_{in} = 1200$ J ($3.75 \times$ threshold); $E_{out} = 1.0$ J. -----	115
6.4.4 Plate #1-1 of 5-4-69: time scale - 39 μ sec/in; wavelength scale - 21 \AA /in; Kodak ND-11 glass rod in 251 cm ring cavity, Q-spoiled with gold film, $D = 0.59$; $E_{in} = 1000$ J ($3.1 \times$ threshold); $E_{out} = 0.3$ J. -----	115
6.4.5 Plate #2-4 of 6-4-69: time scale - 38 μ sec/in; wavelength scale - 31 \AA /in; Kodak ND-11 glass rod in 251 cm ring cavity, Q-spoiled with gold film, $D = 0.3$, on 0.038 mm thick mica plate; $E_{in} = 1400$ J ($4.37 \times$ threshold); $E_{out} = 1.2$ J. -----	116

LIST OF FIGURES (CONTINUED)

	PAGE
6.4.6 Plate #3-6 of 19-9-69: time scale - 86 $\mu\text{sec}/\text{in}$; wavelength scale - 46 $\text{\AA}/\text{in}$; Kodak ND-11 glass rod in 100 cm Fabry-Perot cavity with open Pockel's cell; $E_{\text{in}} = 1000 \text{ J}$ ($3.7 \times$ threshold); $E_{\text{out}} = 1.1 \text{ J}$. -----	116
6.4.7 Plate #1-1 of 16-8-69: time scale - 96 $\mu\text{sec}/\text{in}$; wavelength scale - 52 $\text{\AA}/\text{in}$; Schott LG-56 glass rod in 251 cm ring cavity; $E_{\text{in}} = 800 \text{ J}$ ($1.95 \times$ threshold); $E_{\text{out}} = 1.0 \text{ J}$. -----	117
6.4.8 Plate #4-8 of 20-8-69: time scale - 51 $\mu\text{sec}/\text{in}$; wavelength scale - 27 $\text{\AA}/\text{in}$; Schott LG-56 glass rod in 251 cm ring cavity, Q-spoiled with gold film, $D = 0.24$; $E_{\text{in}} = 1400 \text{ J}$ ($3.4 \times$ threshold); $E_{\text{out}} = 0.24 \text{ J}$. -----	117
6.4.9 Plate #1-1 of 10-9-69: time scale - 79 $\mu\text{sec}/\text{in}$; wavelength scale - 42.5 $\text{\AA}/\text{in}$; Schott LG-56 glass rod in 100 cm Fabry-Perot cavity with Pockel's cell, Q-spoiled 100 μsec after pump pulse begins; $E_{\text{in}} = 1200 \text{ J}$ ($4.0 \times$ threshold); $E_{\text{out}} = 0.55 \text{ J}$. -----	118
6.4.10 Drawings illustrating the five pulse types. -----	119
7.2.1 Spot size ($1/e$) of the TEM_{00} mode for a 60 cm cavity with one plane mirror and one curved mirror, as a function of the focal length of the curved mirror; at the plane mirror (solid line), 72 cm from the plane mirror (broken line), and 250 cm from the plane mirror (broken and dotted line). -----	130
7.4.1 Plate #1-1 of 15-10-69: time scale - 101 $\mu\text{sec}/\text{in}$; wavelength scale - 54 $\text{\AA}/\text{in}$; Kodak ND-11 glass rod in 60 cm Fabry-Perot cavity with grating and telescope; $E_{\text{in}} = 800 \text{ J}$; $E_{\text{out}} = 1.15 \text{ J}$. -----	133
7.4.2 Normalized slope efficiency (triangles) and reciprocal of the threshold (squares) as a function of wavelength for Kodak ND-11 glass. -----	134
7.4.3 Normalized square root of slope efficiency (circles) and reciprocal of the threshold (squares) as a function of wavelength for Kodak ND-11 glass. -----	135
7.4.4 Normalized slope efficiency (triangles) and reciprocal of the threshold (squares) as a function of wavelength for Schott LG-56 glass. -----	136
7.4.5 Normalized square root of slope efficiency (circles) and reciprocal of the threshold (squares) as a function of wavelength for Schott LG-56 glass. -----	137

LIST OF FIGURES (CONTINUED)

	PAGE
8.3.1 Density plot of $\phi(v,t)$ for cross-relaxation rate = 0. -----	146
8.3.2 Density plot of $\log_{10}[\phi(v,t)]$ for cross-relaxation rate = 0. -----	147
8.3.3 Density plot of $\phi(v,t)$ for cross-relaxation rate = 10^4 sec^{-1} . -----	148
8.3.4 Density plot of $\log_{10}[\phi(v,t)]$ for cross-relaxation rate = 10^4 sec^{-1} . -----	149
8.3.5 Density plot of $\phi(v,t)$ for cross-relaxation rate = 10^6 sec^{-1} . -----	150
8.3.6 Density plot of $\log_{10}[\phi(v,t)]$ for cross-relaxation rate = 10^6 sec^{-1} . -----	151
8.3.7 Graph of photon density versus time for cross- relaxation rate = 0: * - $0.9477 \times 10^4 \text{ cm}^{-1}$; + - $0.9468 \times 10^4 \text{ cm}^{-1}$; = - $0.9458 \times 10^4 \text{ cm}^{-1}$; -- - $0.9499 \times 10^4 \text{ cm}^{-1}$; B - $0.9439 \times 10^4 \text{ cm}^{-1}$. -----	152

51. INTRODUCTION

1.1. Problems Investigated

The first successful glass laser used Nd^{3+} as the active ion (Snitzer 1961). Since then several other ions such as Er^{3+} and Yb^{3+} as well as certain combinations of rare-earth and transition elements have been found to lase in a glass host (Young 1969). However, Nd^{3+} still holds the most interest for many investigators. It is a four-level laser whose terminal level has a very short lifetime, with a number of broad absorption bands in the visible, all coupled to the metastable level. It thus has a low threshold, exhibits efficient operation using broad-band pumping sources and should be capable of very high power densities. In addition, the excellent optical properties of glass and the occurrence of emission in the near infra-red region ($1.06 \mu\text{m}$) mean that conventional optical techniques can be used, and large rod volumes can be easily manufactured.

Neodymium is a rare-earth element, the optical spectra of the trivalent ion originating from the partially shielded 4f electrons. Because of the shielding, the positions of excited levels do not shift greatly with a change in ionic environment. Thus, in glass, the assignment of the laser line to the ${}^4\text{F}_{3/2} \rightarrow {}^4\text{I}_{11/2}$ transition is in no doubt, based on studies of the ion in various crystalline hosts. The shape and position of the peak of the relevant fluorescent line varies somewhat in different glass compositions but, in general, it is broad and featureless, considerably skewed on the long wavelength side, and has a full width at half maximum of $300 - 350 \text{ \AA}$ at room temperature. In

crystals, this line is observed to be split into a number of components, each of which have a half width of 5 - 30 Å depending on the crystal quality and the degree of matching of the Nd³⁺ ion to the host lattice. It is suggested that the fluorescent line in glass is an unresolved composite of several lines which have been broadened as a result of the many different possible environments in which a Nd³⁺ ion may be found in a vitreous host.

The laser output exhibits the following salient features. First of all, if it is allowed to operate normally, the oscillating linewidth is observed to increase as the flashlamp energy is increased until a maximum of ~ 100 Å is reached (Snitzer 1964). If the laser is Q-switched by means of a rotating mirror or an electronic shutter, the linewidth is 20 - 30 Å and is nearly independent of pump energy (see §6). Secondly, like many solid state lasers, the output is pulsating. High quality glass rods having outputs with narrow angular divergence exhibit spikes random in time and amplitude with a half width of ~ 1 µsec and a peak power of 2 - 5 kW. If clad rods or fibres are used, the output may consist of periodic pulse trains whose amplitude follows the shape of the pump pulse (limit cycle operation), or it may be steady state with ringing at the leading edge (damped oscillations). In the case of random spiking, the spectral output is a series of sharp lines, whereas with the latter two types of pulsations, the spectral output is smooth with broad maxima (Snitzer 1964).

These observations raise a number of important problems to which we address ourselves in this thesis. In the first place, what is the nature of the broadened line and what mechanisms, if

any, are there to transfer energy from one part of the line to another? It is clear that the only way a line can have such a great width is if different parts of it are due to separate groups of ions, and in this sense the active medium is inhomogeneous. Time resolution studies of the broad maxima of clad rods show that no two adjacent maxima oscillate simultaneously and that each contributes independently to produce the observed total output (Snitzer 1964). Vanukov, Issayenko and Lubimov (1964) have obtained some low resolution time-resolved spectrograms of a laser rod exhibiting random spiking which show that each succeeding spike uses a different part of the spectrum. These results seem to indicate that the energy from one part of the line is not available to any other part. On the other hand, Michon (1966) and Boyden and Clark (1966) have performed experiments which show that energy is available from any part of the fluorescent line to sustain lasing in a 10 - 20 Å band at the fluorescent peak. They interpret these results as indicating a very fast energy exchange mechanism (cross relaxation) between ions with different emission wavelengths. It is important that these conflicting results be resolved, since a thorough understanding of energy storage and transport in the medium is essential to further development of the Nd³⁺ glass laser.

Secondly, there is the question of the source of the spiked output and its relation to the population inversion and pump rate. The rate equations (Statz-deMars equations) for a two level laser have been studied by a number of authors (Makhov 1962, Sinnott 1962, Korobkin and Uspenskii 1963) with the conclusion

that unless additional terms (various sorts of non-linearities) are inserted, limit cycle behaviour cannot occur. In ruby, limit cycle operation readily occurs when only a single longitudinal mode is oscillating, and the random spiking has been shown to be due to the selective spatial depletion of inversion which occurs in a Fabry-Perot resonator cavity (Tang, Statz and deMars 1963). The Nd^{3+} glass laser is certain to be a more complex situation if for no other reason than its very great bandwidth compared with ruby. In the latter, only one mode oscillates at a time, but this is certainly not true of Nd^{3+} glass. Nevertheless, it appears that mode interactions of some sort can influence the temporal behaviour of the output.

1.2. Methods of Investigation

These two problems are certainly related, since the pulsations are indicative of fluctuations in the population inversion, which is in turn influenced by the line structure. We have investigated them using three approaches. Firstly, we have made a thorough review and theoretical study of processes affecting the line shape. In §2, the spectroscopy of Nd^{3+} is reviewed and related to the properties of glasses in order to emphasize the differences between glasses and crystalline hosts. Group theory is applied to the analysis of term splitting to show that the fluorescence at $1.06 \mu\text{m}$ must be a composite of twelve unresolved lines, although little can be said of the degree of splitting or the intensity of these components. §3 discusses the various sources of line broadening in the solid state. This exposition is necessary because there has apparently been no previous attempt to

relate the work of Van Vleck (1948), Bloembergen, Shapiro, Pershan and Artman (1959) and others on line broadening in magnetic resonance experiments to the similar processes in the electronic transitions of lasers. This has resulted in considerable confusion in the literature, not only in the use of descriptive names of various broadening effects, but also in the manner in which they can be expected to affect the laser transitions. All the major mathematical equations and derivations used in the experimental sections have been grouped into §4.

Secondly, two sets of experiments have been carried out to investigate the nature of the broadened line and the source of the spiked output. In the first set of experiments (§6), the spectra of the laser output was studied as it varied in time (time-resolved spectroscopy) by coupling the output of a high resolution spectrograph to a rotating mirror streak camera. Two glasses were investigated to get an estimate of the effect of different glass hosts on the behaviour of the active ions, and observations were made with two cavity arrangements, both when the laser was allowed to operate normally, and when it was Q-spoiled by various methods. The two cavity resonators studied were the usual Fabry-Perot resonator and a three mirror ring resonator. In the former arrangement, standing waves must exist for each cavity mode, resulting in uneven depletion of active ions in the lasing medium (spatial hole burning). Standing waves could also occur in the ring laser through the interaction of the two waves travelling in opposite directions having the same mode number. However, there should be sufficient perturbation to ensure that the frequencies of the modes are "pulled" so as to prevent the form-

ation of standing waves with their accompanying uneven depletion. By using different cavities and observing any changes in the spiking behaviour, some estimate can be obtained of the influence of the resonant cavity on the laser. Similarly, by Q-spoiling the laser using different methods, one can study the laser under pulsed and shock-excited conditions. In the first method of Q-spoiling, a glass plate with a thin gold film deposited on it was inserted into the cavity. When a thin absorbing film is used as a shutter, the first pulse destroys the film, opening it for the rest of the pump pulse. Thus one is able to study the transient behaviour of a laser, since it is suddenly switched on after an appreciable inversion has built up in the active medium. A similar action was obtained by modifying an electronic shutter (Pockel's effect cell) so that it remained open after switching for the duration of the pump pulse. By observing the bandwidth and wavelength structure of individual pulses and comparing adjacent spikes, it is also possible to investigate the nature of the fluorescent line. This is especially true when Q-spoiling with thin films, since lasing may start at almost any part of the central 20 - 30 Å of the fluorescent line or, in some cases, simultaneously over the entire band. Thus one is able to probe different groups of the inversion population and observe the effect on adjacent ones. An organic dye shutter was also studied, and the output was found to consist of one or two Q-spoiled pulses with a spectral width of less than 2 Å. Apparently special steps must be taken to observe the mode locking described by Stetzer and DeMaria (1966).

In the second set of experiments (described in §7), the laser was forced to oscillate in a very narrow bandwidth ($< 5 \text{ \AA}$) by using a diffraction grating as one of the reflectors in a Fabry-Perot cavity. The slope efficiency of the laser as a function of frequency, $dE_{\text{out}}/dE_{\text{in}}$, was then computed from measurements of the output. Clearly, if there are fast energy transfer mechanisms between groups of ions, or if all parts of the fluorescence share a common energy pool, then this measurement of the energy conversion efficiency should not be strongly dependent on the wavelength of oscillation. In addition, by comparing the spiking pattern when the laser is operating in a narrow band with normal wide-band operation, the effect of the number of oscillating modes on spiking can be estimated.

The third approach to the study of Nd^{3+} glass behaviour was to examine the behaviour of the rate equations derived for a model which is thought to be a reasonable approximation of the real laser. In §8, the results of a computer simulation of the coupled equations are presented. This method of investigating the stability of the equations was used rather than the analytic approach of Sinnett (1962) because of the mathematical difficulties involved. The results are correlated with those of Peressini and Linford (1968), who investigated the spectral properties of a similar model for a steady-state condition (i.e. no pulsations).

1.3. Conclusions

On the basis of previous studies of glasses, the ${}^4\text{F}_{3/2}$ level is known to be split and it is shown that this implies that the degeneracy of the ${}^4\text{I}_{11/2}$ level must also be completely removed.

This means that the observed fluorescence at 1.06 μm must be a composite of the twelve possible lines due to transitions from the two sublevels of the ${}^4\text{F}_{3/2}$ term to the six sublevels of the ${}^4\text{I}_{11/2}$ term. Each of these lines experiences inhomogeneous broadening due to the many possible ionic environments in a glass host. However, unlike a similar structure in a magnetic resonance experiment where each line arises from a different population, there is one source (the ${}^4\text{F}_{3/2}$ level) for all these lines, and one cannot speak of energy transfer between the unresolved lines.

On the other hand, it is possible for cross relaxation to occur, i.e., for ions which contribute to different parts of a given line to exchange energy. Our measurements indicate that this process does take place, but that it is very slow compared to other processes. A value for the width of the broadened sublevels is obtained by relating the peak of the fluorescent line to the major transition of the unresolved lines.

The spiking behaviour was found to be little influenced by any of the changes in the type of resonant cavity or the bandwidth of the oscillations. Thus, if the source of the instability arises from mode interactions, then it is not a strong function of the number or type of cavity modes. The computer simulation of the rate equations indicates that neither cross relaxation nor the finite lifetime of the terminal level can account for the observed random spiking. However, certain giant pulsations observed in some of the time-resolved experiments appear to be correctly described by these equations.

§2. SPECTROSCOPY OF Nd^{3+} IN GLASS

2.1. Introduction

There has been considerable interest in the spectroscopy of the rare-earth elements since about 1940, when they were found to be useful as sensitizers in phosphors, and later when their suitability as active ions in quantum-mechanical up-converters became apparent (Urbach, Perlman and Hemmendinger 1946, Brown, Shand and Whiting 1965, Porter 1965). This interest, and the discovery of lasing action in several rare-earth doped crystals, has led to a growing number of papers on the spectral properties of these ions in various crystal hosts (see, for example, Kisliuk, Krupke and Gruber 1964, Carnall, Fields and Wybourne 1965, Brown, Whiting and Shand 1965, Brandewie and Telk 1967).

However, although it may reasonably be expected that many of the results of studies of the properties of ions in crystals can be extended to glass, some care must be exercised. Glass certainly has an ordered structure on the scale of several atomic distances, but in many other respects it behaves more as a liquid than a solid. Thus, in the subsections that follow we first review the spectroscopy of the rare earths as applied to Nd^{3+} , and then discuss some relevant properties of the vitreous state. This is followed by a review of the observed properties of Nd^{3+} in glass. The spectral properties of an ion are determined largely by the symmetry of the crystal fields surrounding the ionic site and, in order to discuss these effects in §2.6, a background sketch of the necessary theory is given in §2.5. The section concludes with a statement of the theoretical results and

a comparison of them with the experimental observations.

2.2. Spectral Properties of Nd^{3+}

In the trivalent rare-earth ions, of which Nd^{3+} is typical, all energy levels below 50000 cm^{-1} are $4f^n$ configurations (with the exception of Tb^{3+}), and being well shielded by the completed 5s and 5p shells, the effect of the external environment on the position of the levels is minimal. Transitions between 4f configurations are forbidden by the normal selection rules and thus tend to have small oscillator strengths even in a highly perturbing environment. The ions follow Russell-Saunders coupling to a great extent and the levels are named accordingly. Because of the shielding, the main differences in ionic spectra for a given ion in various hosts are in the degree and extent of splitting of the terms. The position of the level does not change appreciably from host to host and the energy level assignment can be made unambiguously. Thus, for Nd^{3+} , the results of Dieke and Crosswhite (1963) and others can be applied to the glass matrix to make assignments to the transitions observed in absorption and fluorescence. Nothing can be said, however, about the number of sublevels or the magnitude of their separation without a knowledge of the symmetry of the sites of the ion in a given host.

2.3. The Glass Matrix

A good definition of a glass is a super-cooled liquid whose viscosity is greater than 10^{14} poise (Mackenzie 1960a). Thus, any short-range order such as the formation of complex ions,

or the creation of ligands around the ion, can be expected to be "frozen" in the liquid as it cools. However, most substances which commonly form glassy states are distinguished by a high viscosity even in the liquid state. Thus, at 1700° C fused silica has a viscosity of 10^7 poise and at 2000° C, where it begins to sublime, the viscosity is still 10^4 poise (Mackenzie 1960b), compared with water which has a viscosity of about 2×10^{-2} poise at its melting point. The addition of metal oxides such as Na_2O , Li_2O and PbO to form the binary and ternary compounds which characterize our optical and window glasses drastically decreases the viscosity of the melt, lowering it to about 10^2 poise for 20% mole fraction of a metal oxide (Mackenzie 1960b). Such high viscosities at melting point may frustrate the attainment of equilibrium conditions in a reasonable time and inhibit the formation of co-ordinating complexes between the base oxide (silica) and the metal ions. On the other hand, once equilibrium has been attained, the high viscosity will prevent new equilibria from being established as the glass is cooled past its transition point.

It is generally agreed that the structure of fused silica consists of a random network of SiO_4^{2-} tetrahedra and it is this network which accounts for its high viscosity. Despite the randomness of the structure, the angle of the bonds formed between neighbouring tetrahedra by the shared oxygen atom, and the distance between neighbouring silicon atoms are quite constant. If the number of Si-O-Si bonds versus angle or the number of silicon atom pairs versus distance is plotted, the resulting distributions about the mean value have a full width at half maximum of only about 10% of the mean (Mozzi and Warren 1969). On

the addition of metal oxides, the picture is not quite as clear. There is a discontinuity in many of the properties of glasses in the region of 12 - 20% mole fraction of metal oxide and this has been taken to mean a change in structure from the network model for pure silica. In the range 12 - 66%, where the composition corresponds to the orthosilicate, suggestions as to the structure vary all the way from conjectures about the production of infinite sheets or chains to hypotheses proposing the formation of large ring and globular anionic complexes, isolated from one another and bonded by the metal ions (Mackenzie 1960a and 1960b). Structures such as $\text{Si}_6\text{O}_{15}^{6-}$ and $\text{Si}_8\text{O}_{20}^{8-}$ illustrated in Mackenzie (1960b) are of interest because they have large enough dimensions to act as sequestering agents for a rare-earth ion and would provide a highly stable and symmetrical ligand field.

2.4. Rare-Earth Ions in Silica-Based Glasses

A large number of transitions in rare-earth elements, when in solution with suitable solvents and anions, tend to form stable groupings called complexes. These complexes consist of the metal ion surrounded by a well ordered arrangement of anions or polar molecules which either neutralise or distribute the cationic charge over a greater area, hence reducing the interaction between the cation and its surroundings. For example, such ions as Cu^{2+} , Cr^{3+} AND Ni^{2+} in aqueous solutions are surrounded by six water molecules with the oxygen atoms of each in octahedral symmetry about the ion. If suitable anions are present, such as SO_4^{2-} , one of these may substitute for two water molecules to neutralise the

charge (in the case of divalent cations). In some cases of organic solvents and anions the complex so formed is highly stable. The co-ordinating anions are bonded together in a shell around the cation and the complex may even be precipitated out of solution. Such compounds are known as sequestering (hiding) agents. In fact, most early attempts to produce a liquid laser involved sequestering rare-earth ions (especially Nd^{3+}) in a variety of organic sequestering agents. Anions and molecules which are co-ordinated in this manner with cations are known as ligands, and the number of atoms, ions or molecules associated in a regular manner with the ion is called the co-ordination number of the cation. The electrostatic field formed by the ligands is known as the "ligand field" and its symmetry reflects that of the surrounding ligands in a manner similar to the field of a crystal lattice surrounding an ion in a regular solid. Indeed, since the cation field decays inversely as the fifth power of the distance (Bates 1962), next-nearest neighbour symmetry effects are generally of little consequence, and ions in a crystal lattice behave to first order as if they were in a ligand field formed by nearest neighbours only.

The work that has been done on transition elements indicates that the complexes formed by them in solution and in glasses are of very high symmetry. The most common co-ordinate number is six, which can give a field of full cubic (octahedral) symmetry. The ions appear at the centre of the cube and the six co-ordinating sites of the ligands occupy the centres of the six faces of the cube. Cubic symmetry can also arise if eight co-ordinating sites are arranged at the corners of a cube. Four

co-ordinating sites in crossed, opposing diagonal corners of a cube have tetrahedral symmetry, which is the lowest commonly encountered. Of course, it is possible for a number of reasons to have distortion which could lower the symmetry still further. As an example, should it happen that the ground state of the cation would be degenerate in the full symmetry of the ligand field, the cation field will distort the ligand sites in such a manner as to remove this degeneracy, a consequence of the Jahn-Teller effect (see, for instance, Landau and Lifshitz 1958). While we are not aware of detailed work published on the co-ordination of rare-earth ions in glasses, they should behave in a manner similar to the transition metals. There is good evidence that some transition metals form complexes with the SiO_4^{2-} tetrahedra which have octahedral symmetry or some subgroup of it. Laser glassmakers are evidently aware of this since they control the site symmetry to some extent,† probably through the use of additives which affect the fluidity of the melt and hence the time for complexes to reach equilibrium. If the anionic structures discussed by Mackenzie (1960b) exist in the binary silicate glasses, they could act as sequestering agents for the Nd^{3+} ion. However, there is no need for such permanent structures and similar fields would be produced by the oxygen atoms of silicon tetrahedra (whether free or partially bound in a network) as long as there is sufficient mobility in the melt for the ligand to form.

† "Our glass composition was chosen to give the neodymium ions low symmetry, high field sites, and consequent short fluorescence lifetime. As you have observed, this is contrary to the philosophy employed by other laser glass manufacturers." (Eastman Kodak, private communication 1969)

We should note that a general problem which occurs with the inclusion of transition and rare-earth ions in glasses (and even in solutions) is the control of the valence of the ion. Fortunately, in the case of neodymium, the trivalent state is always found unless rigorous steps are taken to suppress it. The confusion of interpretation of results due to lack of knowledge of the valence of the ion does not occur and will not be discussed further.

2.5. Aspects of Symmetry

Because of the intention to deduce some general conclusions based on symmetry properties, the following brief review is given to emphasize their nature. Most objects, whether man-made or otherwise, possess certain obvious properties of symmetry. For example, one part may be the mirror image of another, i.e., the object possesses a plane of symmetry. Or, the object may look the same after being rotated through some fraction of a circle about some axis. In this case it is said to be axisymmetric and possesses rotational symmetry. In addition, if there is an obvious centre through which an imaginary line may be passed such that it always intersects identical positions on opposite sides, the object is said to be centrosymmetric and to possess a centre of inversion. The possible combinations of the three operations of reflection, rotation and inversion can be classified by group theory, and the groups so formed are known as point groups. Objects such as spheres, cylinders and cones are symmetric under all rotations of their axes and belong to the

study of infinite rotation groups. Those which are brought into coincidence by finite rotations are classed under finite groups. If we also demand that these objects fit into a regular three-dimensional lattice, where translations of the lattice bring the objects into coincidence and rotations of the objects bring the lattice into coincidence, we find that the rotations are restricted to values of $\pm 2\pi/n$, where $n = 2, 3, 4$ or 6 . There are only 48 point groups compatible with these operations. In group theory, operators (or generators) are associated with the three basic operations, and these can be used to generate all the elements of the group. For instance, the operation associated with the symmetry of a flat equilateral triangle is a rotation about an axis of $2\pi/3$, and is called C_3 . The elements are $[C_3, C_3^2 = \bar{C}_3 = C_3^{-1}, C_3^3 = E$ (the "identity" element)]. The importance of this is that one can associate square matrices with these symmetry operations which, when multiplied together, obey the same transformation rules as the symmetry operations themselves. In addition, there is a fixed number of "different" sets of matrices (known as representations) which one can find to associate with a given finite group. Any other possible matrix, vector, or number set which one can devise can be shown to be linear combinations of these associations (McWeeny 1963). The matrices can be chosen to be unitary and orthogonal in the sense that if one forms vectors by extracting the same element from every matrix in a representation, any two different vectors, either from the same representation or from other representations, give zero length when multiplied together. In addition, no matter what unitary transform is applied to these

matrices to change the particular representation, the trace of the matrix does not change and it can be used to identify the representation. Such representations are known as "irreducible representations of the group" and can be completely specified by tables of their traces rather than tables of the matrices themselves. The trace of a representation for a given element of a group is known as the "character" and is denoted by the symbol χ . The character of the identity element is always equal to the dimension of the representation, since it is clear that the identity must be a matrix with ones on the diagonal and zeros elsewhere if it is to leave the other elements of the group unchanged when multiplied by it. It is customary to denote one-dimensional representations (number sets) of a group by the letters A or B, two-dimensional representations (vectors) by E, three- by F or T, four- by G, etc. In addition, many groups of higher symmetry contain groups of lower symmetry as subgroups, and it is always possible to find a linear combination of irreducible representations of the subgroups which reproduce the representations of those elements in the higher group common to both groups. The representation of the higher group is said to be "carried" by those of the lower group.

In the case of the infinite rotation groups, there is an infinite but denumerable number of representations (Landau and Lifshitz 1958), and they may be of infinite dimension. An infinite group which we shall be discussing is the "three-dimensional full rotation group", which is the group of all possible rotations about a point. Its generator is the infinitesimal rotation $d\phi$.

We now consider the relationship between symmetry and the splitting of energy levels in an ion or atom. For free ions (or atoms) the solution of the eigenvalue problem associated with the Hamiltonian operator on the electron wave functions,

$$\hat{H}\psi = \left[\frac{-\hbar^2}{2m} \nabla^2 + V(R) \right] \psi = E\psi, \quad \dots \quad (2.5.1)$$

yields different values of the energy associated with the principle quantum number n . There is not, however, a unique wave function associated with each energy level since the angular momentum commutes with the Hamiltonian, and its wave functions must therefore be wave functions of the Hamiltonian. There are $2L + 1$ independent wave functions associated with any energy level, where L is the angular momentum quantum number. The energy level is said to be degenerate of order $2L + 1$.

Let us look at it another way. Consider now an ion that is surrounded by an electrostatic field produced by a crystal lattice. We replace $V(R)$ with $V(X,Y,Z)$ in eqn. (2.5.1) and note that the solutions to this new eigenvalue problem will not change if the co-ordinate system is rotated in such a way that the field is once again brought into coincidence. This is in effect a symmetry operation of the wave functions, and since this operation does not change the energy eigenvalues it clearly commutes with the Hamiltonian. Thus, the (possibly degenerate) wave function(s) associated with the energy level form a representation of the rotation group in question. The symmetry operations merely transform one linear combination of degenerate wave functions associated

with an energy eigenvalue into another linear combination, each combination being associated with a symmetry element. The number of degenerate wave functions of an energy eigenvalue is equal to the dimension of the irreducible representation, and the proper representation may be found from a consideration of the symmetry of the free ion.

As the crystal field is "turned on" about the free ion, the free ion level splits into new levels and the energy eigenfunctions of the new levels are linear combinations of the energy eigenfunctions of the old levels. Thus, what is needed is a rule for re-ordering the $2L + 1$ degenerate wave functions of an energy eigenvalue of the free ion to form sets of wave functions which transform like the operations of the symmetry group of the lattice. Now the angular momentum operator is in fact an operator of the full rotation group (since the centrosymmetric field of the ion distinguishes no particular direction in space) and the wave functions associated with an energy level form a $2L + 1$ -dimensional representation of the full rotation group. This group has a character

$$\chi(\phi) = \frac{\sin[(L + 1/2)\phi]}{\sin[\phi/2]}, \quad \dots \quad (2.5.2)$$

(Landau and Lifshitz 1958). The finite rotation groups are subgroups of the full rotation group and any representation of the full group can be reproduced by a linear combination of the irreducible representations of the finite group. The representations in the linear combination are the correct representations

for the levels of the ion in the crystal lattice, and the total number of these representations determines the degree of splitting. The dimensions of the representations determine the degree of degeneracy of the new levels. The rule for finding the linear combination is to calculate the characters of the full rotation group for angles corresponding to allowed rotations in the finite group, and consult the character table of the irreducible representations of the finite group in order to find a linear combination whose characters add up to the characters of the full rotation group.

When electron spin is included, conservation of angular momentum strictly applies only to the total angular momentum J of the ion. It is this which commutes with the Hamiltonian and forms a representation of the full rotation group. In Russell-Saunders coupling, which is most applicable to Nd^{3+} , spin-orbit interaction is small compared with spin-spin coupling, and the sum of the orbital angular momentum L and the sum of the spins S are constants of the motion to a first approximation. These are therefore used as labels for the terms which in the free ion are degenerate of order $2J + 1$. Thus the angular momentum can take on half-integral values and we note that when such is the case, the character of the full rotation group given by eqn. (2.5.2) becomes minus the character of the identity when $\phi = 2\pi$, rather than being equal to it as it should. A further rotation of 2π restores the positive identity. This is a direct result of the two-valued nature of the electron wave function, due to spin, and must be taken into consideration when comparing the characters of the full rotation

group with tables of the finite groups. Bethe (Landau and Lifshitz 1958, Knox and Gold 1964) developed a convenient method of handling this by introducing the concept of a "double group", in which a fictitious operator Q was introduced, such that $Q^2 = E$. Such double groups have other representations in addition to those corresponding to the normal groups, and it is these which are used to represent the double-valued terms. Tables of the double groups of interest to us are given in appendix I, where representations given below the dotted line are the ones to be used for the double-valued representation. It is emphasized that any results obtained by these group theoretical approaches are completely general; if the configurations of the terms are known (and they are in no doubt for Nd^{3+}), then given a specific ligand field symmetry, the degree of removal of degeneracy can be determined exactly. The calculation of the difference in energy between the split terms and its sign is, however, an extremely difficult task which depends on a detailed knowledge of the wave functions of the term and the strength of the ligand field.

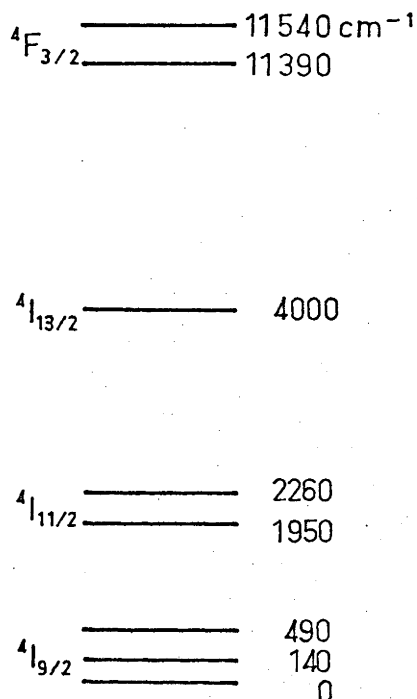
2.6. Discussion of Observations as Compared with Theory

The spectral lines of Nd^{3+} ions in a glass matrix vary considerably from one glass to another, and also from the spectrum of the ion in crystalline hosts (Lengyel 1966, Young 1969). The latter tend to have narrow lines both in absorption and emission, these being sharpest when the crystal is of high quality and when the Nd^{3+} ion fits the crystal lattice well. All the glasses, however, exhibit broad, diffuse lines with poorly defined split-

ting. This is attributed to the large number of non-equivalent sites, that is, to the variety of different possible ligand configurations available in a glass matrix. Of course, there will be only a certain few different point group symmetries represented, but quite considerable variations in the field strength will exist and hence the magnitude of the splitting varies from ion to ion. In addition, next-nearest neighbours will play some part, especially in a solid where thermal motion cannot cause the background field to fluctuate about a mean of spherical symmetry as in a liquid. The lines are therefore inhomogeneously broadened and the resulting lineshape can be thought of as the superposition of the individual lines of all the ions, each of these having a finite linewidth due to homogeneous broadening.

Thus, the assessment of the behaviour of the ions in the glass matrix is extremely difficult and one must be careful about making generalizations from glass to glass, where not only do the lineshapes vary, but the fluorescent lifetimes also range over an order of magnitude. Fig. 2.6.1 is an energy level diagram of experimentally observed splittings of the relevant levels, based on Snitzer and Young (1968). In glass, Nd^{3+} has a number of strong, broad absorption lines in the visible and near infrared, strong because many are allowed transitions, and broad because of high multiplicities and the splitting of both the ground and excited states in the glass matrix. All these states decay by radiationless transitions in a rapid cascade process to the ${}^4\text{F}_{3/2}$ state. It is metastable because there are no allowed transitions to lower levels and because it is separated by 6000 cm^{-1} from the next lower

Fig. 2.6.1



Energy level diagram of Nd³⁺, indicating the experimentally resolved sublevels, after Snitzer and Young (1968).

level, too much for the energy to be easily yielded to the crystal lattice in a non-radiative transition. In glass, for concentrations of around 2 - 3% atomic weight (below which co-operative energy transport phenomena do not occur), this excited state then decays predominantly to the ⁴I_{11/2} level, but also the ground state (⁴I_{9/2}) and to the ⁴I_{13/2} level. Careful measurements by DeShazer and Komai (1965) account for all the absorbed energy, and indicate that only 40% of the absorbed photons are emitted in fluorescence. This is relatively independent of the absorbing band, and varies only slightly from glass to glass, indicating either that the metastable level does have some non-radiative by-pass processes, or that there is always a certain fixed fraction of ions in the

matrix which never fluoresce. It is probable that the latter is closer to the truth (Edwards 1966). The fluorescent ratios found by DeShazer and Komai are 0.24, 0.60 and 0.16 for decay to the ${}^4I_{9/2}$, ${}^4I_{11/2}$ and ${}^4I_{13/2}$ levels, respectively. Measurements by others of different glasses confirm these observations.

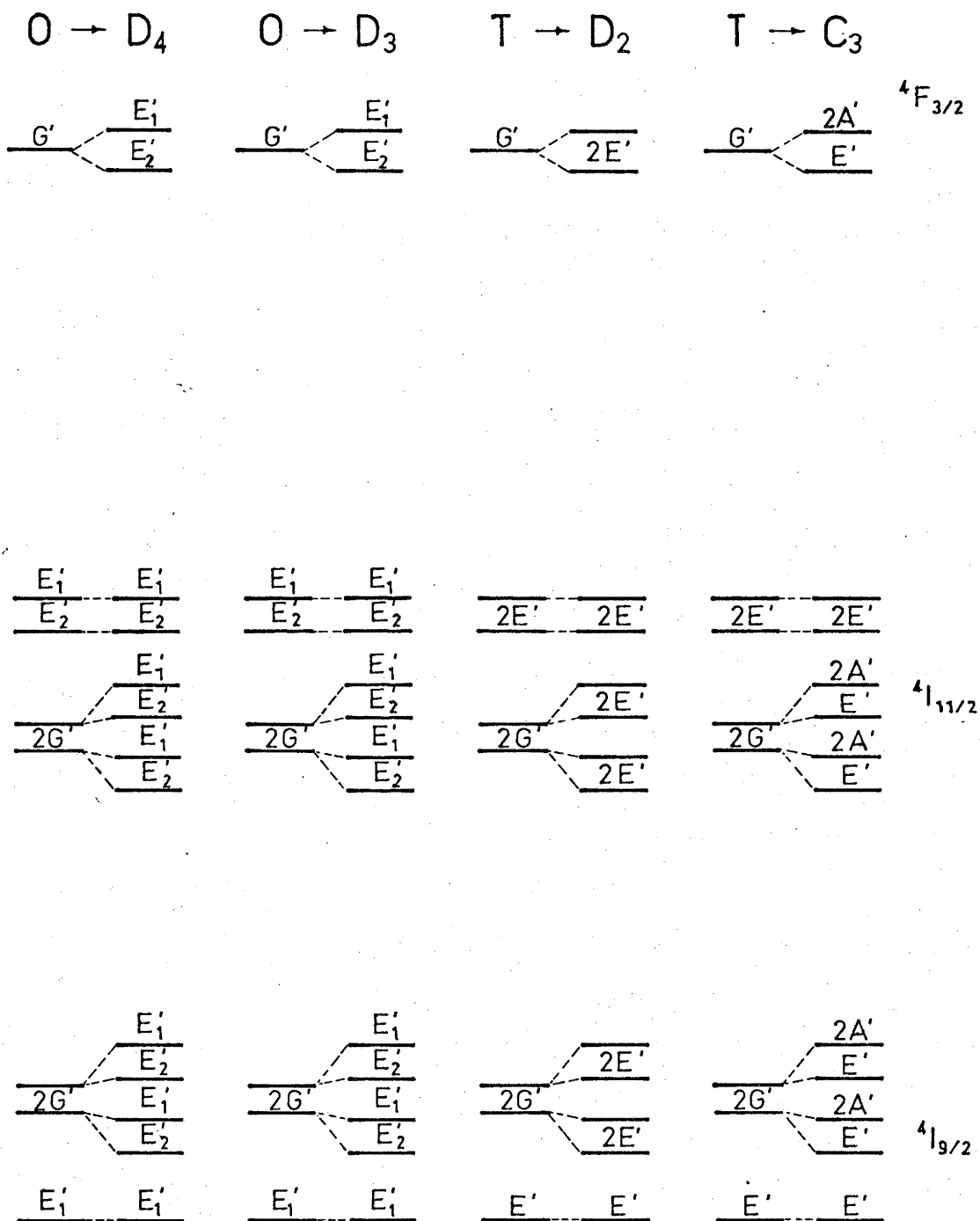
The glass associated with the energy level diagram shown in fig. 2.6.1 was chosen by Snitzer and Young (1968) because its narrow lines facilitated resolution of any possible structure. It appears to be representative of other glasses. The splitting of the ${}^4F_{3/2}$ level is observed in absorption and is well resolved at 77° K. This line has been found to be split in all glasses. The number of sublevels in the ground state was obtained by fluorescence at $0.88 \mu\text{m}$ and 77° K. It is known to vary from glass to glass. The splitting of the ${}^4I_{11/2}$ line is uncertain, but it has at least two sublevels.

Before turning to the discussion on the results of application of symmetry theory, a remark should be made about the maximum number of sublevels possible. The degeneracy of a term is $2J + 1$, but a theorem due to Kramer (Landau and Lifshitz 1958) states that in the case of half-integral values of the angular momentum quantum number, the degeneracy cannot be completely lifted in the presence of purely electrostatic fields. All the levels must remain at least doubly degenerate. This is why nearly all the special double groups previously considered are even dimensioned, and in the case of two which happen to be type A, a representation must be taken using these in pairs which are not split. (It is interesting to speculate on the effect of the strong magnetic

fields often associated with glass lasers due to the close proximity of the flash lamps.)

Fig. 2.6.2 illustrates energy level diagrams obtained from group theory for various symmetries of the ligand field. Figs. 2.6.2(a) and 2.6.2(b) show the splittings due to a ligand field possessing full cubic (octahedral) symmetry and two of its subgroups D_4 (tetragonal) and D_3 (trigonal) to which such a field can be reduced by distortion, indicating how the lines are further split when passing from octahedral to a lower symmetry. Figs. 2.6.2(c) and 2.6.2(d) are similar illustrations for the tetrahedral group of cubic symmetry. In the figures, the positions and the magnitudes of the sublevels have been arbitrarily chosen for the cubic symmetries, except that E'_1 must be the ground state because of the Jahn-Teller effect. The positions of the sublevels of the lower symmetries follow from the choice for the cubic groups. The conclusion that in glass the degeneracy of all the levels of interest must be completely removed (as much as is allowed by Kramer's theorem) follows from the experimental fact that the ${}^4F_{3/2}$ level is always found to be a well resolved doublet, and from the theoretical result that all symmetries which remove this degeneracy also remove it in the other levels. The importance of this conclusion will be brought out in later sections. Unfortunately, because all symmetries lower than the cubic completely remove the degeneracy, one can say little more using this approach about the actual ligand fields surrounding the ion.

Fig. 2.6.2



Energy level diagram of the ${}^4F_{3/2}$, ${}^4I_{11/2}$ and ${}^4I_{9/2}$ levels, showing how the terms split as the symmetry is lowered by distortion, from O (octahedral) to D_4 (tetragonal) and D_3 (trigonal), and from T (tetrahedral) to D_2 (orthorhombic) and C_3 (trigonal).

§3. LINEWIDTH

3.1. Introduction

There has been considerable confusion in the literature over the use of the terms "homogeneous broadening", "inhomogeneous broadening" and "cross relaxation". This has sometimes led to a misrepresentation of the properties of the observed linewidth of Nd^{3+} in glass and of the energy exchange between the radiation field and the ions. The confusion has arisen in part because the terms were originally used to describe line broadening mechanisms in magnetic resonance experiments. The broadening of the electronic transitions of lasers has the same sources, but the effects will differ in important ways since the observables being measured in the two cases are quite separate. It would appear that this has not always been appreciated and that care has not been taken to avoid confusing the sources of line broadening. Because of this, and because such processes are central to the theme of this thesis, it has been thought desirable to review what is known of the mechanisms that produce line broadening and attempt to categorise them and their effects.

In the subsections which follow, the mechanisms which produce homogeneous broadening in paramagnetic ions - interaction between ions and the radiation field, ion-ion interactions, and interactions between ions and the host material - are classified and discussed. Then, in §3.5, a hypothetical experiment is used to illustrate the source of inhomogeneous broadening and to show how it differs from homogeneous broadening. The final subsection clarifies the relation between homogeneous broadening and energy

transfer mechanisms (cross relaxation) in an inhomogeneously broadened line.

3.2. Interaction with the Radiation Field

In considering the interaction between ions and a radiation field, the simplest system is one in which the ions are spaced far enough apart that radiation of a photon by one ion does not affect the radiation of other ions. If some of the ions are in an excited state, they will decay at random and emit radiation of frequency

$$\nu = (E_i - E_f)/h = \Delta E/h ,$$

where ΔE is the difference in the energy of the initial and final states. The emitted radiation is not monochromatic but has a measurable linewidth. This arises because of the uncertainty in the frequency measurement of any wave train of finite length and is described mathematically by the Fourier transform of the function representing the wave train. When radiation from all the ions is considered, the linewidth is described by the Fourier components of a quasi-continuous wave which is continually being interrupted and started again, with a phase relation random to that previous to the interruption. If τ is the lifetime of the excited state, related to the Einstein coefficient for spontaneous emission A by $\tau = 1/A$, then the average rate of interruption is just A . The shape of a line whose width is due to the above process is the Lorentzian, which has a normalized intensity distribution about ν_0 given by

$$g(\nu) = \frac{\Delta\nu}{2\pi} \cdot \frac{1}{(\nu - \nu_0)^2 + (\Delta\nu/2)^2}, \quad \dots \quad (3.1)$$

where

$$\Delta\nu = 1/\pi\tau.$$

See, for example, Vuylsteke (1960 §4.5). Any other process which can interrupt the radiation (or absorption) of a photon by an ion will also contribute to the linewidth. In a gas, an example of this is collision broadening. In a solid containing paramagnetic ions, the radiation can be interrupted by the sudden change in local fields due to an alteration of the configuration of adjacent ions (see §3.3). The total linewidth is just the sum of the linewidths arising from any one of these sources of interruption, i.e.,

$$\Delta\nu_{\text{tot}} = \Delta\nu_1 + \Delta\nu_2 + \Delta\nu_3 + \dots + \Delta\nu_n.$$

In cases where the ion spacing is not small compared to the wavelength of the emitted radiation, an additional effect (Lamb shift) arises due to co-operation among neighbouring ions. Its effect is to further broaden and shift the line so that it is no longer Lorentzian (Fain and Khanin 1969 §33).

3.3. Interactions between Elements of the Ion System

Interactions between the ions may also cause broadening of the line by slightly shifting the energy levels of the ions from the mean position. The profile of the resulting line does not have the Lorentzian shape. In the case of paramagnetic ions, these effects are much greater than those contributing to the Lorentzian line and completely obscure it. The sources of this

broadening were first considered in connection with relaxation effects and line broadening observed in susceptibility and magnetic resonance experiments with dilute solutions of paramagnetic ions in crystals and liquids. It is discussed lucidly in papers by Bloembergen, Purcell and Pound (1948) and Van Vleck (1948). The effects of interest here are due to the interaction between the electrons in the ions which are in partly filled shells (in the case of Nd^{3+} , the 4f electrons). The Hamiltonian for these effects is

$$H = - \sum_{j>i} 2J_{ij} \hat{S}_i \cdot \hat{S}_j + g^2 \mu_B^2 \sum_{i>j} [r_{ij}^{-3} (\hat{S}_i \cdot \hat{S}_j) - 3r_{ij}^{-5} (\hat{r}_{ij} \cdot \hat{S}_i)(\hat{r}_{ij} \cdot \hat{S}_j)] , \quad \dots \quad (3.2)$$

where J_{ij} is the exchange integral between two electrons i and j , \hat{S}_i is the spin operator, g is the Landé factor, and μ_B is the Bohr magneton. \hat{r}_{ij} is the vector distance between the two electrons. The summation is taken over all the electrons not in closed shells in the crystal. This is the Hamiltonian of the internal or coupling energy of the system. There is obviously a large number of different ways that the electrons and spins can be distributed, and thus the energy stored in the interaction may vary over a considerable range.

The first term is due to the exchange interaction and arises from the Pauli exclusion principle (Dicke and Wittke 1960 §17.4). The bringing together of ions in the same energy state such that their electron wave functions overlap causes a splitting of the (previously) single level. With a large number of ions

such as found in a solid, the level smears out into a band.

The second term is the dipole approximation to the spin-spin interaction and was first investigated by Kronig and Bouwkamp (1938) in order to explain relaxation in the magnetization of paramagnetic ions. See also Casimir and Du Pré (1938) and Waller (1932). Each electron finds itself in a local magnetic field produced by the magnetic moments of all other unpaired electrons and thus has a different energy according to whether its spin is parallel or anti-parallel to this field. Once again, there is a large number of possible states with slightly different energies, and a broadening of the line results.

Of course, one cannot separate the effects of the two processes since, for instance, interchange of two electrons will change the local field acting on the electron dipole. The picture that arises is that the spin system (i.e., the ion system) as a whole has a definite energy but, on the microscopic scale of a single ion, the energy levels are seen to shift around at a rapid rate due to interchange and local re-arrangement of the magnetic energy in the dipole-dipole (spin-spin) interaction.

If an external magnetic field is applied, there is now a preferred direction in space and the terms can be sorted out according to their properties, obtaining

$$H = A + B + C + D + E + F , \quad \quad (3.3)$$

where,

$$A = \sum_{j>i} [-2J_{ij} + g^2\mu_B^2 r_{ij}^{-3} (1 - 3\cos^2\phi_{ij})] S_{iz} S_{jz} ,$$

$$B = \sum_{j>i} [-J_{ij} - (1/4) g^2\mu_B^2 r_{ij}^{-3} (1 - 3\cos^2\phi_{ij})] (S_{i+} S_{j-} + S_{i-} S_{j+}) ,$$

$$C = \sum_{j>i} (-3/2) g^2\mu_B^2 r_{ij}^{-3} \sin\phi_{ij} \cos\phi_{ij} (S_{i+} S_{jz} + S_{iz} S_{j+}) \exp(-\theta_{ij}) ,$$

$$D = \sum_{j>i} (-3/2) g^2\mu_B^2 r_{ij}^{-3} \sin\phi_{ij} \cos\phi_{ij} (S_{i-} S_{jz} + S_{iz} S_{j-}) \exp(+\theta_{ij}) ,$$

$$E = \sum_{j>i} (-3/4) g^2\mu_B^2 r_{ij}^{-3} \sin^2\phi_{ij} S_{i+} S_{j+} \exp(-2\theta_{ij}) ,$$

$$F = \sum_{j>i} (-3/4) g^2\mu_B^2 r_{ij}^{-3} \sin^2\phi_{ij} S_{i-} S_{j-} \exp(+2\theta_{ij}) ,$$

$S_{i\pm} = (S_{ix} \pm iS_{iy})$, the spin creation and annihilation operators, and ϕ and θ are angles in polar co-ordinates which are related to the direction cosines α_{ij} , β_{ij} and γ_{ij} of r_{ij} with respect to the x, y and z axes by

$$\alpha = \sin\phi \cos\theta, \quad \beta = \sin\phi \sin\theta, \quad \gamma = \cos\phi,$$

(after Bloembergen et al. 1959). Term A can now be seen to consist of the interaction of the z-components of the angular momentum and thus represents the energy of one electron due to the local field formed by other neighbouring electrons. Term B is the energy on interchange of the spins of two electrons (or two adjacent spin flips of opposite sign). Terms C and D are terms where there is a net change of one spin, while terms E and F correspond to a net change of two spins. If higher approximations had been used instead of the dipole interaction, there would also

be terms included for three and more spin flips. Only the first two terms commute with the Hamiltonian for the Zeeman energy and thus only these terms conserve Zeeman energy. This can be understood when one remembers that if the spin system is in isolation, conservation of angular momentum is required of the system and thus terms involving a net change of spin cannot contribute. Van Vleck (1948) has shown that the broadening of the electron magnetic resonance (EMR) line due to spin-spin interaction is approximately Gaussian but, if exchange terms are appreciable, the effect is to narrow the line at halfwidth at the expense of producing broad wings on the shape function.

That the spin system is indeed isolated from its surroundings (in particular, from the host material) is illustrated in relaxation experiments of the type described by Casimir and Du Pré (1938), Kronig and Bouwkamp (1938) and Purcell and Pound (1951). The implications are discussed very thoroughly by Abragam and Proctor (1958) in an article on the interpretation of spin temperature. In a magnetic field, the unpaired electron of a paramagnetic ion loses its Kramer's degeneracy, and the ratio of the number of electrons in each level follows the Boltzmann distribution. The magnetic moments line up with the external field and the magnetization will be a function of temperature given approximately by

$$\hat{M} \approx N \hat{\mu}_e^2 \cdot \hat{H} / 3kT, \quad \dots \dots \dots (3.4)$$

where $\hat{\mu}_e$ is the magnetic moment of the electron and k is

Boltzmann's constant. In fact, when an experiment is performed to measure the magnetization of a dilute paramagnetic salt, it is usually found that considerable time is needed for the magnetization to reach equilibrium after the application of the magnetic field, sometimes of the order of minutes. This is the time needed for the spin system to come into equilibrium with its surroundings and indicates how well isolated it is. Suppose now that the spin system has been allowed to come into equilibrium with its surroundings and that the magnetic field is suddenly lowered to a new value. The magnetization does not change and thus according to eqn. (3.4), the spin temperature must have dropped since the Zeeman energy is now less. For constant \hat{M} , the internal energy of a system is given by the balance equation

$$dU = dQ - \hat{M} \cdot d\hat{H} ,$$

(see, for instance, Kittel 1958 §18) and since the spin system is in isolation from its host ($dQ = 0$), the interaction energy $\hat{M} \cdot d\hat{H}$ must have been taken up into the internal energy of the system. This has been brought about by a re-arrangement of the spins in the system, the net spin-up : spin-down ratio being conserved. Of course, if the field should pass through zero, one can no longer speak of the spin (angular momentum) being conserved. Nevertheless, if the magnetic field is now increased again to its former value the magnetization is found to be the same as before. The entire Zeeman energy can be supplied or taken up by a re-arrangement of the spin system.

The above discussion illustrates a number of points; firstly, it is apparent that there is a rapid interchange of energy between the magnetic interaction (or Zeeman) energy and the internal energy of the spin system, brought about by relaxation of the spin configuration. The time constant for this relaxation is of the order of 10^{-9} sec or less and is known as the "transverse relaxation time". It is the reciprocal of the linewidth measured in an EMR experiment due to interchange and spin-spin interactions. If equilibrium is attained in the entire system on this time scale, changes at any one atomic site must occur at least this fast. Unless one examines the system on time scales typically of the order of 10^{-12} sec no inhomogeneities will be found. We will return to this point later.

3.4. Interactions between the System and the Host Material

Secondly, in order for the spin system to come into equilibrium with its surroundings, there must be interaction, however weak, with the host material. Waller (1932) first investigated this interaction and was able to show that energy could be transferred by means of emission or absorption of phonons, or by scattering of phonons. It is difficult to see how this can be effective in hosts other than highly perfect crystals, and even then it is relatively slow. This was realized by Bloembergen, Purcell and Pound (1948) who had been investigating relaxation effects in liquids. They developed a theory based on Brownian-type motions which could be very effective in transferring energy and angular momentum from the spin system to the host via the

ligand field. This interaction can also be effective in disordered solids.

The time for the spin system to come into equilibrium with the host material is known as the "longitudinal relaxation time". In most solids, it is much longer than the transverse relaxation time and therefore its contribution to the linewidth is negligible (this may not be true in a liquid). Its main effect, along with spin flips and interchanges, is as an interrupting mechanism on the interaction with the radiation field.

3.5. Inhomogeneous Broadening

Suppose that one is studying a dilute paramagnetic ion in a crystalline host, and that there are two non-equivalent sites in which ions may be situated. Alternate sites will differ at least in the separation of sublevels and, if of different symmetry, may also have a different number of sublevels. One will then observe two sets of lines, whether in an EMR experiment or in an experiment involving electronic transitions. Not only this, but any experiment which is done on one set of lines will have no effect on the other set. For all practical purposes there are two different systems and each will exhibit line broadening in the same manner as the systems discussed above. If we now consider the ion to be in a liquid or in a highly disordered solid such as a glass, there will be a very large number of different sites and a very large number of distinct lines, all of them broadened by the abovementioned processes and all overlapping to form one broad line. But each group of ions (however small in number) with the same site will still be a separate system. It will be possible to

perform experiments on this system without disturbing the others. The resonant line of such a system is called an "inhomogeneously broadened line" and we choose to limit the use of the term to the case described above, where one can distinguish systems of non-equivalent ions. The inhomogeneity is entirely on a microscopic scale and is not to be confused with effects due, say, to inhomogeneous applied fields or to gradients in the concentration of impurity ions in the host. In particular, it is not to be confused with spatial inhomogeneities in the inversion population of an excited ion in a laser material in a Fabry-Perot cavity. This periodic variation of the inversion population along the optic axis is brought about by the standing waves of the induced radiation field. We shall refer to such effects as "spatial hole burning" and to any possible diffusion of energy from regions of higher inversion density to regions of lower inversion density as "spatial cross relaxation". This distinction will be amplified in §9.2. In addition, some of the confusion in the literature has arisen from the use of the term "inhomogeneous broadening" to describe the linewidth arising from the exchange and spin-spin interactions. In fact, for times that are short compared to the transverse relaxation rate, the ions appear to be "frozen" in a given configuration and behave as if the linewidth were inhomogeneously broadened in the sense that we use the term. But these times are very short and may be of the order of the oscillation period of the radiation field, in which case there is no possible experiment that can show up this inhomogeneity. If the relaxation time were of the order of 10^{-9} sec, it would presumably be possible to perform an experiment which would measure only the Lorentzian linewidth.

We shall refer to the combined effect of the Lorentzian linewidth and the exchange and spin-spin interactions as the homogeneous linewidth and justify the use later.

It should be clear from what has been said that there is considerable difference in the behaviour between lines that are broadened homogeneously and those broadened inhomogeneously. Consider, for instance, an absorption experiment on an inhomogeneously broadened species. An intense monochromatic source of radiation is allowed to impinge on a sample, and at the same time the absorption as a function of wavelength is measured by using a weak probe beam at right angles to the intense source. The absorption curve will then be observed to have a notch in it at the wavelength of the intense beam. This is due to the fact that the absorbing transition has been saturated; there are fewer ions in the ground state at that wavelength to contribute to absorption of the probe beam. Such an effect is known as "hole-burning". In the case of a species which is homogeneously broadened only, the sole effect observed would be an overall decrease in the entire absorption curve of the material when the intense source is on, as compared to when the source is turned off. This is because any one ion can absorb the monochromatic radiation a certain fraction of time (or, what is equivalent, can absorb sometimes). Thus, the absorption peak is decreased by the fraction of ions which are in the excited state and unable to absorb the probe beam. On the contrary, an inhomogeneously broadened species always has some ions which can never absorb at the intense monochromatic wavelength. It is this fundamental difference which prompts us to choose the definition of inhomogeneous broadening given above. It

is now clear that in order to justify using the term "inhomogeneous broadening" to describe exchange and spin-spin effects, one must be performing the equivalent of the above experiment, but in a time which is short compared with the transverse relaxation time. It is also clear that if the radiation pulses necessary to perform the experiment are so short that their Fourier transforms give linewidths comparable to the linebreadth being measured, then such an experiment has no meaning.

3.6. Cross Relaxation

In fact, it would be difficult to find a substance on which our simple experiment could be successfully performed. It was recognized that separate spin systems do come into equilibrium with one another, and that this time is usually much shorter than the longitudinal relaxation time but longer than the transverse relaxation time (Abragam and Proctor 1958). However, until the fundamental paper of Bloembergen et al. (1959), the mechanism of the energy transfer between the different spin systems remained obscure. In a magnetic resonance experiment involving ions in two dissimilar sites, if there is not too great a difference in their Zeeman energies, then the spin-spin and exchange energy is common to both systems. Bloembergen et al. were able to show that under such conditions Zeeman energy could be transferred from one ion type to another, with the energy balance being maintained by a rearrangement of the spin system. The terms in eqn. (3.3) which are involved are those labelled C, D and E, F. Spin is not conserved, but the angular momentum can be coupled to the host through the ligand fields and angular momentum of the solid as a whole is con-

served. It is clear from the discussion in §3.3 that the spin system has an adequate energy reservoir to supply the energy increment (or decrement). The strength (and hence the rate) of this "cross-relaxation" effect is proportional to the overlap of the shape functions of the two lines. The inhomogeneously broadened line was also discussed by Bloembergen et al., who generalized the above to the case of an infinite number of closely spaced homogeneously broadened lines.

Our interest, however, is in electronic transitions in zero magnetic field. Nevertheless, Nd^{3+} is a paramagnetic ion and exhibits spin-spin and interchange interactions between its unpaired electrons and between any unpaired electrons in the ligands surrounding them. The only difference is that now there is no preferred axis (for the spin system) and the interactions cannot neatly be dissected mathematically into components. One cannot carry the step from eqn. (3.2) to eqn. (3.3). Now, exchange of electronic excitation between the ions in two non-equivalent sites takes place with the balance of the energy being taken up by the spin system. Indeed, it is this sort of process which can be postulated for the rapid cascade of excitation to the metastable state discussed in §2.6. We have previously mentioned that exchange processes had the effect of narrowing the line at the expense of greatly enhancing the wings. This is just the sort of thing that makes for good overlap and hence fast cross relaxation, and it is this which Bloembergen et al. consider to be important. A more recent paper on such energy transport in rare earth ions (Birgenau 1968) indicates that exchange and "super-exchange" (exchange with the orbital parameters considered) effects

have large matrix elements, at least for Nd^{3+} in a crystal lattice. These effects of course decrease quite rapidly with distance between ions, but there is no dependence on symmetry or order and so they can be expected to make comparable contributions in a glass matrix. It is thus entirely possible to have rapid cross relaxation in the inhomogeneously broadened line of Nd^{3+} in glass, but even an order of magnitude estimate of the rate is impossible, and it must be determined experimentally.

§4. LASER RATE EQUATIONS WITH INHOMOGENEOUS BROADENING

4.1. Introduction

All the major mathematical equations which are used in the succeeding sections are grouped together here. Starting with a realistic model of the behaviour of the Nd^{3+} ion which includes inhomogeneous broadening and cross relaxation, the rate equations for a three level approximation are derived. These are subsequently tested for stability in a computer simulation described in §8. A two level approximation is obtained from the three level equations by assuming the lifetime of the terminal level to be infinitely short. Two relations which couple observables with theory are then derived. The first is the relation between the internal and external photon density and the second is the relation between the threshold for laser operation and the lineshape function. The final subsection is devoted to a study of the steady-state equations obtained from the two level approximation. From these come expressions for the shape of the laser output as a function of frequency for the limiting cases of infinite cross relaxation and no cross relaxation. They are then compared with the experimental results in §7.

4.2. Three Level Approximation

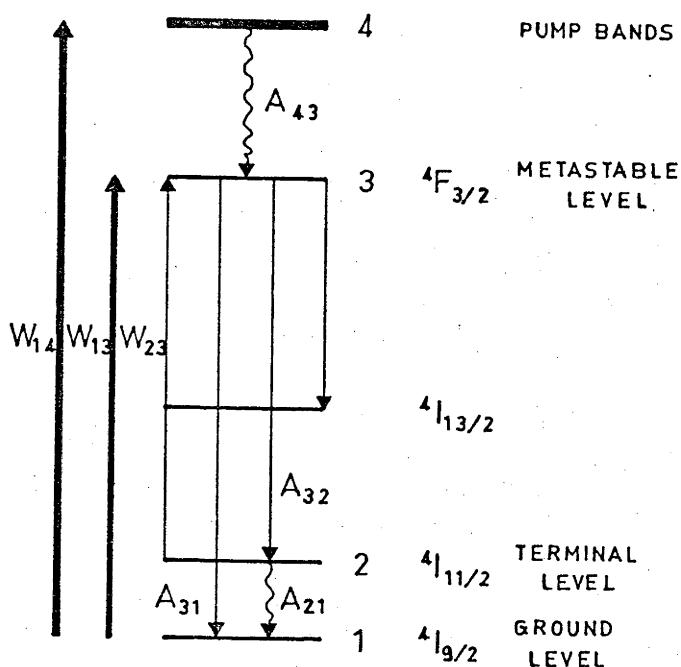
4.2.1. Model Adopted and Basis for Assumptions

The rate equations for the Nd^{3+} glass laser are based on the following model (see fig. 4.2.1):

1. The lifetime of the terminal level is 20 nsec.

This is smaller than the upper limit set by Michon (1966) and agrees with a recent experiment (Dunstan 1970).

Fig. 4.2.1



Energy level diagram of model for three level approximation.

2. All transitions induced by the pump light can be lumped together to give an equivalent pump rate from the ground state to the metastable state.

All pump light at the wavelength of the $1 \rightarrow 2$ transition is absorbed by the glass matrix, and the terminal level (2), because it is 2000 cm^{-1} above the ground state and because of its short lifetime, can be expected to be almost empty. Thus the only pumping from the terminal level to the metastable level that is of any importance is that due to absorption of the laser beam itself.

Since the cascade from the pump bands is extremely rapid compared to the pump rate W_{14} , it is equivalent to pumping the metastable level directly.

3. The ions can be divided into two groups - those which always decay to the ground state by non-radiative transitions, and

those which always decay by radiative transitions.

DeShazer and Komai (1965) indicate that the quantum efficiency of the ${}^4F_{3/2}$ level is about 40%, and of this energy 24% is emitted in the ${}^4F_{3/2} \rightarrow {}^4I_{9/2}$ transition, 16% in the ${}^4F_{3/2} \rightarrow {}^4I_{13/2}$ transition and 60% in the ${}^4F_{3/2} \rightarrow {}^4I_{11/2}$ transition. The assumption that the populations which fluoresce and those which decay non-radiatively are independent is necessary to make the problem tractable and is discussed by Edwards (1966) who concludes that it is probably a reasonable assumption.

4. The levels are homogeneously broadened.
5. There is no splitting of the levels.

This is certainly not a correct assumption. Its effects will be discussed in detail later.

6. A cross-relaxation rate, W_c , is assigned to the metastable level.

A list of the symbols used in the following subsections is given below. Although functional relationships and subscripts are listed in full below, these are only included in the equations where necessary. Symbols which do not conform to the list are defined in the text.

SYMBOLS

N_0	number density of the ions in the active medium which fluoresce
ℓ'	true length of the active medium
L'	true length of the Fabry-Perot cavity
η	index of refraction of host material relative to air, at the lasing wavelength
ℓ	$= \eta \ell'$ equivalent free air optical length of the active medium

- $L = L' + (\eta - 1)\ell'$ equivalent free air optical length of the cavity
- A' cross-sectional area of the active medium
- $V' = A' L$ equivalent free air volume of the cavity
- $V = A' \ell$ equivalent free air volume of the active medium
- $N_m' = N_m'(v, t)$ total number of ions in state m per unit wavenumber
- $N_m = N_m(v, t) = N_m'/V$ number density of ions in state m per unit wavenumber
- $n_m = n_m(v, t) = N_m'/N_0$ normalised number density, equal to the fraction of ions per unit wavenumber in state m
- $N_{ms}' = N_{ms}'(t) = \int_0^{\infty} N_m'(v, t) dv$ number density of ions in state m
- $n_{ms}' = n_{ms}'(t) = \int_0^{\infty} n_m(v, t) dv$ normalised number density of ions in state m
- $P' = P'(v, t)$ total number of photons per unit wavenumber in the cavity
- $\phi = \phi(v, t) = P'/V'$ photon density per unit wavenumber in the cavity
- $\phi = \phi(v, t) = L\phi/\ell N_0$ normalised photon density, equal to the number of photons per ion in the cavity, per unit wavenumber
- $\phi_s = \phi_s(t) = \int_0^{\infty} \phi(v, t) dv$ normalised photon density
- $W_p = W_p(t)$ pump rate, photons per second per ion
- W_c cross-relaxation rate between excited ions in the meta-stable state and ions in the ground state, per second per ion
- A_{nm} spontaneous decay rate from state n to state m
- $B_{nm} = c^3 A_{nm} / 8\pi h \nu^3 n^3$ Einstein coefficient for stimulated emission from state n to state m

$k(\nu)$ absorption coefficient of an absorber, defined in the equation

$$I(\nu, x) = I_0(\nu) \cdot \exp\{-k(\nu)x\}$$

$\alpha'(\nu)$ = $-k(\nu)$ gain coefficient when the medium is amplifying

$\sigma_a(\nu)$ = $k(\nu)/N_m$ absorption cross section per ion

$\sigma(\nu)$ = $\alpha'(\nu)/N_m$ stimulated emission cross section per ion

β a constant which is equal to the fraction of fluorescent photons which contribute to the cavity photon density

$\alpha(\nu, t)$ photon loss rate from the cavity due to all processes

R mirror reflectivity

g_m = $2J + 1$ multiplicity of level m

K = $c\ell N_0/L$ a constant

4.2.2. Relationship between Absorption Coefficient and Stimulated Emission Cross Section

There are basically two ways to obtain the stimulated emission cross section of a laser material - by absorption measurements of the desired transition, or by gain measurements with a known inversion. As will be seen, for four level lasers, they yield different results and the cross section to which one is referring must be specified exactly. For Nd^{3+} in glass, Mauer (1964) made measurements of absorption by heating the glasses sufficiently to populate the terminal level, and Edwards (1966) obtained a value of the stimulated emission directly by measuring beam gain in a carefully controlled experiment. Both methods refer to the Fuchtbauer-Ladenberg formula

$$\int_0^{\infty} k(\nu) d\nu = - \int_0^{\infty} \alpha'(\nu) d\nu = \frac{h\nu_0 \eta}{c} \left(B_{mn} N_m - B_{nm} N_n \right), \quad (4.2.1)$$

where

$$N_m = \int_0^{\infty} N_m(\nu) d\nu.$$

Using the relations

$$g_n B_{nm} = g_m B_{mn}, \quad A_{nm} = \frac{8\pi h \nu^3 \eta^3}{c^3} B_{nm}, \quad \dots \quad (4.2.2)$$

one obtains

$$\int_0^{\infty} k(\nu) d\nu = \kappa \left[N_m - \frac{g_m}{g_n} N_n \right], \quad \dots \quad (4.2.3)$$

where

$$\kappa = \frac{c^2 A_{nm}}{8\pi \eta^2 \nu_0^2} \frac{g_n}{g_m}. \quad \dots \quad (4.2.4)$$

(See, for instance, Lengyel 1966.)

If an absorption measurement is made, there are very few ions in the upper state, i.e., $N_n \ll N_m$, and

$$\int_0^{\infty} k(\nu) d\nu \approx \kappa N_m = N_m \int_0^{\infty} \sigma_a(\nu) d\nu = N_m \overline{\sigma_{na}} \Delta\nu_n,$$

then

$$\overline{\sigma_{na}} = \frac{\kappa}{\Delta\nu_n}, \quad \dots \quad (4.2.5)$$

where $\Delta\nu_n$ is the full width at half maximum of the absorption line,

and $\overline{\sigma}_{na}$ is the mean peak absorption cross section per ion.

On the other hand, if the cross section is determined by gain measurements we have from eqns. (4.2.1) and (4.2.3)

$$\int_0^{\infty} \alpha'(\nu) d\nu = \kappa \left(\frac{g_m}{g_n} N_n - N_m \right). \quad \dots \dots (4.2.6)$$

In this case, the terminal state is almost empty, i.e., $N_m \ll N_n$,

$$\text{and} \quad \int_0^{\infty} \alpha'(\nu) d\nu \approx \kappa \frac{g_m}{g_n} N_n = N_n \int_0^{\infty} \sigma(\nu) d\nu = N_n \overline{\sigma}_n \Delta\nu_n.$$

Thus

$$\overline{\sigma}_n = \frac{\kappa}{\Delta\nu_n} \frac{g_m}{g_n}, \quad \dots \dots \dots (4.2.7)$$

and $\overline{\sigma}_n$, the peak stimulated emission cross section per ion, is related to the peak absorption cross section per ion by

$$\overline{\sigma}_n = \frac{g_m}{g_n} \overline{\sigma}_{na}. \quad \dots \dots \dots (4.2.8)$$

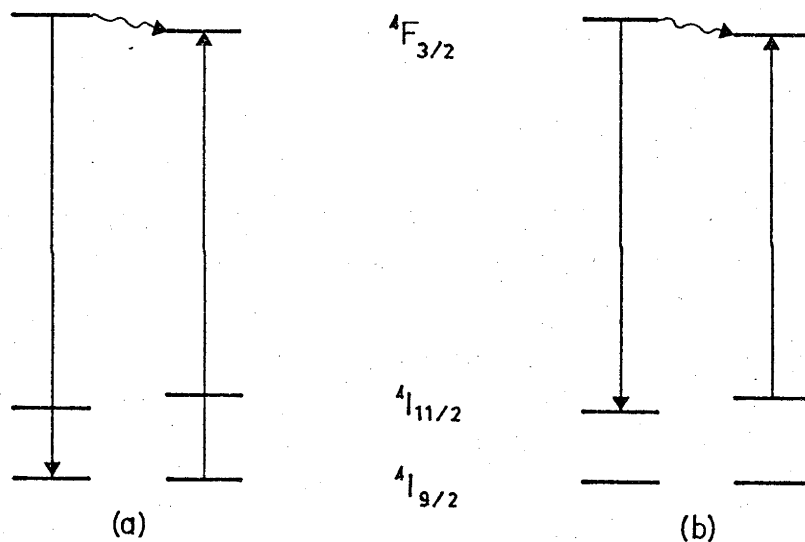
In the case of Nd^{3+} , $g_m/g_n = 3$.

4.2.3. The Cross Relaxation Term in the Rate Equations

Fig. 4.2.2 illustrates the two possible forms of cross relaxation that could occur with our model. In the first case, cross relaxation takes place between an ion in the excited state (which decays then to the ground state) and an ion in the ground state (fig. 4.2.2(a)). The second case, illustrated in

fig. 4.2.2(b), involves the transfer of energy from an ion in the excited state to an ion in the terminal state, the first ion decaying to the terminal state. This latter process will not be considered here because there are always so few ions in the terminal state as to make such transfers highly improbable even with cross relaxation rates the same size as the terminal level decay rate.

Fig. 4.2.2



Energy level diagrams of possible cross relaxation processes.

We assume that any ion in a given ligand field has a preferred emission frequency ν , and that the number density of ions in the host material capable of emitting in a region $d\nu$ about ν is $N_0 g(\nu) d\nu$, where $g(\nu)$ is the normalised lineshape function describ-

ing the inhomogeneously broadened line. Each ion experiences homogeneous broadening and has a stimulated emission differential cross section per ion, $\sigma(\nu, \nu')$, centred on ν with full width at half maximum of $\Delta\nu_n$ such that

$$\int_0^{\infty} \sigma(\nu, \nu') d\nu' = \bar{\sigma} = \overline{\sigma}_n \Delta\nu_n. \quad \dots (4.2.9)$$

Note that the integrated cross section per ion and the peak cross section per ion, etc., are assumed to be the same for any ion no matter what its surroundings, and that the total shape function of the fluorescent line is assumed to be due to the number distribution of the ions as a function of their emitting frequency.

We assume that any excited ion is able to transfer its excitation energy to any ground state ion, with a cross section $\sigma_{cr} = \chi/r^n$, where χ may be some function of the energy defect (but which will be assumed to be a constant), r is the radial distance between ions, and $n \geq 6$ (see Bates 1962, Birgeneau 1968). First consider the influx of ions from the ground state to the excited state which are capable of emitting in a frequency region $d\nu$ about ν . This influx is due to the interaction of excited ions not capable of emitting in this region with ground state ions which, if excited, could emit in the region. The number density of excited ions not capable of emitting in the region $d\nu$ about ν is

$$N_{3S} - N_3(\nu)$$

and the number density in the ground state which, if excited, could emit in the region is

$$N_1(\nu) = N_0g(\nu) - N_2(\nu) - N_3(\nu).$$

The fraction of ground state ions which can interact in a region dr at a distance r from an excited state is $4\pi r^2 dr [N_1(\nu)]$, and the probability density of interaction is

$$4\pi r^2 dr [N_1(\nu)] \sigma_{cr} = \frac{4\pi\chi}{r^{n-2}} [N_0g(\nu) - N_2(\nu) - N_3(\nu)] dr.$$

The probability of interaction of any ground state ion in the whole volume is

$$\begin{aligned} & 4\pi\chi [N_0g(\nu) - N_2(\nu) - N_3(\nu)] \int_0^\infty \frac{dr}{r^{n-2}} \\ & = [N_0g(\nu) - N_2(\nu) - N_3(\nu)] \frac{4\pi\chi}{(n-3)R^{n-3}}, \end{aligned}$$

where R is the nearest neighbour distance. There are $[N_{3S} - N_3(\nu)]$ ions per unit volume which can interact, and thus the influx is

$$[N_{3S} - N_3(\nu)] [N_0g(\nu) - N_2(\nu) - N_3(\nu)] W_c,$$

where

$$W_c = \frac{4\pi\chi}{(n-3)R^{n-3}}$$

is the cross relaxation rate per ion. Similarly, consider the efflux of ions from the excited state to the ground state which are capable of emitting in the region $d\nu$ about ν . This can only happen if excited ions which emit in the region transfer energy to ground state ions which, if excited, would emit outside the region. The number of ground state ions which would emit outside the region is

$$[N_{1s} - N_1(\nu)] = [\{N_0 - N_{2s} - N_{3s}\} - \{N_0g(\nu) - N_2(\nu) - N_3(\nu)\}],$$

and by similar considerations to the above, the efflux is

$$N_3(\nu) [N_{1s} - N_1(\nu)] W_c.$$

The net flow rate is influx minus efflux, or

$$\left(\frac{dN_3(\nu)}{dt} \right)_{\text{cross}} = W_c [N_{3s} \{N_0g(\nu) - N_2(\nu)\} - N_3(\nu) (N_0 - N_{2s})] = N_0 F(\nu).$$

Dividing through by N_0 , one obtains the dimensionless cross relaxation rate

$$\left. \begin{aligned} \left(\frac{dn_3(\nu)}{dt} \right)_{\text{cross}} &= W_c [n_{3s} \{g(\nu) - n_2(\nu)\} - n_3(\nu) (1 - n_{2s})] \\ &= - \left(\frac{dn_1(\nu)}{dt} \right)_{\text{cross}} = F(\nu) \end{aligned} \right\} \quad (4.2.10)$$

That this form is proper can be seen by noting that it fulfils certain very general conditions required of the cross-relaxation term. These are:

1. There can be no cross relaxation when there is no inversion or when there is maximum inversion, i.e., $F(\nu) \equiv 0$ when $n_{3s} = 0$ or $n_{3s} = 1$.
2. Cross relaxation does not change the total inversion but rather exchanges inversion with ions capable of emitting at different frequencies, therefore

$$\int_0^{\infty} F(\nu) d\nu = 0.$$

3. There should be no cross relaxation if the system is in equilibrium and the distribution density of ions in all three states is the same, i.e. if

$$n_3(\nu) = k_3g(\nu), \quad n_2(\nu) = k_2g(\nu),$$

$$n_1(\nu) = k_1g(\nu), \quad k_1 + k_2 + k_3 = 1.$$

4.2.4. The Stimulated Emission Term in the Rate Equations

Let $\Delta P'(\nu)$ be the number of photons in a region $d\nu$ about ν which are produced by stimulated emission in a time Δt . During this time, a photon travels a distance $\Delta l = c\Delta t$. There are on the average $N_3'(\nu')\Delta l d\nu'/V'$ ions per unit area in the volume traversed by a photon in time Δt that can emit in a region $d\nu'$ about ν' , and the differential probability dP that a photon of frequency ν will stimulate emission in one of these ions is

$$dP = p(\nu, \nu') d\nu' = \sigma(\nu, \nu') \frac{N_3'(\nu')}{V'} \Delta l d\nu',$$

and the total probability for all frequencies is

$$P = \frac{\Delta l}{V'} \int_0^\infty \sigma(\nu, \nu') N_3'(\nu') d\nu'.$$

Thus
$$\Delta P'(\nu) = \frac{P'(\nu)}{V'} \Delta l \int_0^\infty \sigma(\nu, \nu') N_3'(\nu') d\nu',$$

or
$$\frac{\Delta P'(\nu)}{\Delta t} = \frac{cP'(\nu)}{V'} \int_0^\infty \sigma(\nu, \nu') N_3'(\nu') d\nu',$$

since $\Delta l = c\Delta t$. Thus

$$\lim_{t \rightarrow 0} \frac{\Delta P'(v)}{\Delta t} = \left(\frac{dP'(v)}{dt} \right)_{\text{stim}} = \frac{c \ell P'(v)}{L} \int_0^{\infty} \sigma(v, v') N_3(v') dv',$$

and normalising

$$\left(\frac{d\phi(v)}{dt} \right)_{\text{stim}} = \frac{c \ell N_0 \phi(v)}{L} \int_0^{\infty} \sigma(v, v') n_3(v') dv'. \quad (4.2.11)$$

Now consider the loss of excited ions $\Delta N'(v)$ in a region dv about v due to stimulated emission. The differential probability that $P'(v)$ photons in the region dv' about v' will stimulate one ion to emit radiation is

$$dP = p(v') dv' = P'(v') \sigma(v, v') dv',$$

or

$$P = \int_0^{\infty} P'(v') \sigma(v, v') dv',$$

and there are $N_3'(v) \Delta \ell / V' = N_3'(v) c \Delta t / V'$ excited ions per unit area in the volume traversed by a photon in time Δt . Thus

$$\lim_{t \rightarrow 0} \frac{\Delta N_3'(v)}{\Delta t} = \left(\frac{dN_3'(v)}{dt} \right)_{\text{stim}} = - \frac{c N_3'(v)}{V'} \int_0^{\infty} P'(v') \sigma(v, v') dv',$$

or

$$\left(\frac{dn_3(v)}{dt} \right)_{\text{stim}} = -n_3(v) \frac{c \ell N_0}{L} \int_0^{\infty} \phi(v') \sigma(v, v') dv' = - \left(\frac{dn_2(v)}{dt} \right)_{\text{stim}} \quad (4.2.12)$$

To these terms are added expressions for the pump rate and the fluorescent losses to obtain the following equations:

$$\begin{aligned} \frac{dn_3}{dt} = & W_p [g - n_2 - n_3] + W_c [n_{3S}(g - n_2) - n_3(1 - n_{2S})] \\ & - K \left[n_3 - \frac{n_2}{3} \right] \int_0^\infty \phi(v') \sigma(v, v') dv' - A_3 n_3, \end{aligned} \quad (4.2.13)$$

$$\frac{dn_2}{dt} = K \left[n_3 - \frac{n_2}{3} \right] \int_0^\infty \phi(v') \sigma(v, v') dv' + A_{32} n_3 - A_2 n_2, \quad (4.2.14)$$

$$\frac{d\phi}{dt} = K\phi \int_0^\infty \sigma(v, v') \left[n_3(v') - \frac{n_2(v')}{3} \right] dv' + \beta n_3 - \alpha\phi. \quad (4.2.15)$$

Terms have been added to correct for absorption of cavity photons by the terminal level, derived in a manner similar to the emission term but with the cross section corrected for the multiplicities of the two levels. A_3 is the measured decay rate from level 3 and contains contributions to all levels, while A_{32} is the decay rate to level 2 only. The expression for the pump rate is simply the product of the pump rate per ion W_p and the number density of ions in the ground state which, if excited, would emit in a region dv about v .

4.2.5. Two Level Approximation

The two level approximation is obtained by assuming that $A_2 \rightarrow \infty$ and hence $n_2 \rightarrow 0$. Thus, from eqns. (4.2.13) and 4.2.15), one obtains

$$\frac{dn_3}{dt} = W_p [g - n_3] + W_c [gn_{3S} - n_3] - Kn_3 \int_0^\infty \sigma(v, v') \phi(v') dv' - A_3 n_3, \quad (4.2.16)$$

$$\frac{d\phi}{dt} = K\phi \int_0^{\infty} \sigma(v, v') n_3(v') dv' + \beta n_3 - \alpha\phi. \quad (4.2.17)$$

These equations are formally identical to those obtained by Peressini and Linford (1968).

4.2.6. Relationship between Internal and External Photon Flux Density

On the average, half of the P' photons in the cavity are travelling in each direction. Thus, if one of the end mirrors were suddenly removed, P'/A' photons per unit area would be seen for $2L/c$ seconds, a flux of

$$\frac{P' c}{2A' L} = \frac{c\Phi}{2} = \frac{c\ell N_0}{2L} \phi.$$

The cavity flux density, Ψ' , is twice this because there are photons travelling in both directions. Thus

$$\Psi' = c\Phi = \frac{c\ell N_0}{L} \phi.$$

If one of the mirrors is partially transmitting, with transmission $(1 - R)$, then the external flux density, Ψ , is

$$\Psi = \frac{c(1 - R)}{2} \Phi = \frac{c\ell N_0 (1 - R)}{2L} \phi. \quad \dots (4.2.18)$$

If the only cavity loss is the mirror, then the cavity loss rate is related to the reflectivity by

$$\alpha = \frac{c(1 - R)}{2L}, \quad \dots \dots \dots (4.2.19)$$

as can be seen by noting that each photon is incident upon the exit mirror $c/2L$ times per second. Thus

$$-\Delta P' = P' \frac{c}{2L} (1 - R) \Delta t,$$

or
$$\frac{dP'}{dt} = -\frac{c(1 - R)}{2L} P' = -\alpha P'.$$

4.2.7. Threshold

We wish to relate the threshold condition to the line-shape function, $g(\nu)$. Referring to the integral equation from which eqn. (4.2.7) is derived, we note that for an inhomogeneously broadened line

$$\alpha'(\nu) = N(\nu) \int_0^{\infty} \sigma(\nu, \nu') d\nu' = N(\nu) \overline{\sigma_n \Delta \nu_n}.$$

At threshold, the gain per pass just equals the losses in the cavity (assumed here to be due entirely to the output mirror) and the number density of excited ions will be in equilibrium, i.e. $N(\nu) = N_s g(\nu) = N_0 n_s^{\infty} g(\nu)$. If the pump rate is less than the threshold value, then the inversion population reaches an equilibrium level such that the fluorescent loss rate is just equal to the pump rate, i.e.,

$$W_{pt}(1 - n_s^{\infty}) = A n_s^{\infty}, \quad \text{or} \quad n_s^{\infty} = \frac{W_{pt}}{W_{pt} + A}.$$

Thus
$$\alpha'(\nu) = \frac{\ell n R}{2\ell} = N_0 n_s^\infty g(\nu) \overline{\sigma_n \Delta \nu_n} = N_0 g(\nu) \overline{\sigma_n \Delta \nu_n} \left(\frac{W_{pt}}{W_{pt} + A} \right),$$

or
$$g(\nu) = \frac{\ell n R}{2\ell N_0 \overline{\sigma_n \Delta \nu_n}} \left(1 + \frac{A}{W_{pt}} \right), \quad \dots \dots (4.2.20)$$

i.e.,
$$g(\nu) \propto \frac{1}{W_{pt}},$$

where W_{pt} is the pump rate at threshold. This equation is meaningful only if the laser is oscillating at a single frequency at threshold. If the laser can be forced to oscillate at a single frequency and tuned over the fluorescent linewidth, then the line-shape function $g(\nu)$ can be obtained from the threshold as a function of frequency.

4.3. Equilibrium Equations

4.3.1. Introduction

We now consider the case where the pump rate, the populations of the ionic energy levels and the photon density can be assumed constant. These equations were first considered by Peressini and Linford (1968), who used them in a discussion of the spectral properties of inhomogeneously broadened lasers exhibiting fast cross relaxation. The solution of these equations gives a description of the steady state spectral output of the laser, and a question arises concerning their validity in the description of a spiking laser. The ions excited to the metastable state can only decay by fluorescence or through stimulated emission and any conservation equations which include both terms will be correct when averaged over the duration of the pumping pulse. In a laser

which is operating well above threshold, the stimulated emission exceeds the fluorescence by several orders of magnitude and thus the equations should also be approximately correct for the energy output due to stimulated emission, even though spiking is taking place and causes gross changes in the rate of stimulated emission over a short time scale. The accuracy of the description of the spectral character of the output is a different problem. It should be clear that if cross relaxation is the same order of magnitude as the spike period, or is slow compared to the pump pulse duration, then the equations will not correctly describe the spectral shape of the output.

In what follows, we re-derive the basic equations {(4.3.3), (4.3.4), (4.3.6), (4.3.7), (4.3.9)} of Peressini and Linford with the exceptions that no assumption is made on the magnitude of the cross relaxation, and fluorescent losses are included. From eqns. (4.2.16) and (4.2.17) one obtains the following equilibrium equations:

$$\frac{dn}{dt} = 0 = W_p (g - n) + W_c (gn_s - n) - n \left[K \int_0^\infty \sigma \phi dv' + A \right], \quad (4.4.1)$$

$$\frac{d\phi}{dt} = 0 = \phi \left[K \int_0^\infty \sigma n dv' - \alpha \right] + \beta n. \quad (4.3.2)$$

We integrate over all v to get

$$W_p (1 - n_s) - An_s = K \int_0^\infty n(v) \int_0^\infty \phi(v') \sigma(v, v') dv' dv, \quad (4.3.3)$$

$$\int_0^\infty \alpha(v) \phi(v) dv - \int_0^\infty \beta n(v) dv = K \int_0^\infty \phi(v) \int_0^\infty n(v') \sigma(v, v') dv' dv. \quad (4.3.4)$$

The limits of integration may be interchanged, and equating (4.3.3) and (4.3.4), one obtains the fundamental conservation equation

$$\int_0^{\infty} \alpha \phi dv - \int_0^{\infty} \beta ndv = W_p (1 - n_s) - An_s. \quad \dots (4.3.5)$$

4.3.2. Single Frequency Operation

Our interest is in the case where the laser is constrained to oscillate in only a few modes such that the oscillation linewidth $\Delta\nu_0 \ll \Delta\nu_n$, the homogeneous linewidth. In the steady state case, the term containing β can be ignored since it is very small compared to the total flux ϕ_s , and only has an appreciable effect as a noise source at the onset of the oscillations in a given mode. Thus, for $\phi(\nu) = \phi_s \delta(\nu - \nu_a)$, (4.3.5) becomes

$$\phi_s = \frac{W_p (1 - n_s) - An_s}{\alpha}. \quad \dots (4.3.6)$$

In addition, for $\phi(\nu) > 0$, from (4.3.2)

$$\int_0^{\infty} n(\nu') \sigma(\nu, \nu') d\nu' = \alpha/K,$$

or

$$\int_0^{\infty} n(\nu') \sigma(\nu_a, \nu') d\nu' = \alpha/K. \quad \dots (4.3.7)$$

Solving eqn. (4.3.1) and using eqn. (4.3.6) and the relation

$$\int_0^{\infty} \phi(\nu') \sigma(\nu, \nu') d\nu' = \phi_s \sigma(\nu, \nu_a),$$

we obtain

$$n(\nu) = \frac{\gamma g(\nu)}{1 + \epsilon \sigma(\nu, \nu_a)}, \quad \text{where } \zeta = W_p + W_c + A,$$

$$\gamma = \frac{W_p + W_c n_s}{\zeta}, \quad \epsilon = \frac{W_p (1 - n_s) - A n_s \cdot K}{\zeta \cdot \alpha} = \frac{\phi_s}{\zeta} K. \quad (4.3.8)$$

When the cross relaxation is infinite, the value of n_s can be found by noting that the distribution of excited states is always in equilibrium, i.e. $n(\nu) = n_s^\infty g(\nu)$. Applying this to eqn. (4.3.7),

$$\frac{\alpha}{g(\nu_a) K n_s^\infty} = \int_0^\infty \sigma(\nu_a, \nu) d\nu = \bar{\sigma} = \bar{\sigma}_n \Delta \nu_n,$$

i.e.
$$n_s^\infty = \frac{\alpha}{K g(\nu_a) \bar{\sigma}} \dots \dots \dots (4.3.9)$$

One can relate the total inversion, n_s , for a given cross relaxation to n_s^∞ , by inserting eqn. (4.3.8) into eqn. (4.3.7). Thus,

$$\gamma \int_0^\infty \frac{g(\nu_a) \sigma(\nu_a, \nu)}{1 + \epsilon \sigma(\nu_a, \nu)} d\nu = \frac{\alpha}{K} \dots \dots \dots (4.3.10)$$

It will now be assumed that $g(\nu)$ is a normalized Gaussian centred about ν_0 with full width at half maximum $\Delta \nu_d$,

$$g(\nu) = \left(\frac{4 \ln 2}{\pi} \right)^{1/2} \cdot \frac{1}{\Delta \nu_d} \exp \left\{ -4 \ln 2 \left[\frac{\nu - \nu_0}{\Delta \nu_d} \right]^2 \right\},$$

and that $\sigma(\nu, \nu')$ is a Gaussian with peak σ_n and width $\Delta \nu_n$ at half maximum

$$\sigma(\nu, \nu') = \sigma_n \exp \left\{ -4 \ln 2 \left[\frac{\nu - \nu'}{\Delta \nu_n} \right]^2 \right\},$$

$$\int_0^{\infty} \sigma(v, v') dv' = \Delta v_n \sigma_n \left(\frac{\pi}{4 \ln 2} \right)^{1/2}.$$

We set $\int_0^{\infty} = \int_{-\infty}^{\infty}$ since the functions are nearly zero except for a small region in the positive half of the plane. $g(v)$ and $\sigma(v, v')$ have the forms

$$g(v) = \frac{\beta}{\Delta} \exp \left[-\frac{\beta^2}{\Delta^2} (v - v_0)^2 \right],$$

$$\sigma(v, v') = \sigma_n \exp \left[-\frac{\beta^2}{\delta^2} (v - v')^2 \right],$$

Thus eqn. (4.3.10) becomes, on setting $x^2 = \frac{\beta^2}{\delta^2} (v - v_a)^2$,

$$I = \int_{-\infty}^{\infty} \frac{e^{-\theta^2(x-a)^2} e^{-x^2}}{1 + \sigma_n \epsilon e^{-x^2}} dx = \frac{\alpha \sqrt{\pi}}{\gamma \theta \sigma_n K}, \quad (4.3.11)$$

where $\theta = \frac{\delta}{\Delta}$, $a = \frac{\beta}{\delta} (v_0 - v_a)$.

4.3.3. Case I: $\sigma_n \epsilon < 1$

The requirement $\sigma_n \epsilon < 1$ corresponds to the case of little hole burning. This can be seen from eqn. (4.3.8) where the term $\epsilon \sigma(v, v')$ perturbs $n(v)$ from the equilibrium shape $g(v)$. The condition is met at threshold, where $W_p (1 - n_s) \approx A n_s$, or if the cross relaxation rate $W_p \approx 5 \times 10^4$, or greater, based on typical values of parameters for Nd^{3+} in glass and a pump rate of 100 sec^{-1} . With this condition, the term in θ in eqn. (4.3.11) is seen to be very slowly varying compared to the term involving $\sigma_n \epsilon$. We expand the term in θ {eqn. (4.3.11)} about $x = 0$

$$e^{-\theta^2(x-a)^2} = e^{-\theta^2 a^2} [1 + 2\theta^2 ax + \dots], \quad (4.3.12)$$

and approximate the expansion to zero order since $e^{-x^2} \approx 0$ for $x \neq 0$.

$$I \approx e^{-\theta^2 a^2} \int_{-\infty}^{\infty} \frac{e^{-x^2}}{1 + \phi e^{-x^2}} dx,$$

where

$$\phi = \sigma_n \epsilon.$$

Let $x^2 = -\ln y$. Then I becomes

$$I = e^{-\theta^2 a^2} \int_0^1 \frac{dy}{\sqrt{\ln(1/y)} (1 + \phi y)}.$$

Using eqn. 17, p.551 of Gradshteyn and Ryzhik (1965),

$$\int_0^1 [\ln(1/x)]^{p-1} \frac{x^{q-1} dx}{1 - ax^q} = \frac{1}{aq^p} \Gamma(p) \sum_{k=1}^{\infty} \frac{a^k}{k^p},$$

$$[p > 0, q > 0, |a| < 1],$$

one obtains

$$I \doteq \sqrt{\pi} e^{-\theta^2 a^2} \left(1 - \frac{\phi}{\sqrt{2}} + \frac{\phi^2}{\sqrt{3}} - \dots \right),$$

or

$$\frac{\alpha \sqrt{\pi}}{\gamma \theta \sigma_n K} \doteq \sqrt{\pi} e^{-\theta^2 a^2} \left(1 - \frac{\sigma_n \epsilon}{\sqrt{2}} \right)$$

to first order in $\sigma_n \epsilon$. We note that

$$\frac{\beta e^{-\theta^2 a^2}}{\sqrt{\pi} \Delta} = g(v), \quad \bar{\sigma} = \frac{\sigma_n \delta \sqrt{\pi}}{\beta}.$$

Thus

$$\frac{\alpha}{\gamma K \bar{\sigma} g(v_a)} = \frac{n_s^\infty}{\gamma} = \left(1 - \frac{\sigma n \epsilon}{\sqrt{2}} \right),$$

or

$$n_s^\infty = \frac{W_p + W_c n_s}{\zeta} \left(1 - \frac{W_p (1 - n_s) - A n_s \cdot \frac{K \sigma n}{\sqrt{2} \alpha}}{\zeta} \right)$$

$$= \frac{W_p + W_c n_s}{\zeta} \left\{ 1 - \frac{W_p (1 - n_s^\infty) - A n_s \left(\frac{2 \ell n 2}{\pi} \right)^{1/2} \cdot \frac{1}{g(v_a) n_s^\infty \Delta v_n}}{\zeta} \right\}$$

$$= \frac{W_p + W_c n_s}{\zeta} \left(1 - \frac{W_p (1 - n_s) - A n_s}{\zeta \rho n_s^\infty} \right)$$

where

$$\rho = \left(\frac{\pi}{2 \ell n 2} \right)^{1/2} g(v_a) \Delta v_n.$$

(4.3.13)

The form of this expansion will remain the same even if $g(v)$ and $\sigma(v, v')$ are not Gaussian in shape, although the expression for ρ will be dependent upon them.

This relationship is now used to provide a value for the cavity flux density in terms of the fundamental constants of the system. Using eqn. (4.3.6) to give ϕ_s in terms of n_s , after some manipulation, one obtains

$$\left(\frac{\alpha \phi_s}{\zeta} \right)^2 - \frac{\alpha \phi_s}{\zeta} \left(\rho n_s^\infty + \frac{W_p}{W_c} \right) + \left(W_p (1 - n_s^\infty) - A n_s^\infty \right) \frac{\rho n_s^\infty}{W_c} = 0.$$

Now $\frac{\alpha \phi_s}{\zeta} < 10^{-2}$, so we linearize to get

$$\left. \begin{aligned} \frac{\phi_s}{\phi_s^\infty} &= \frac{\zeta}{W_c} \cdot \frac{1}{1 + \frac{W_p}{\rho W_c n_s^\infty}}, \\ \phi_s &= \frac{W_p (1 - n_s^\infty) - A n_s^\infty}{\alpha}. \end{aligned} \right\} \dots (4.3.14)$$

where

$$\text{Also } \left. \frac{d\phi_S}{dW_p} = \phi'_S = \left[\frac{1 - n_S^\infty}{\alpha} \right] \left[\frac{1}{W_c \theta} \right] \left\{ \left[W_p - \frac{\alpha A n_S^\infty}{1 - n_S^\infty} \right] \left[1 - \frac{\zeta}{\rho W_c n_S^\infty \theta} \right] + \zeta \right\}, \right\}$$

where $\theta = 1 + \frac{W_p}{\rho W_c n_S^\infty}$,

(4.3.15)

and $\lim_{W_c \rightarrow \infty} \phi'_S = \frac{1 - n_S^\infty}{\alpha}$ (4.3.16)

Now, the slope efficiency $dE_{\text{out}}/dE_{\text{in}}$ is proportional to ϕ'_S , and using eqn. (4.2.18) for the external flux density, and eqns. (4.2.19) and (4.3.9), one obtains

$$\frac{dE_{\text{out}}}{dE_{\text{in}}} = N_0 V \{1 - n_S^\infty\} = N_0 V \left[1 - \frac{\alpha}{K g(\nu) \bar{\sigma}} \right]. \quad (4.3.17)$$

Thus, for fast cross relaxation, the slope efficiency is independent of the pump rate W_p and is only weakly dependent on the oscillation frequency over the central portion of the fluorescent linewidth. (See §7.4.)

4.3.4. Case II: $\sigma_n \epsilon > 1$

This condition corresponds to deep hole burning into the equilibrium distribution of the inversion density, and can be expected to occur with moderate pumping rates and slow cross relaxation.

We write the integral of eqn. (4.3.11)

$$I = \frac{\alpha \sqrt{\pi}}{\gamma \theta \sigma_n K} = \int_{-\infty}^{\infty} \frac{dx}{(\sigma_n \epsilon + e^{x^2}) e^{\theta^2 (x - a)^2}} = \int_{-\infty}^{\infty} \frac{dx}{D_1 D_2}$$

and expand e^{x^2} and $e^{\theta^2 (x - a)^2}$ about $x = 0$ to second order,

$$e^{\theta^2(x-a)^2} = e^{\theta^2 a^2} [1 - 2\theta^2 ax + \theta^2(1 + 2\theta^2 a^2)x^2],$$

$$\phi + e^{x^2} = [1 + \phi + x^2], \quad \text{where } \phi = \sigma_n \epsilon.$$

Then the denominator is separated into two fractions

$$\int_{-\infty}^{\infty} \frac{dx}{D_1 D_2} = \int_{-\infty}^{\infty} \left(\frac{ax + b}{1 + fx + gx^2} \right) + \frac{cx + d}{k + x^2} dx,$$

where $f = -2\theta^2 a$, $g = \theta^2(1 + 2\theta^2 a^2)$, $k = 1 + \phi$.

The solutions to the equations are

$$a = \frac{fg}{\xi}, \quad b = \frac{\xi - \eta}{k\xi}, \quad c = \frac{f}{\xi}, \quad d = \frac{\eta}{\xi},$$

where $\eta = 1 - gk$, $\xi = fk + \eta^2$.

The following integrals can be obtained from any standard table:

$$\int_{-\infty}^{\infty} \frac{dx}{ax^2 + 2bx + c} = \frac{\pi}{\sqrt{ac - b^2}}, \quad [ac > b^2],$$

$$\int_{-\infty}^{\infty} \frac{xdx}{ax^2 + 2bx + c} = \frac{b}{a} \frac{\pi}{\sqrt{ac - b^2}}, \quad [ac > b^2].$$

Thus

$$I = \pi e^{-\theta^2 a^2} \left\{ \frac{1}{\theta \sqrt{1 + \theta^2 a^2}} \left(\frac{\xi - \eta}{k\xi} + \frac{a}{1 + 2\theta^2 a^2} \cdot \frac{fg}{\xi} \right) + \frac{1}{\sqrt{1 + \phi}} \cdot \frac{\eta}{\xi} \right\}$$

to second order in both terms. Since $\theta \ll 1$, $a \approx 1$,

$$\eta = 1 - \theta^2(1 + 2\theta^2 a^2)(1 + \phi)$$

$$\approx 1 - \theta^2(1 + \phi) + \text{terms of order 4 and higher in } a \text{ and } \theta.$$

$$\xi = 4\theta^4 a^2(1 + \phi) + [1 - \theta^2(1 + 2\theta^2 a^2)(1 + \phi)]^2$$

$$\approx [1 - \theta^2(1 + \phi)]^2 = \eta^2 + \text{terms of order 6 and higher.}$$

Thus

$$I = \pi e^{-\theta^2 a^2} \left\{ \frac{1}{\theta \sqrt{1 + \theta^2 a^2}} \left[\frac{1}{1 + \phi} \left[1 - \frac{1}{1 - \theta^2(1 + \phi)} \right] + \frac{2\theta^4 a^2}{[1 - \theta^2(1 + \phi)]^2} \right] + \frac{1}{\sqrt{1 + \phi}} \cdot \frac{1}{1 - \theta^2(1 + \phi)} \right\}$$

$$\approx \frac{\pi e^{-\theta^2 a^2}}{1 - \theta^2(1 + \phi)} \left(\frac{1}{\sqrt{1 + \phi}} - \theta \right) \text{ to second order in } \theta,$$

$$= \frac{\pi e^{-\theta^2 a^2}}{[1 + \theta \sqrt{1 + \phi}] \sqrt{1 + \phi}} = \frac{\alpha \sqrt{\pi}}{\gamma \theta \sigma_n K}$$

i.e.

$$\frac{1}{[1 + \theta \sqrt{1 + \phi}] \sqrt{1 + \phi}} = \frac{\alpha e^{\theta^2 a^2}}{\sqrt{\pi} \gamma \theta \sigma_n K} = \frac{n_s^\infty}{\sqrt{\pi} \gamma}$$

Let

$$m = n_s^\infty / \sqrt{\pi} \gamma, \quad k = 1 + \phi.$$

Thus

$$1/m^2 = (1 + \theta^2 k + 2\theta \sqrt{k}) k.$$

We wish a solution of k in terms of θ and m . If the cross relaxation rate is assumed to be zero, then $\gamma = W_p / (W_p + A) \approx 10^{-2}$ [eqn. (4.3.8)], and $\phi \approx 10$, $m \approx 1/2$. If the fluorescent linewidth is assumed to be 150 \AA and the homogeneous linewidth 10 \AA , then $\theta \approx 1/16$. Re-arranging terms in the above equation

$$\left(\frac{1}{km^2} - (1 + \theta^2 k) \right)^2 = \frac{1}{k^2 m^4} + 1 + 2\theta^2 k + \theta^4 k^2 - \frac{2(1 + \theta^2 k)}{km^2} = 4\theta^2 k,$$

or
$$(km^2 - 1)^2 + (1 - k\theta^2)^2 k^2 m^4 = k^2 m^4 \left(1 + \frac{2\theta^2}{m^2} \right).$$

Let
$$f(k) = (km^2 - 1)^2 + (1 - k\theta^2)^2 k^2 m^4 - k^2 m^4 \left(1 + \frac{2\theta^2}{m^2} \right)$$

$$= 1 - 2km^2 + k^2 m^2 (m^2 - 2\theta^2) - 2k^3 m^4 \theta^2 + k^4 m^4 \theta^4 = 0$$

be the solution. Since $k > 1$ and $\theta < m < 1$, a first approximation is $k = 1/m^2$. A better approximation (to second order) can be obtained by the Newton-Raphson method, using

$$k_1 = k_0 + \frac{f(k_0)}{f'(k_0)}.$$

$$\frac{f(k)}{f'(k)} = \frac{1 - 2km^2 + k^2 m^2 (m^2 - 2\theta^2) - 2k^3 m^4 \theta^2 + k^4 m^4 \theta^4}{-2m^2 + 2km^2 (m^2 - 2\theta^2) - 6k^2 m^4 \theta^2 + 4k^3 m^4 \theta^4},$$

and
$$k_1 = \frac{1}{m^2} + \frac{1}{2m^2} \frac{\theta^4 - 4\theta^2 m^2}{2\theta^4 - 5\theta^2 m^2} = \frac{1}{2m^2} \frac{5\theta^2 - 14m^2}{2\theta^2 - 5m^2}$$

$$\approx \frac{1.4}{m^2} \left(1 + \frac{3}{70} \frac{\theta^2}{m^2} \right) \text{ to second order in } \theta.$$

i.e.,
$$1 + \sigma_n \varepsilon = \frac{1.4\pi\gamma^2}{n_s^{\infty 2}} \left(1 + \frac{3}{70} \frac{\theta^2 \pi \gamma^2}{n_s^{\infty 2}} \right), \quad \dots (4.3.18)$$

or using eqn. (4.3.8),

$$1 + \frac{\sigma_n \phi_s K}{\zeta} = \frac{1.4 \pi}{\zeta^2 n_s^{\infty 2}} \left(W_p + \frac{W_c (W_p - \alpha \phi_s)}{W_p + A} \right)^2$$

$$\left\{ 1 + \frac{3\pi}{70} \left(\frac{\theta}{n_s^{\infty}} \right)^2 \left(W_p + \frac{W_c (W_p - \alpha \phi_s)}{W_p + A} \right)^2 \right\}.$$

This is multiplied out and separated into powers of $\frac{\alpha\phi_s}{\zeta} < 10^{-2}$ to second order, to yield

$$\begin{aligned} & \frac{1.4\pi}{(n_s^\infty)^2} \left(\frac{W_p}{W_p + A} \right)^2 \left\{ \left(\frac{W_c}{W_p} \right)^2 \left(1 + \frac{6\pi}{70} \left[\frac{\theta W_p}{n_s^\infty (W_p + A)} \right]^2 \right) \right. \\ & \quad \left. + \frac{12\pi}{70} \left(\frac{\theta W_c}{n_s^\infty (W_p + A)} \right)^2 \right\} \left(\frac{\alpha\phi_s}{\zeta} \right)^2 \\ & + \left\{ \frac{2.8\pi}{(n_s^\infty)^2} \left(\frac{W_p}{W_p + A} \right)^2 \left(\frac{W_c}{W_p} \right) \left(1 + \frac{6\pi}{70} \left[\frac{\theta W_p}{n_s^\infty (W_p + A)} \right]^2 \right) - \frac{K\sigma_n}{\alpha} \right\} \left(\frac{\alpha\phi_s}{\zeta} \right) \\ & + \left\{ \frac{1.4\pi}{(n_s^\infty)^2} \left(\frac{W_p}{W_p + A} \right)^2 \left(1 + \frac{3\pi}{70} \left[\frac{\theta W_p}{n_s^\infty (W_p + A)} \right]^2 \right) - 1 \right\} = 0, \end{aligned}$$

and linearizing, one obtains

$$\phi_s^0 = \lim_{W_c \rightarrow 0} \phi_s = \frac{W_p + A}{K\sigma_n} \left\{ \frac{1.4\pi}{(n_s^\infty)^2} \left(\frac{W_p}{W_p + A} \right)^2 \left(1 + \frac{3\pi}{70} \left(\frac{\theta}{n_s^\infty} \right)^2 \left(\frac{W_p}{W_p + A} \right)^2 \right) - 1 \right\},$$

$$\begin{aligned} \text{and } \frac{d\phi_s^0}{dW_p} = \phi_s^{0'} &= \frac{1}{K\sigma_n} \left\{ \frac{1.4\pi}{(n_s^\infty)^2} \left(1 - \left(\frac{A}{W_p + A} \right)^2 \right) \right. \\ & \quad \left. \left(1 + \frac{3\pi}{70} \left(\frac{\theta}{n_s^\infty} \right)^2 \left(\frac{W_p + 4A}{W_p + 2A} \right) \left(\frac{W_p}{W_p + A} \right)^2 \right) - \frac{W_p}{W_p} \right\}. \end{aligned} \quad (4.3.19)$$

The first term in eqn. (4.3.19) is large compared with W_p and to second order in n_s^∞ , $\phi_s^{0'} \propto 1/(n_s^\infty)^2$. Using eqns. (4.2.18), (4.2.19) and (4.3.9)

$$\frac{dE_{\text{out}}}{dE_{\text{in}}} \approx \frac{N_0 V \alpha}{K\sigma_n} \cdot \frac{1.4\pi}{(n_s^\infty)^2} = \frac{1.4\pi N_0 V K\sigma_n}{\alpha} \cdot \{g(v) \Delta v_n\}^2. \quad (4.3.20)$$

Thus, when the cross relaxation rate is slow, the slope efficiency is proportional to the square of the lineshape function $g(\nu)$.

(See §7.4.)

§5. EXPERIMENTAL ARRANGEMENT

5.1. Introduction

This section describes the major pieces of equipment used in the experiments, their calibration and, in some cases, their design and construction. §5.2 is concerned with the design of the laser pumping head, while §5.3 deals with the energy storage bank and power supply used to drive the flashlamps. §5.4 describes the design and construction of the 5 m spectrograph, while §5.5 details the calibration and use of the energy and peak power monitors. The construction of the optical bench is briefly outlined in §5.6 and some details of the streak camera are discussed in §5.7.

5.2. Laser Head

5.2.1. Choice of Laser Rods

As the percentage of Nd_2O_3 in the glass is increased above 1% by weight, there is a corresponding reduction in the measured fluorescent lifetime due to concentration quenching. Thus, a trade-off between ion density (which determines gain, energy storage density, and pump light absorption efficiency) and fluorescent lifetime is required. Commercially available material ranges between 1% and 5%, and a choice of 3% seems a reasonable compromise. Rods were chosen doped with 3% by weight of Nd_2O_3 in a silicate-based glass 6 1/2 in. long by 1/4 in. diameter with ends polished flat and parallel and anti-reflection coated. High energy output is not necessary in a study of the spectrographic properties of the Nd^{3+} ion and experience has shown that rods of this size can give a Q-spoiled pulse of several tenths of a joule. The rod length is such

as to give satisfactory gain with a 75% reflectivity output mirror, and the cross section is sufficient to keep energy densities below the level where internal damage is a problem when Q-spoiling is attempted. The anti-reflection coatings are necessary to avoid complications of yet another resonant cavity and possible self-oscillation. They are gradually damaged by Q-spoiling, but are preferable to the alternative of Brewster angle ends because then a resonant cavity with offset mirrors is required, and this is difficult to align. Kodak ND-11 glass was chosen for the original rods, but when experimental results appeared to be at variance with some of the published data using other glasses, a Schott LG-56 glass rod was purchased for comparison. A summary of the relevant properties, as provided by the manufacturers, is given below in table 5.1.

5.2.2. Pumplight Cavity and Flashlamps

Ideally, one wishes to obtain uniform inversion throughout the entire laser rod. Uniformity can be approached by using helical or coaxial flashlamps surrounded by a diffuse reflector and by choosing the laser rod dimensions and doping so that it is optically thin at the pumping wavelengths, thus avoiding gross radial inhomogeneities. There is another important reason for avoiding uneven pumping; the low thermal conductivity of glass can cause temperature gradients and severe thermal distortion if the pump energy distribution is uneven, resulting in rupture of the rod or, at least, undesirable optical distortion (thermal lens formation). Unfortunately, no source could be found to supply helical

Table 5.1. Optical and Physical Properties of Two Laser Glasses

Type	ND-11	LG-56
Basic Glass	Silicate	Silicate
Doping	3% by weight of Nd ₂ O ₃	3% by weight of Nd ₂ O ₃
Emission Wavelength	1.06 ± 0.01 μm	1.06 μm
Fluorescent Linewidth	0.03 μm	Not supplied
Fluorescent Time Constant	360 μsec	650 μsec
Refractive Index n _d	1.592	1.5199
Density	3.09 g/cm ³	2.69 g/cm ³
Young's Modulus	10.65 × 10 ⁶ psi	8.79 × 10 ⁶ psi
Coefficient of Expansion	11.3 × 10 ⁻⁶ /°C (25°C - 200°C)	10.9 × 10 ⁻⁶ /°C (20°C - 300°C)

flashlamps at the time and the more readily available linear flashlamps were used. Those purchased have an arc length of 6 in., a fused quartz envelope 1 mm thick by 9 mm O.D., and a maximum energy input rating of 2000 J.

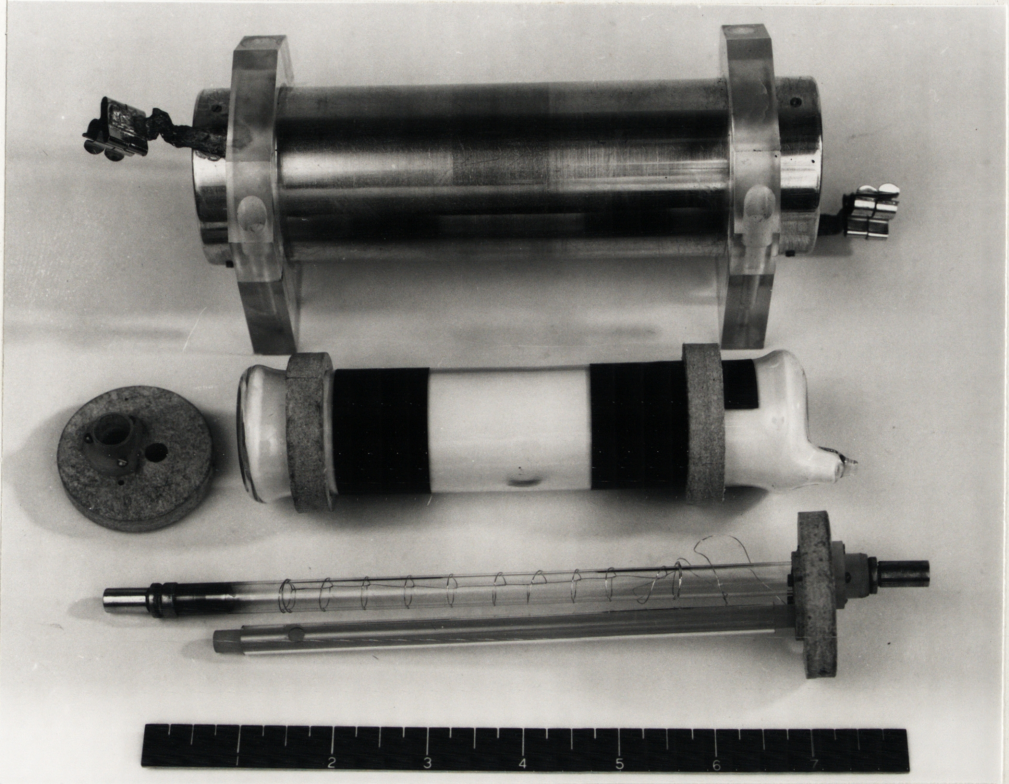
A reflector was constructed by filling the space between two glass tubes with reagent grade powdered MgO which has a high diffuse reflectivity throughout the near ultra-violet, visible and near infra-red spectral regions. The first version of the pumping cavity consisted of a single flashlamp and the laser rod (protected

from solarization by a 1 mm thick soda glass sleeve) mounted symmetrically inside the MgO reflector and aligned by end plugs of asbestos fibre board, the entire assembly being slipped into an aluminium tube for support. Fig. 5.2.1 is a photograph of the assembly. This arrangement was later replaced by that shown in the photograph of fig. 5.2.2 when it was found that one flashlamp was not satisfactory because of saturation. Due to space limitations, a similar coaxial reflector could not be used and it was replaced by a single piece of glass tubing, coated on the outside with a heavy slurry of MgO and water glass. This reflector was not as satisfactory as the former since the flashlamp caused discoloration of the coating. In addition, it was found necessary to cool the second assembly with forced air.

5.2.3. Flashlamp Triggering Circuit

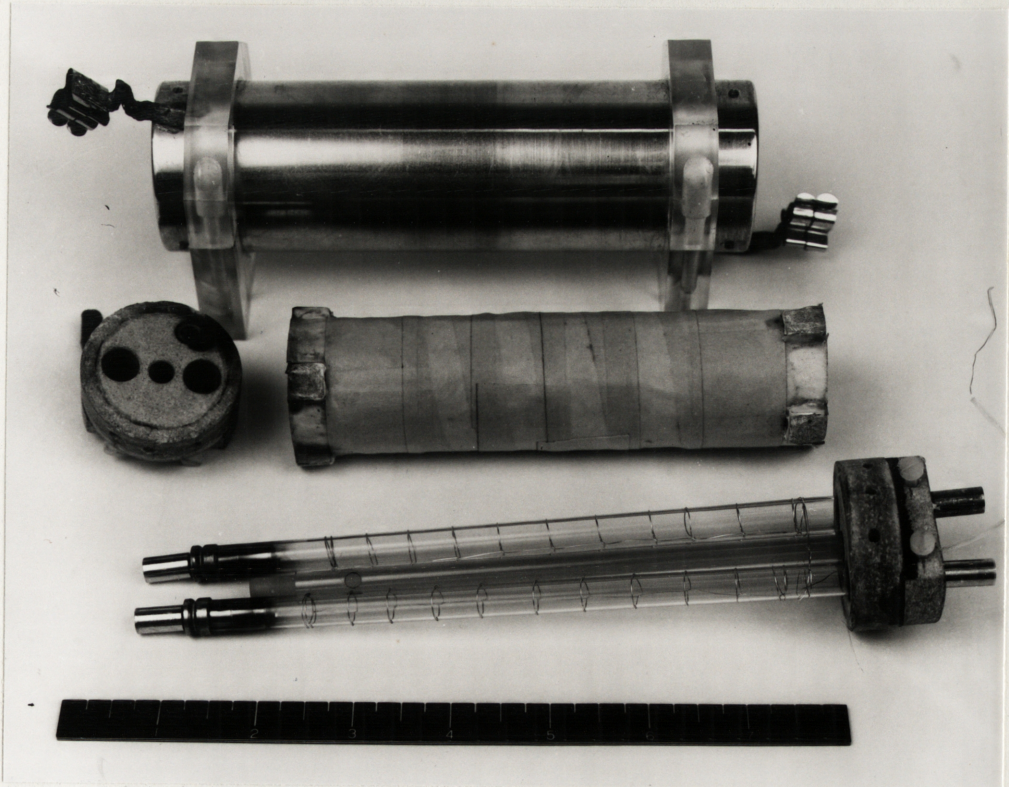
There are two common ways of firing the flashlamp. The first is to inject an additional voltage pulse in series with the capacitor bank voltage sufficient to exceed the breakdown potential of the lamp (usually about 8 kV). The second is to initiate breakdown in the lamp by applying a short, high voltage pulse to a plate or wire in close contact with the flashlamp envelope. The latter method was adopted because of its greater simplicity. To prevent the radiation of the high-voltage pulse from interfering with measuring equipment, the entire pulse circuitry (except its power supply) was enclosed along with the laser pump cavity in a carefully shielded box. Both ends of the flashlamp were earthed by coupling them with small by-pass capacitors to the box. All cables

Fig. 5.2.1



Photograph of the single flashlamp pumping cavity.

Fig. 5.2.2



Photograph of the double flashlamp pumping cavity.

to the laser head were coaxial, and the charging network was floated above earth. The degree of success of these steps can be judged from oscillograms which show no pickup from the high voltage pulse and less than 20 mV inductive pickup from the flashlamp discharge current, even when the external circuitry contained some unavoidable ground loops. Fig. 5.2.3 is a schematic diagram of the circuit.

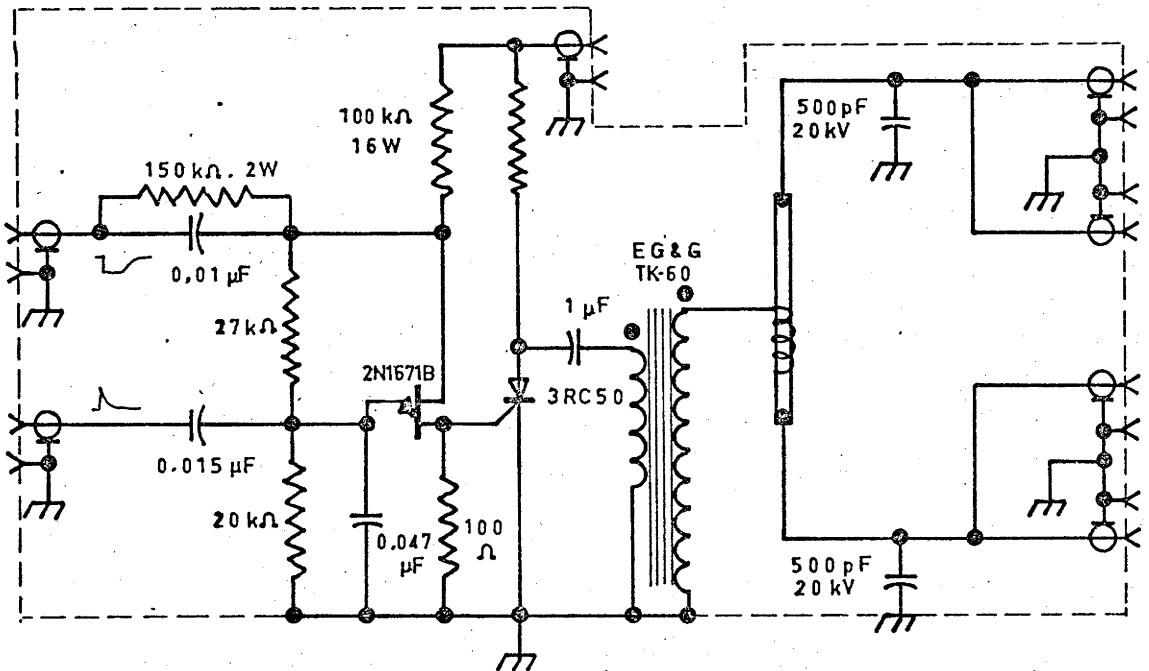
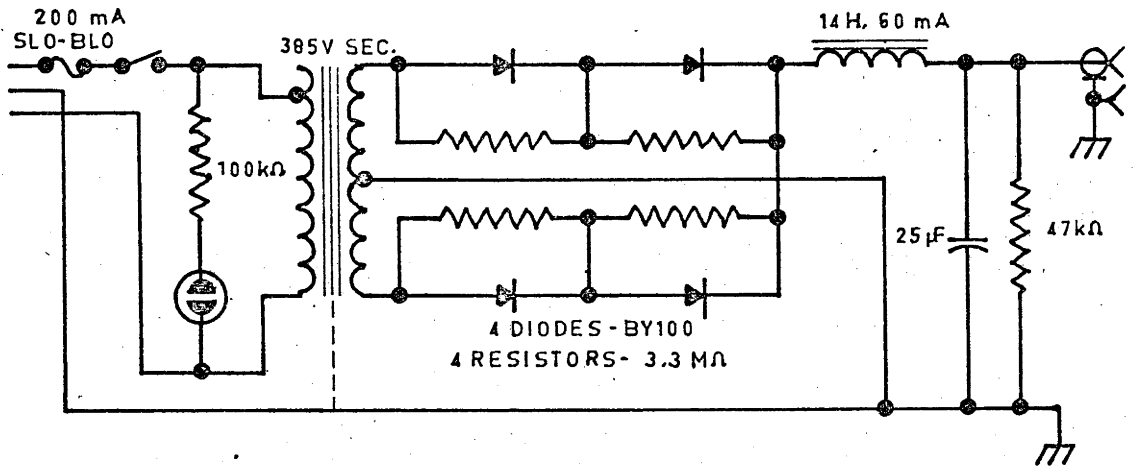
5.3. Flashlamp Energy Storage Bank and Power Supply

5.3.1. Design of the Energy Storage Bank

The design of a power supply and energy storage unit turns out to be rather sensitive to the type of flashlamp and the range of energies over which it must operate. It is also dependent upon the type of laser material which is being pumped. This is illustrated in the following discussion.

The circuit is assumed to be a classical LCR network, where the inductance is used to limit the current and the flashlamp impedance is the resistive element. This impedance is a function of the current (Perlman 1967), but for the flashlamps used is relatively constant at about 0.6Ω once the arc channel has fully expanded. Since laser energy storage capacitors are not designed to withstand ringing and their life is severely shortened if it is allowed to occur, only critically damped or over-damped discharges can be allowed. This limits the size of inductor that can be used with a given flashlamp-capacitor combination. In addition, the flashlamp will not work reliably if the applied voltage is less than 1.5 kV. Since the threshold for lasing is of the order of

Fig. 5.2.3



Schematic diagram of the flashlamp pulser and its power supply.

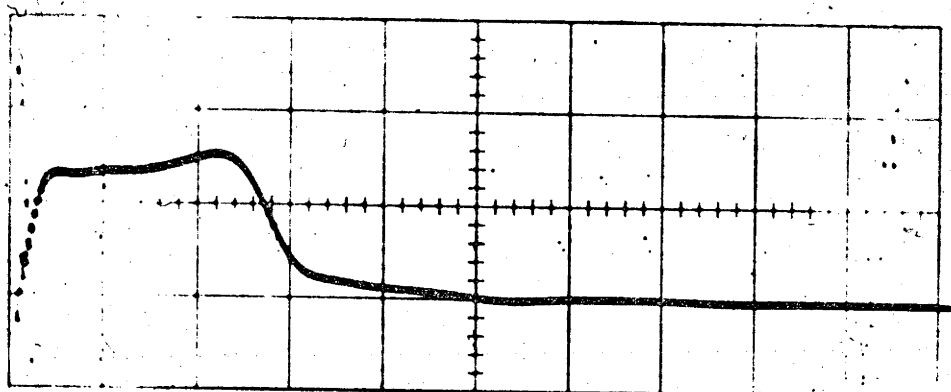
200 J when the rod and flashlamp are coupled as described above, a capacitance of 200 μF is chosen so that this energy is stored in the bank at the minimum flashlamp voltage. If ringing is to be prevented the inductance for this circuit must be $\leq 180 \mu\text{H}$. This will produce a pulse whose width at 1/3 of the peak is 360 μsec . However, according to the manufacturers data, a pulse of this width will cause immediate explosive failure of the flashlamp if the energy exceeds 2500 J. For a lifetime of 1000 shots, recommended maximum operation energy is 40% of the explosion energy, or 1000 J, which is less than the maximum energy desired. An additional factor which must also be considered is the need for the pump energy to be delivered in a time short compared with the fluorescent lifetime of the active ion in order to obtain high inversion. For the laser glasses used here, this time is 360 and 650 μsec (table 5.1). Thus, there are a number of conflicting design criteria and a compromise solution must be obtained. One solution is to distribute the total capacity among several capacitors and to construct a lumped constant delay line to give a square pulse. This has two advantages. Firstly, for a given energy input and time interval, a square pulse will have the lowest possible peak current and will thus cause less wall loading of the flashlamp. (This is offset somewhat by the possibility of lamp failure due to plasma shockwaves if the current risetime is too fast.) Secondly, the pulse shape lends itself to easy calculation of inversion population.

The final design consisted of a five section delay line approximating a trapezoidal pulse with risetime equal to 8% of the

pulsewidth, based on a network in Pettit (1959). Assuming a flashlamp resistance of 0.6Ω the calculated pulse width is 264 μsec .

Fig. 5.3.1 is an oscillogram of the current waveform.

Fig. 5.3.1



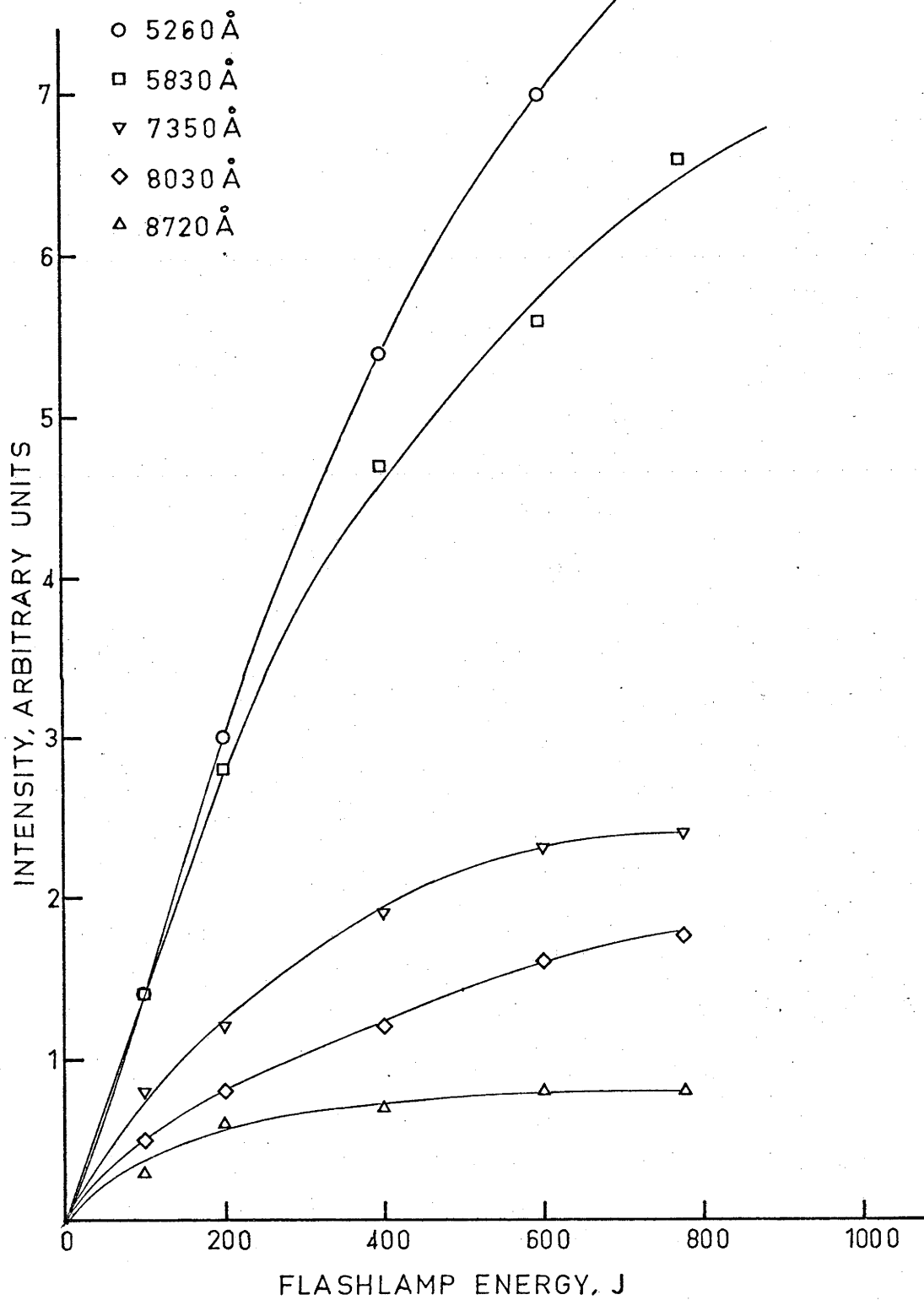
Oscillogram of current versus time for the single flashlamp circuit:
vertical scale - 860 A/div.; horizontal scale - 100 $\mu\text{sec}/\text{div}$.

Using the single flashlamp laser cavity described above, and with 100% and 75% reflectivity mirrors, laser threshold was 80 J and the slope efficiency 0.6%. The largest output obtained was 3.5 J, and saturation was found to be severe at 3 J output. These performance figures are significantly poorer than estimates by one manufacturer (Kodak) that their laser rods are capable of delivering $3 \text{ J}/\text{cm}^3$, or about 14 J for the rod size used. This should be compared with 130 J if the entire ion population could be inverted, based on the known quantum efficiency (DeShazer and Komai 1965) and the ion density in the glass host. The saturation effect was thought to arise from nonlinearity in the flashlamp due to opacity of the plasma to its own emission at the longer wavelengths (see Emmett, Schawlow and Weinberg 1964). Measurements

were made of the light in the pumping cavity as a function of wavelength and input energy for the five main pumping bands of Nd^{3+} and the results are indicated in fig. 5.3.2. The photodiode used in the measurements was checked for linearity in the range of outputs measured but was not calibrated for sensitivity as a function of wavelength, although the published sensitivity curve indicates a variation factor of less than 1.5 over the wavelength region covered. The graphs show that nonlinearity of three of the pumping bands is quite severe for energies greater than 400 J.

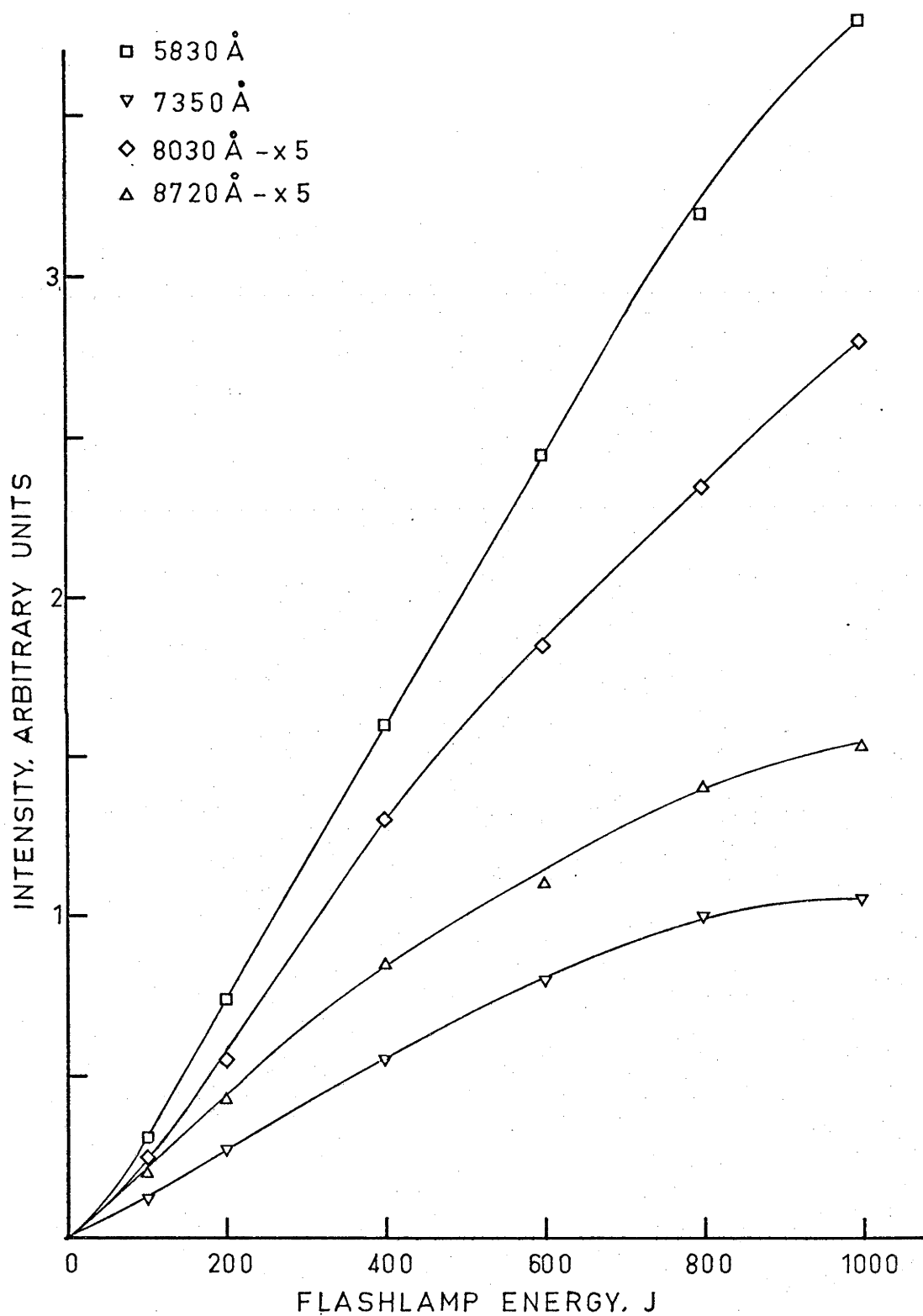
Because of the desire to make quantitative measurements of laser output versus inversion, it was necessary to modify the pumping arrangement in order to improve the linearity. This was accomplished by using two flashlamps in series as described earlier. The pulse-forming network was redesigned to drive an impedance of 1.2Ω , resulting in a calculated pulsewidth of 527 μsec . It can be seen from fig. 5.3.3 that there is considerable improvement in the linearity, although the waveform of the current pulse driving the flashlamps is not as flat as that obtained with the single flashlamp (fig. 5.3.4). Because the coupling between the laser rod and the flashlamps in the new pump cavity was not as efficient as in the old arrangement, the performance was degraded considerably, the new threshold being 140 J and the slope efficiency 0.42%. Despite the improvement in the flashlamp output linearity, there was not an accompanying improvement in the performance of the laser and the maximum energy that could be obtained was 3.6 J. Later measurements and the sharp cutoff of the energy output tend to indicate that the saturation was due entirely to the laser material itself.

Fig. 5.3.2



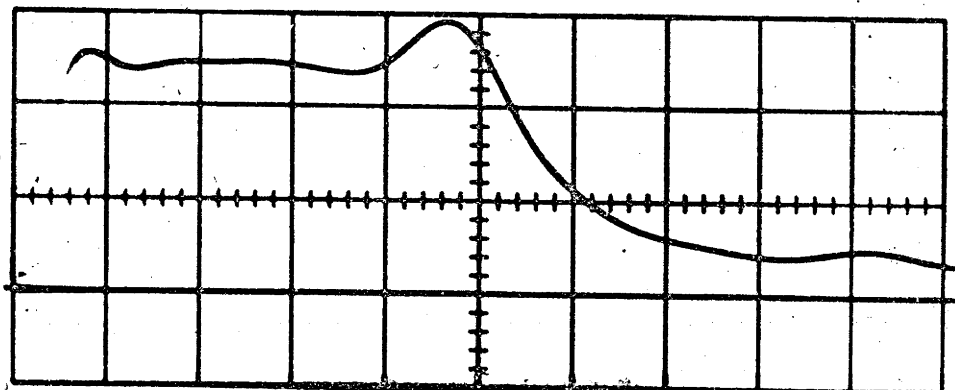
Emission intensity versus pump energy at the wavelength of the Nd³⁺ absorption bands, for the single flashlamp.

Fig. 5.3.3



Emission intensity versus pump energy at the wavelength of the Nd^{3+} absorption bands, for two flashlamps in series.

Fig. 5.3.4



Oscillogram of current versus time for the double flashlamp circuit:
vertical scale - 172 A/div.; horizontal scale - 100 μ sec/div.

5.3.2. Power Supply

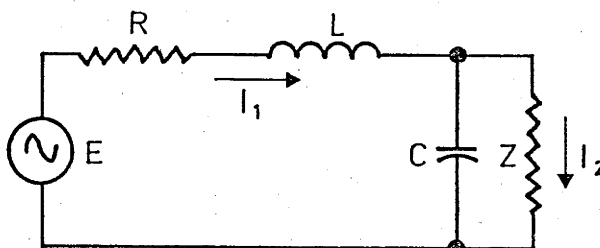
There were two reasons for designing and constructing the power supply rather than purchasing one: firstly, one of the experiments required that the output should be as reproducible as possible from shot to shot, necessitating careful control of the capacitor bank voltage; secondly, for the reasons previously discussed, it was desirable to float the capacitor bank above earth. Neither of these features is readily available in commercial designs.

Our solution to the problem is to use a constant current power supply and compare the charging voltage with an adjustable reference. When the charging voltage and the reference become equal the power supply is turned off and the capacitor bank isolated from it. Two purposes are served by using a constant current power supply, the first being that the capacitors are charged in the minimum time, and the second that the error in the

charging voltage is independent of bank voltage. Because relays must be used to shut down the power supply and isolate the capacitor bank, and they take a finite time to operate, the voltage on the capacitors will differ from the reference value. This difference can be an appreciable fraction of the capacitor bank voltage for small bank voltages, and if a high charging current is used. However, if the current is constant, then the voltage difference between the reference value and the capacitor bank voltage will also be a constant and any error due to jitter in the closing time of the relays will be independent of the capacitor bank voltage. The calibration curve of capacitor bank voltage versus reference voltage will be linear and the only effect of the finite operating time of the relays will be to shift the zero point.

The principle of the constant current source used here is due to Steinmetz as reported by Chandler (1949), and can be understood by referring to fig. 5.3.5, which is a series circuit resonant at mains frequency. R represents resistive and core losses in the inductor, and Z is the load. The magnitudes of the

Fig. 5.3.5



Simplified circuit of the constant current power supply.

inductive current I_1 and the load current I_2 are given by

$$|I_1| = \frac{E(X^2 + Z^2)^{1/2}}{[R^2X^2 + (X^2 + RZ)^2]^{1/2}},$$

$$|I_2| = \frac{EX}{[R^2X^2 + (X^2 + RZ)^2]^{1/2}},$$

and in the limit of no losses in the inductance,

$$\lim_{R \rightarrow 0} |I_1| = \frac{E(X^2 + Z^2)^{1/2}}{X^2},$$

$$\lim_{R \rightarrow 0} |I_2| = E/X,$$

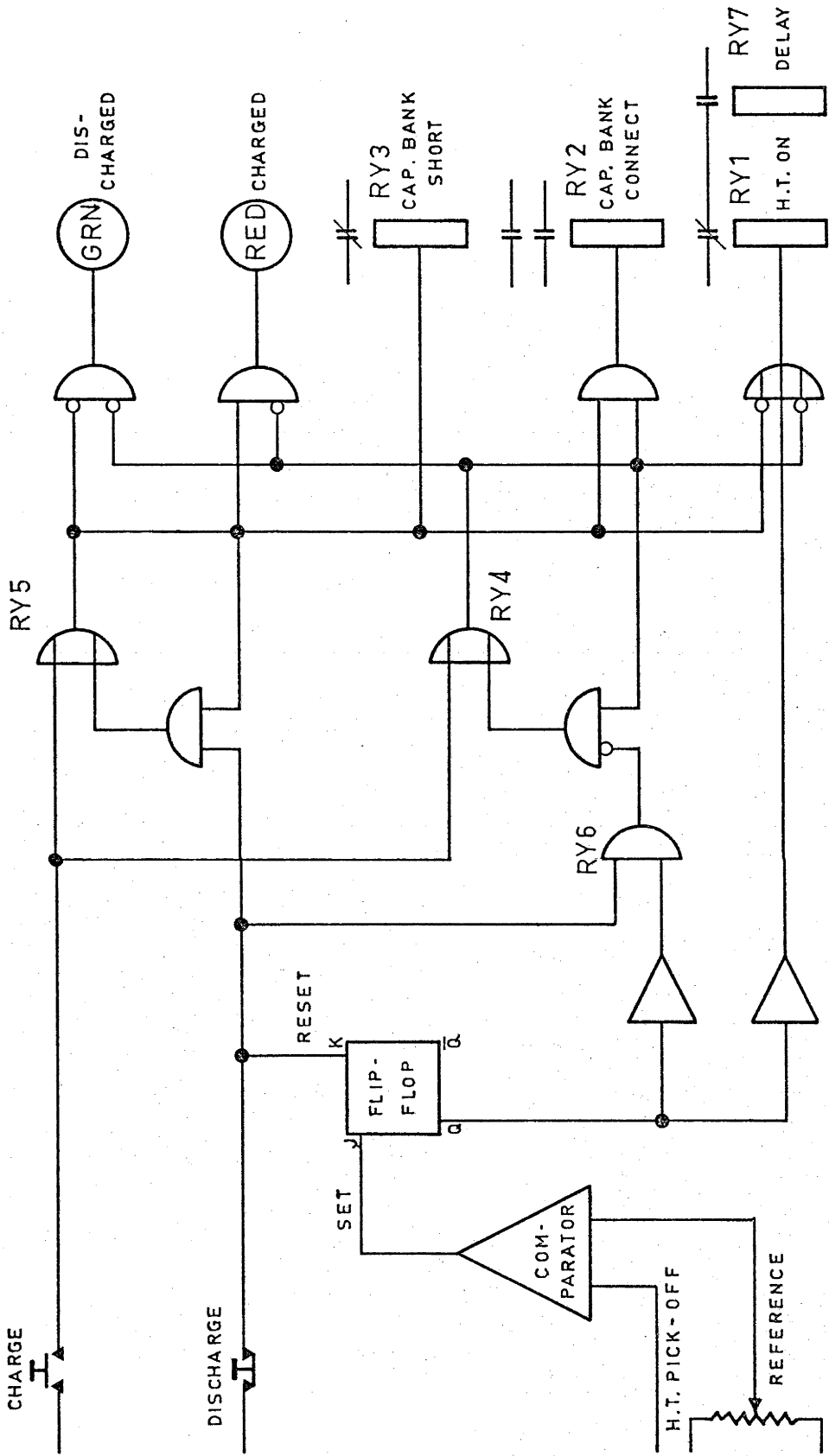
where $X = 2\pi fL = 1/2\pi fC$ at resonance. To a good approximation, the current through Z is a function of X and E only if $R \ll X$ and $RZ \ll X^2$. If computations are made for such a circuit to provide 100 mA charging current to a voltage of 5 kV, the physical size of the inductor turns out to be completely unrealistic. This is overcome by designing a circuit driven by mains voltage to provide a constant current to a low impedance, and using a transformer to match the required high impedance. A special high-voltage transformer is used, rated at 5 kV and 100 mA, but designed to give low leakage inductance by using interleaved windings in a manner similar to a high quality audio transformer. Full wave rectification is used to avoid any direct currents in the windings. The primary reactor must be designed to have a low resistance winding and should have an air gap to avoid saturation.

The switching of heavy inductive currents is always a

problem; in this case a special heavy duty mercury-wetted relay was used, with make-before-break single pole double throw contacts shorting to a quenching resistor. For safety reasons and for circuit protection, the switching logic is quite complicated. A logic diagram is given in fig. 5.3.6. The fast switching relay RY1 has normally closed contacts and RY7 acts as a delayed switch to prevent the high voltage from being energised when the power is first turned on. Safety from accidental charging of the capacitors is assured by RY2 which is normally open and isolates the capacitor bank from the high voltage power supply. In addition, RY3 is normally closed, short circuiting the capacitors. These relays can only be energised if the proper charging sequence is initiated. If the green light is on, then the capacitor bank is shorted and isolated from the power supply. Pressing the charge button turns out the green light, releases the short, connects the power supply and turns it on. When the preset voltage has been reached, the red light is turned on, the power supply turned off and the charged capacitor bank isolated from it. Pressing the discharge button shorts the capacitor bank and turns on the green safety light.

The stability of the power supply charging voltage is largely a function of the stability of the reference voltage, since the resistor chain from which the voltage is sampled consists of pyrolytic carbon film resistors designed to have high stability and a low coefficient of resistive change as a function of voltage. The change in resistance with temperature partially offsets the change in the reference voltage with temperature. The fractional change in voltage $\Delta V/V$ of the capacitor bank voltage as a function

Fig. 5.3.6



Logic diagram of the relay switching in the power supply.

of temperature is calculated to be $-5 \times 10^{-4}/^{\circ}\text{C}$, and the voltage stability with respect to mains variation $dV_{\text{out}}/dV_{\text{in}}$, 1.2×10^{-3} .

Fig. 5.3.7 is a schematic diagram of the power supply.

5.3.3. Calibration of the Power Supply

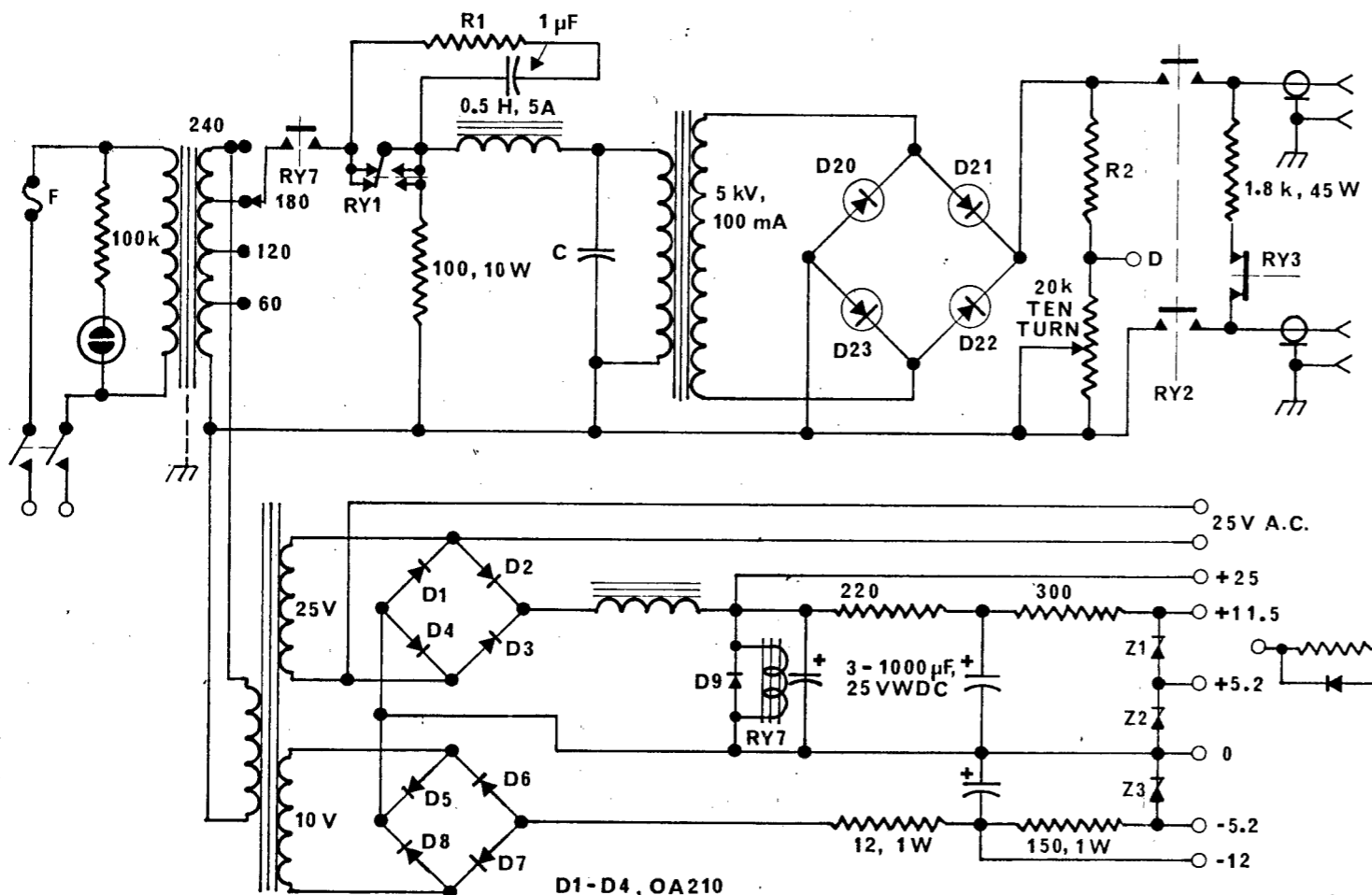
Because the capacitor gradually discharges through the finite input impedance of the voltage measuring device, a dynamic method of measurement must be sought. A suitable arrangement is to use a Tektronix type P6105 high voltage probe feeding into a Tektronix type Z plug-in unit. The probe is a resistive divider with a $100 \text{ M}\Omega$ input resistor, giving a discharge time constant of 2×10^4 sec. All resistances in the probe and the plug-in input were measured with an ESI model 42 Kelvin-Varley bridge with resistance standard accurate to within $\pm 0.005\%$ on all ranges. The type Z plug-in unit is a comparator providing a precise back-off voltage which may be subtracted from an unknown input voltage. Its comparison voltage is accurate to within $\pm 150 \text{ mV}$ on the 10 V range and its potentiometer is linear to $\pm 0.05\%$. The accuracy of the unit was checked against a standard cell before its use in calibrating the power supply. The calibration of the power supply has been found to be resettable to $\pm 5 \text{ V}$ even after two years between checks.

5.4. Five Metre Spectrograph

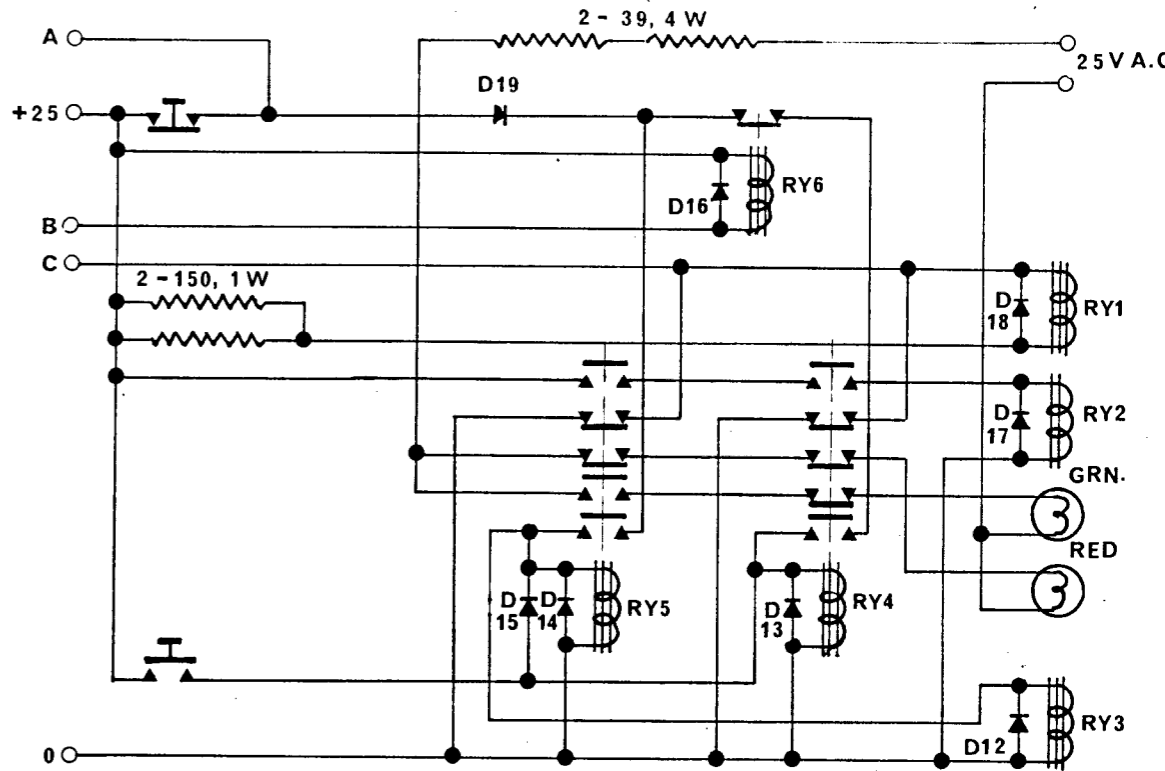
5.4.1. Introduction

The fluorescent line of Nd^{3+} in glass is about 300 \AA wide centred at $1.06 \text{ }\mu\text{m}$. However, the linewidth of the laser oscillator

Fig. 5.3.7

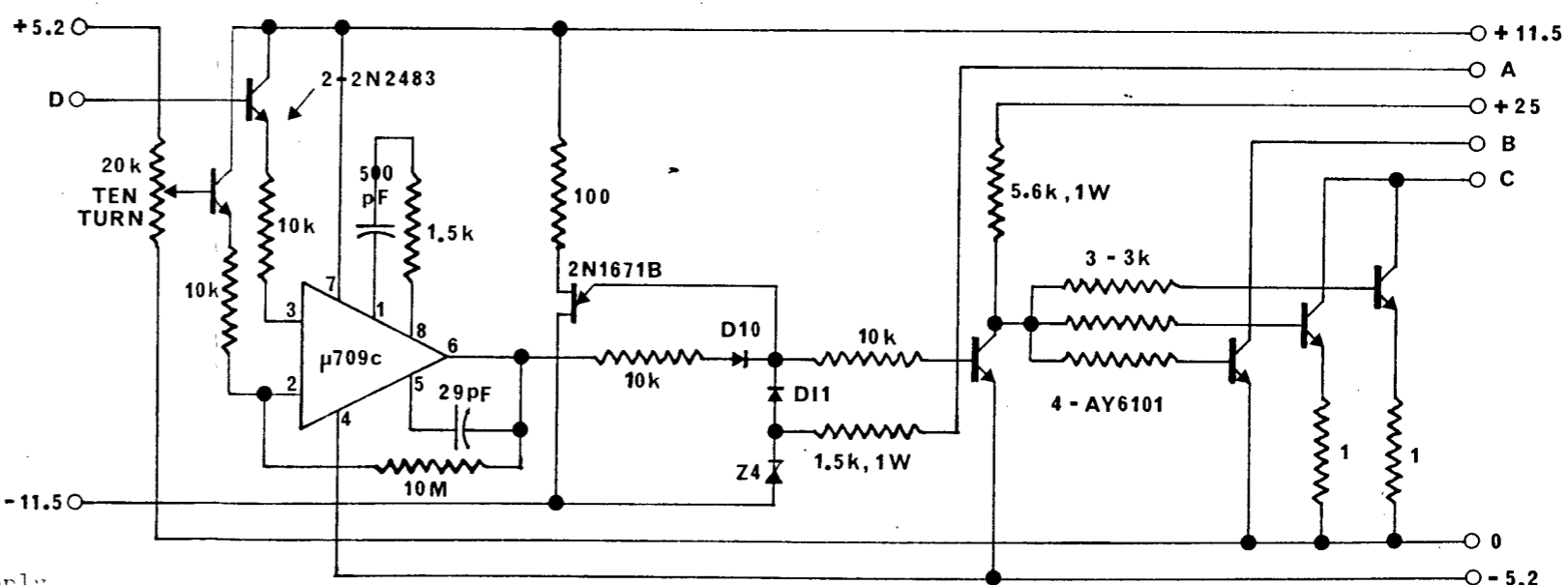


- D1-D4, OA210
- D5-D17, OA202
- D18-D19, AN1105
- F- 3A, SLO-BLO
- Z1-Z3, OAZ201
- Z4- OAZ213, SELECTED
- R1; 2-33, 10 W, IN PARALLEL
- C- SELECTED FOR RESONANCE AT LOAD



DETAIL OF D20 - D23; ALL DIODES - OA670,
ALL RESISTORS - 3.3 M

DETAIL OF R2;
9 - 1M, 1 - 820 k, 1 - 160k, 1 - 10 k, ALL 1 %



Schematic diagram of the capacitor bank charging power supply.

is usually about 30 \AA and is never greater than 180 \AA even with extremely hard pumping unless the laser is mode locked (see DeMaria, Stetser and Glenn 1967, for instance). The mode spacing of a Fabry-Perot resonator is given by $\Delta\lambda = \lambda^2/2L$, where L is the cavity length and λ is the wavelength. Thus, for a cavity length of 50 cm, the mode spacing is only 0.01 \AA and cannot be resolved even with a good grating spectrograph. However, in one set of experiments thin-film absorbers were inserted into the cavity to Q-spoil the laser. These films are deposited on 1 mm thick glass microscope slides, which have a mode separation $\Delta\lambda = 3.75 \text{ \AA}$ if they behave as a Fabry-Perot or a tilted-plate etalon (Snitzer 1966), and the desire to observe this structure determined the minimum resolution of the spectrograph. If any greater resolution were found to be necessary, it would have to be obtained using a Fabry-Perot etalon in conjunction with the spectrograph.

There was no spectrograph or spectrometer available that could easily be converted to operate as a high resolution spectrograph in the near infra-red, and one had to be constructed. It should be stated that original design considerations were dictated by the wish to use an image converter camera with an infra-red sensitive photocathode to observe the variation of the spectrum with time and, although the camera was never used, the choice turned out to be fortuitous. The image converter considered had a limiting resolution of 20 line pairs/mm and hence the spectrograph should have a linear dispersion greater than 20 \AA/mm in order to resolve any possible structure from the thin film plates. In addition, to investigate the time resolved structure of a Q-spoiled

pulse, the image converter camera needed a trigger pulse 50 nsec in advance of the pulse. This would require some sort of an optical delay line, and when preliminary calculations were made on the focal length required to give the desired linear dispersion, it became clear that the folded light path in a 5 m spectrograph would give sufficient delay (67 nsec). The focal length calculations were based on a 600 line/mm grating, blazed at $1 \mu\text{m}$, which was the only reasonable choice among those available from our sources. A plane grating $102 \text{ mm} \times 102 \text{ mm}$ was used, which gives an instrument speed of $f/44$.

5.4.2. Spectrograph Design and Construction

Any realistic design of an instrument this size will use folded reflecting optics, limiting the choice between the Ebert and the Czerny-Turner arrangements. The latter was chosen because its two mirrors allowed more freedom of layout and because the diameter of the single mirror of the Ebert must be as large as the sum of the two used in the Czerny-Turner configuration. The size of the input mirror must be sufficient to illuminate the whole of the grating with light from the entrance slit, i.e., it must be at least the size of the grating. Similarly, the exit mirror must be large enough to contain the diffracted images of the grating at the two extremes of wavelength to be imaged in the exit focal plane. The linear dispersion is given by

$$d\lambda/d\ell = a \cos \theta/mf, \quad \dots \dots \dots (5.4.1)$$

where θ is the angle of incidence, m is the order, a is the spacing

of the grating lines, and f is the focal length of the spectrograph. Thus, for a range of 200 \AA in first order, the image displacement at the exit mirror will be $\Delta l \approx 60 \text{ mm}$. The entrance mirror must therefore contain a square $102 \text{ mm} \times 102 \text{ mm}$, and the exit mirror a rectangle $102 \text{ mm} \times 162 \text{ mm}$. Using these figures, the final diameters chosen were 160 mm and 200 mm for the entrance and exit mirrors, respectively. They were manufactured and coated in the optical workshops at Mt. Stromlo Observatory. Gold was selected as the coating because its reflectivity at 1 \mu m is significantly better than aluminium - 0.982 , as compared with 0.939 (Hass 1955). The focal length of the two mirrors was matched to within 1 mm , although the exact value of the focal length was not controlled to better than 1 or 2 cm . Surface finish and coating quality left something to be desired if the instrument was to be used in the visible and if low scatter and maximum resolution were important, but the optics were perfectly adequate for the near infra-red.

Once the focal length has been chosen, there are yet several variables such as the positions of the grating, entrance slits and focal plane which can be manipulated to reduce aberrations (the most serious of which is coma) as discussed in papers by Allemand (1968) and Chandler (1968). For speeds less than $f/30$, however, the advantage is negligible and these variables were therefore chosen to provide a convenient physical layout. The centre-to-centre distance between the mirrors was kept as small as possible (240 mm) and the grating axis was set in the same plane as the entrance slits and the image plane, 120 mm away from the entrance slits. Fig. 5.6.2 is a plan of the laboratory layout. The theor-

etical resolving power is given by

$$R = \lambda/\Delta\lambda = mN$$

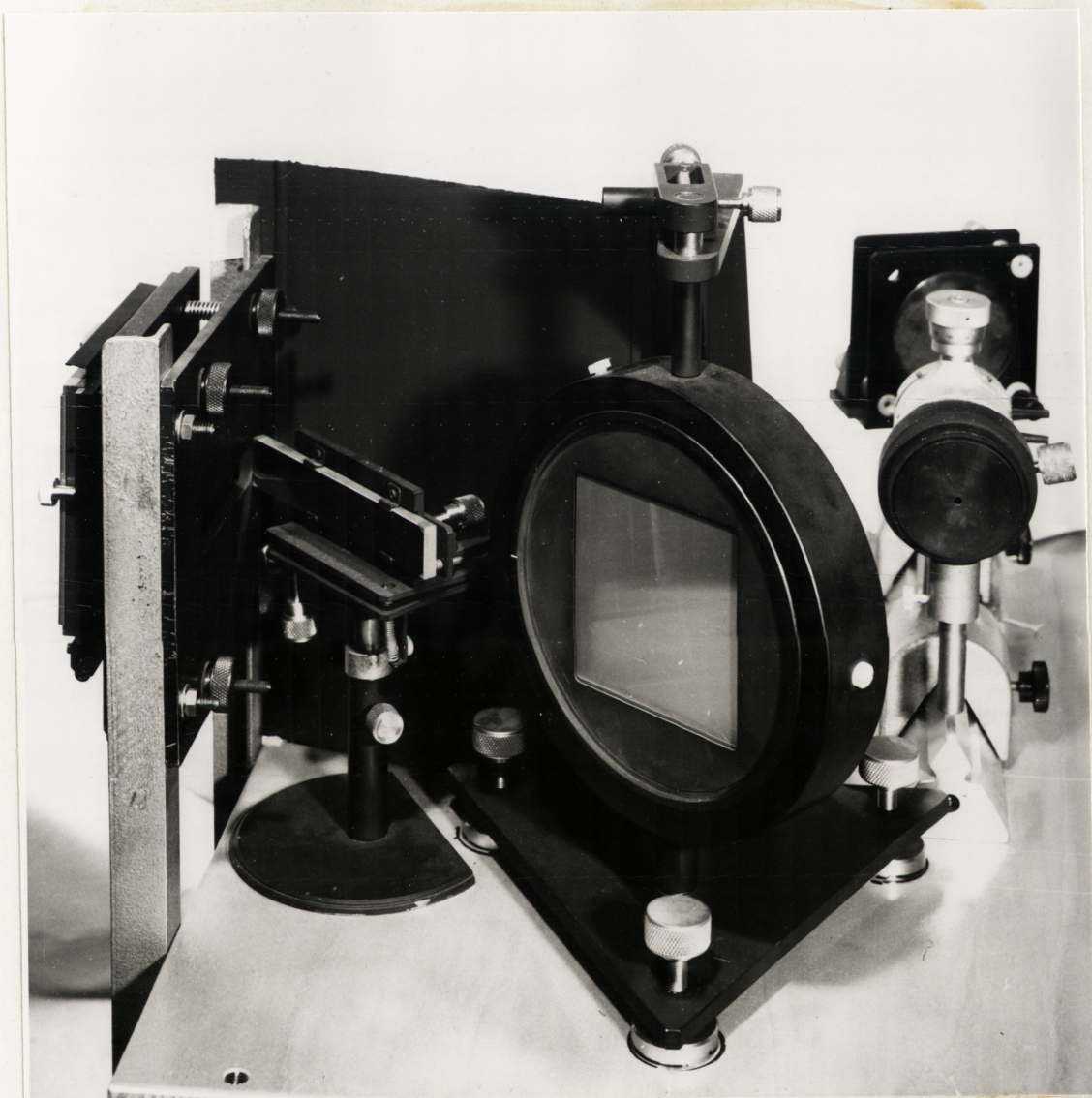
where N is the total number of lines on the grating and $\Delta\lambda$ is the resolution. Thus, in first order, $R = 6.12 \times 10^4$ and $\Delta\lambda = 0.173 \text{ \AA}$. The dispersion, given in eqn. (5.4.1), is 3.18 \AA/mm in first order and 1.59 \AA/mm in second order.

Because of the short duration of the phenomena to be analysed, vibration in the spectrograph is not a problem, and all the heavy construction and isolation usually associated with a spectrograph of this size can be eliminated. In fact, because of the limited space available, it was decided to run the axis of the spectrograph across the diagonal of the laboratory with free access in the centre, and the entire room was made light tight as in a camera obscura. The mirrors are mounted in the standard four point arrangement employed in all large spectrographs and the grating is set on three points for ease of alignment. Fig. 5.4.1 is a photograph of the arrangement.

5.4.3. Energy Collection and Image Brightness

There are still the questions of whether the numerical aperture of the instrument is great enough to provide sufficient energy at the focal plane of the instrument and of how the source is to be imaged on the slits. We discuss the second problem first. For maximum resolution, the energy passing through the entrance slit should fill the width of the first mirror (thus using the entire grating). However, the beam divergence of even a poor qual-

Fig. 5.4.1



Photograph illustrating the arrangement of the grating mount and the slits.

ity laser rod will be much less than the angle subtended by the first mirror at the entrance slits and, in addition, some method should be devised to sample light from every part of the laser rod in case filamenting occurs. This can be done by focusing the laser beam on to the slits with a 5 m focal length lens. Because there was not enough room physically for this to be done, a shorter focal length lens (1.33 m) was used. Even this arrangement was found to be unnecessary as the laser rods used did not oscillate in filaments to any great extent, and no difference in the spectrograms could be seen whether the lens was used or not. Since the lens caused some damage to the mirrors and slits, its use was discontinued. Further consideration indicates that if the slits are set to a width of 90 μm , the first maximum of the diffraction pattern will just fill the area of the first mirror, and the maximum resolution of the system will be attained with this condition. There is no point in making the slits any smaller and the resolution is instrument limited to $\Delta\lambda = 0.29 \text{ \AA}$.

A worst case estimate may be made of the energy density incident upon the focal plane of the spectrograph, under the following assumptions: the laser is assumed to emit a Q-spoiled pulse of 0.04 J (about half that expected) with the energy evenly distributed across its exit aperture and uniformly dispersed in a 200 \AA band; further, the radiation is not focused on to the slits which are set to a width of 100 μm . If there is no loss from the mirrors or grating, then the energy density at the focal plane should be $1.7 \times 10^{-4} \text{ J/cm}^2$ in first order. This exposure should be just adequate for Kodak type I-Z spectrographic plate, the only photographic

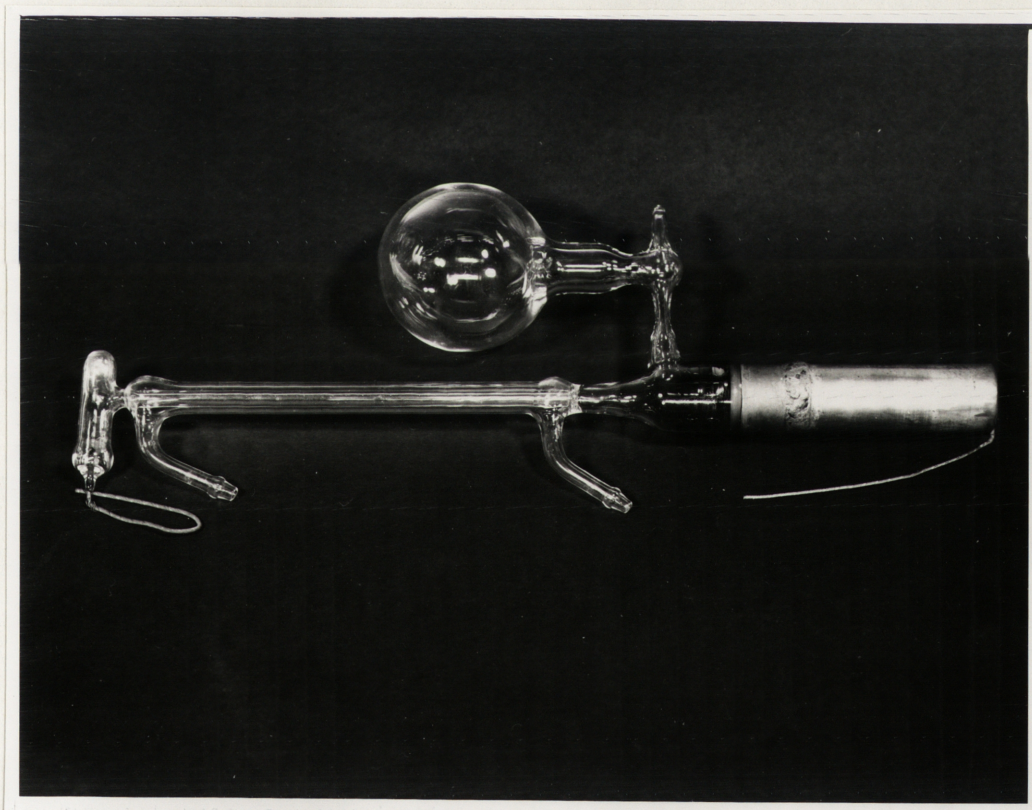
material available which is sensitive at $1 \mu\text{m}$. On the basis of data supplied by Kodak, an exposure of $6.3 \times 10^{-7} \text{ J/cm}^2$ is required to produce a density of 0.6 above gross fog. However, there will be serious reciprocity failure due to the short duration of the laser pulse, and the above exposure will have to be increased by a factor of 10 to 100 to produce the same plate density. An estimate of the image converter sensitivity was much more favourable and indicated that an exposure of $3 \times 10^{-10} \text{ J/cm}^2$ should be detected. Recent indications are that this value is too small by several orders of magnitude and thus the sensitivity of the image converter should be comparable with the plates.

5.4.4. Calibration of the Spectrograph

By far the most vexing problem was calibration of wavelength. An exhaustive search of all spectral sources for strong, distinct lines of any wavelength that would fall within 20 \AA of $1.06 \mu\text{m}$ in first or second order indicated that only argon had lines that might be suitable, and none of these could be classified as strong. The spectrograph could easily be set visually to its approximate wavelength using the resonant line of Thallium at 5350.46 \AA in second order (equivalent to 10700.92 \AA), but I-Z plates are not sensitive to this wavelength. Thallium also has one suitable strong U.V. line at 3529.43 \AA (10588.29 \AA , third order), which was later used as a fiducial mark with the streak camera. However, for most of the work, a strong argon source was used. The principle lines used are listed in appendix II. Fig. 5.4.2 is a photograph of the final version of the numerous lamps tried. It has a water-

cooled capillary discharge about 20 cm long and an air-cooled stainless steel hollow cathode joined by a glass-to-metal seal. Fill pressure is 1 Torr and the lamp is run at 350 mA, dissipating about 160 W. The end of the lamp is placed adjacent to the slits of the spectrograph, the capillary along the optic axis so that the spectrograph "sees" a deep, dense plasma. Good calibration lines are obtained on I-Z plates with the slits set at 100 μm and an exposure time of about 3 min.

Fig. 5.4.2



Photograph of the water-cooled argon spectral lamp.

5.5. Detectors

Two types of quantitative detectors in addition to photographic plates were used in the experiments. Energy was detected with a ballistic thermopile and power with a PIN photodiode.

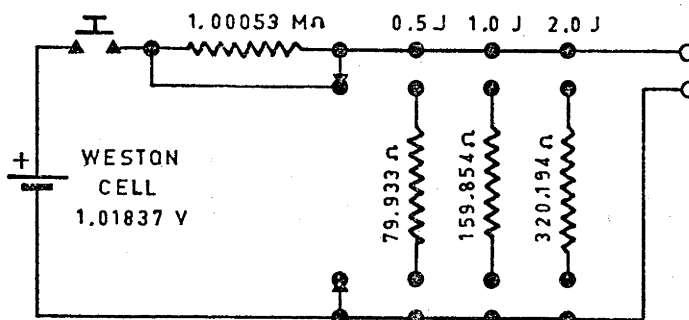
5.5.1. Ballistic Thermopile

The thermopile used was a TRG model 100. It is a calorimetric device in which the beam energy is measured by observing the subsequent temperature rise of a small thermal mass in which the energy is totally absorbed. Two identical nickel-plated silver cones are arranged so that ten series-connected iron-constantan thermocouples have their hot junctions connected to one cone (the receiver) and cold junctions connected to the other (the reference), the energy being totally absorbed in the receiving cone by multiple internal reflection. The instrument has been factory calibrated with standards traceable to NBS and has a sensitivity of $163 \mu\text{V}/\text{J}$, accurate to $\pm 5\%$. The thermal time constant is 80 sec. A permanent record of the energy is obtained by detecting the thermopile voltage with a Keithley model 150A Microvolt/Ammeter connected to a Philips PR 2210A/00 chart recorder. The recorder is calibrated to 0.5, 1.0 and 2.0 J full scale by means of the circuit shown in fig. 5.5.1. All of the resistances in this circuit are adjusted to $\pm 0.2\%$ with the Kelvin-Varley bridge.

5.5.2. PIN Photodiode

The peak power was monitored with a Hewlett-Packard type HPA4205 silicon planar PIN photodiode. It has a quantum efficiency

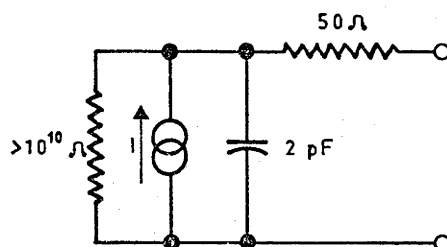
Fig. 5.5.1



Schematic diagram of the circuit used to calibrate the chart recorder to read energy directly in joules.

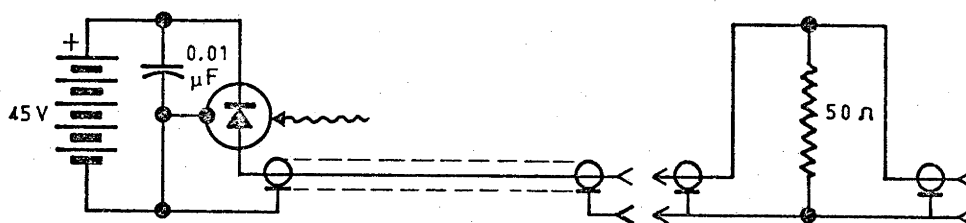
of 75% at 7700 \AA , a rise time of less than 1 nsec, and a sensitive area of $5 \times 10^{-4} \text{ cm}^2$. The equivalent circuit of the photodiode is shown in fig. 5.5.2, and the electronic connections in fig. 5.5.3. By using a $50 \text{ } \Omega$ termination, the 4 nsec rise time of the Tektronix 585 oscilloscope could be fully exploited. The maximum power dissipation is claimed to be 50 mW but diodes were repeatedly subjected to 100 nsec wide pulses of 500 mW and occasionally to pulses of 4 W without any indication of damage. (One diode did fail after repeated exposure to pulses in the range of 1 - 2 W.) Two experimental arrangements for sampling the beam were tried, and are shown in fig. 5.5.4. The beam-splitters used are 2 in. diameter uncoated cellulose-based pellicules $8 \text{ } \mu\text{m}$ thick, obtained from National Photocolor Corp. In the first arrangement, the diode had a lucite light pipe with a $3/8$ in. diameter fine ground light collecting surface.

Fig. 5.5.2



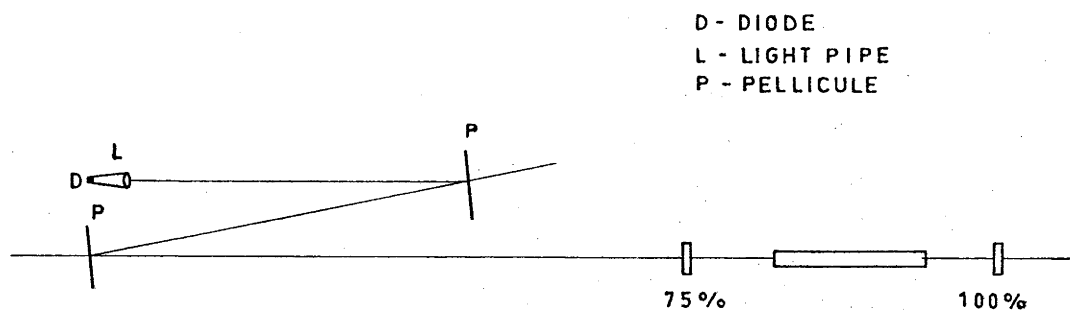
Equivalent circuit for the HPA4205 photodiode.

Fig. 5.5.3

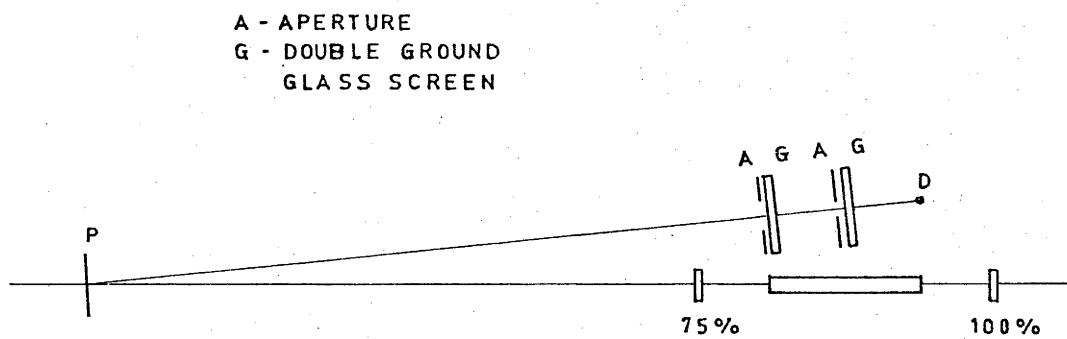


Schematic diagram of the oscilloscope connections to the photodiode.

Fig. 5.5.4



(a)



(b)

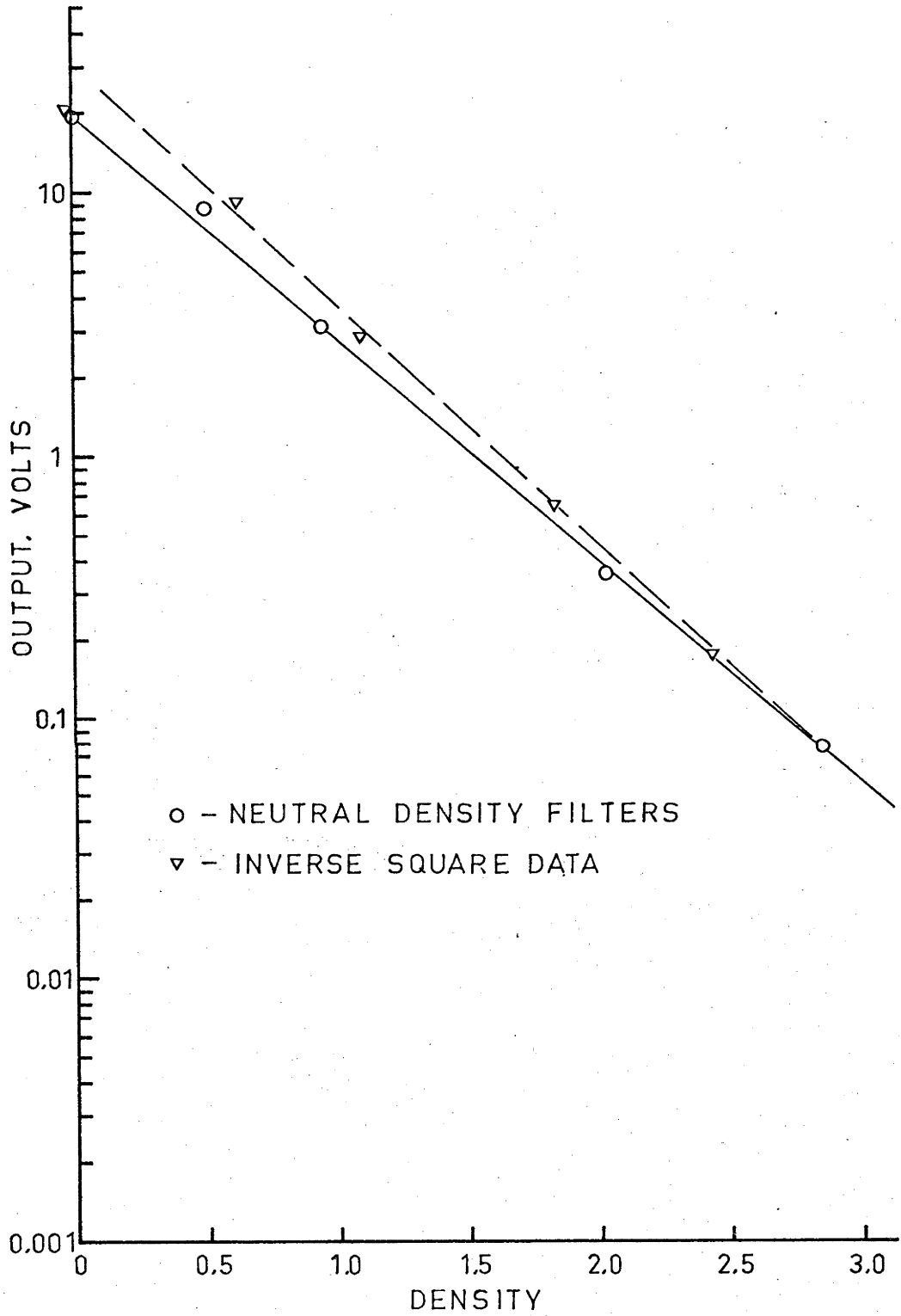
Diagram of the arrangements used to sample the beam for the photo-diode: (a) with light pipe, (b) with ground glass screens.

It was not satisfactory because of non-reproducible results whenever any of the optical components were moved, probably caused by interference effects in the pellicules which were readily observable with the He-Ne laser (see Hillenkamp 1969). To destroy these coherence effects, the second arrangement employed a naked diode behind two ground glass screens in a manner described by Edwards (1969). The Fresnel numbers for the two screens in the second arrangement are 115 and 230.

The linearity of the diode for high power pulses was checked with a Lumatron Electronics argon spark gap light source, which provides a fast-rise, exponentially decaying light pulse with a halfwidth of about 200 nsec. Two methods were used. In the first, calibration was provided over a 200:1 range by observing the intensity of the light source as a function of distance. The spark is nearly a point source and the intensity should follow the inverse square law. In the second method, measurements were made at a fixed distance with a set of calibrated neutral density filters. Corrections were made for changes in the oscilloscope vertical deflection scale range and the results for the two methods normalised to zero density for purposes of comparison. A graph of these results is shown in fig. 5.5.5. There is some departure from linearity for the first set of results and this is attributed to measurements being made too close to the source for the inverse square law to hold. The maximum point on the curve corresponds to a peak diode dissipation of 4.6 W.

Two approaches to calibrating the diode for peak power were tried. In the first, the calibration was obtained from

Fig. 5.5.5



Graph of photodiode output voltage versus density (circles) of the neutral density filters, and equivalent density (triangles) for the inverse square data, referenced to zero density.

measurements of normal lasing. One way was to integrate the output by placing a $0.2 \mu\text{F}$ capacitor across the 50Ω resistor to give a time constant of $10 \mu\text{sec}$. Alternatively, the laser was run at threshold to give 3 or 4 spikes, which were all recorded using a fast sweep on one oscilloscope and multiple exposures. Another oscilloscope was used to count the number of pulses and verify that all were included in the multiple exposure. The areas under each spike were then measured and added together. In either case the results were then compared with the energy measured with the calorimeter to give the calibration factor.

The second approach to calibration of the photodiode was to measure the energy of a single Q-spoiled pulse using the calorimeter and compare this with the area under the intensity-time curve obtained from the photodiode. The two approaches give calibration factors which differ by a factor of 10. No reason can be found for such disparate results unless it is assumed that the response curve of the photodiode has a knee below the point where linearity checks were made. In any case, the measurements made directly on the Q-spoiled pulses give a calibration factor of the expected magnitude and since linearity was checked in the region of the power levels used with Q-spoiling, the latter was adopted as the correct calibration factor.

5.6. Optical Bench

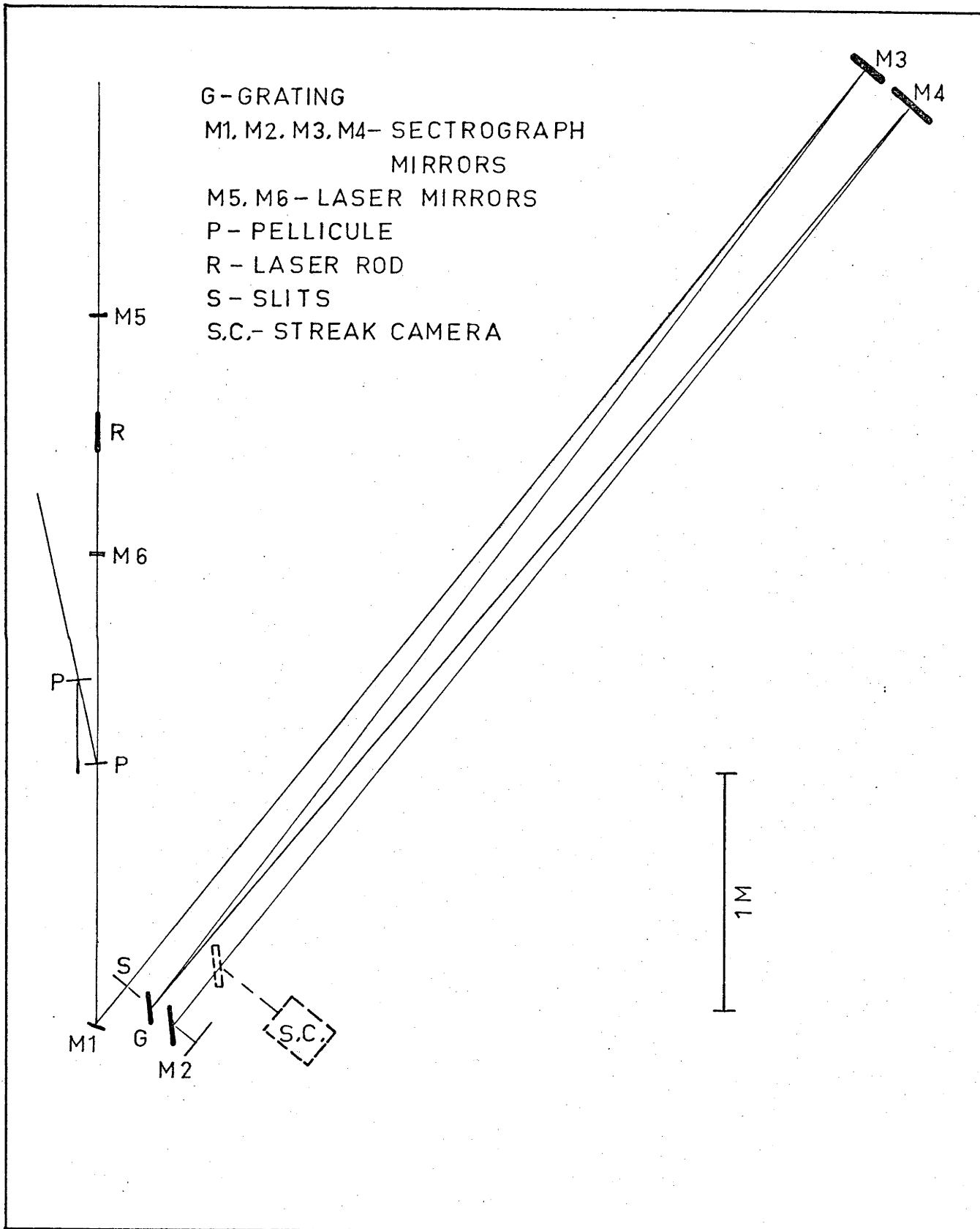
All the optical components excluding the spectrograph were mounted on a 3 m optical bench for stability and ease of alignment. It was constructed using 1 m sections of PTI triangular

rail mounted on steel girders which were braced with angle iron. The rails were carefully shimmed and aligned so that a crosshair mounted on any part of the rails deviated from a true line by less than 0.1 mm in both the horizontal and the vertical direction. Later, another rail was added at right angles to the others in the middle of the bench to provide space for the ring laser (see §6). A plan of the entire setup is shown in fig. 5.6.1 and a photograph is given in fig. 5.6.2.

5.7. Streak Camera

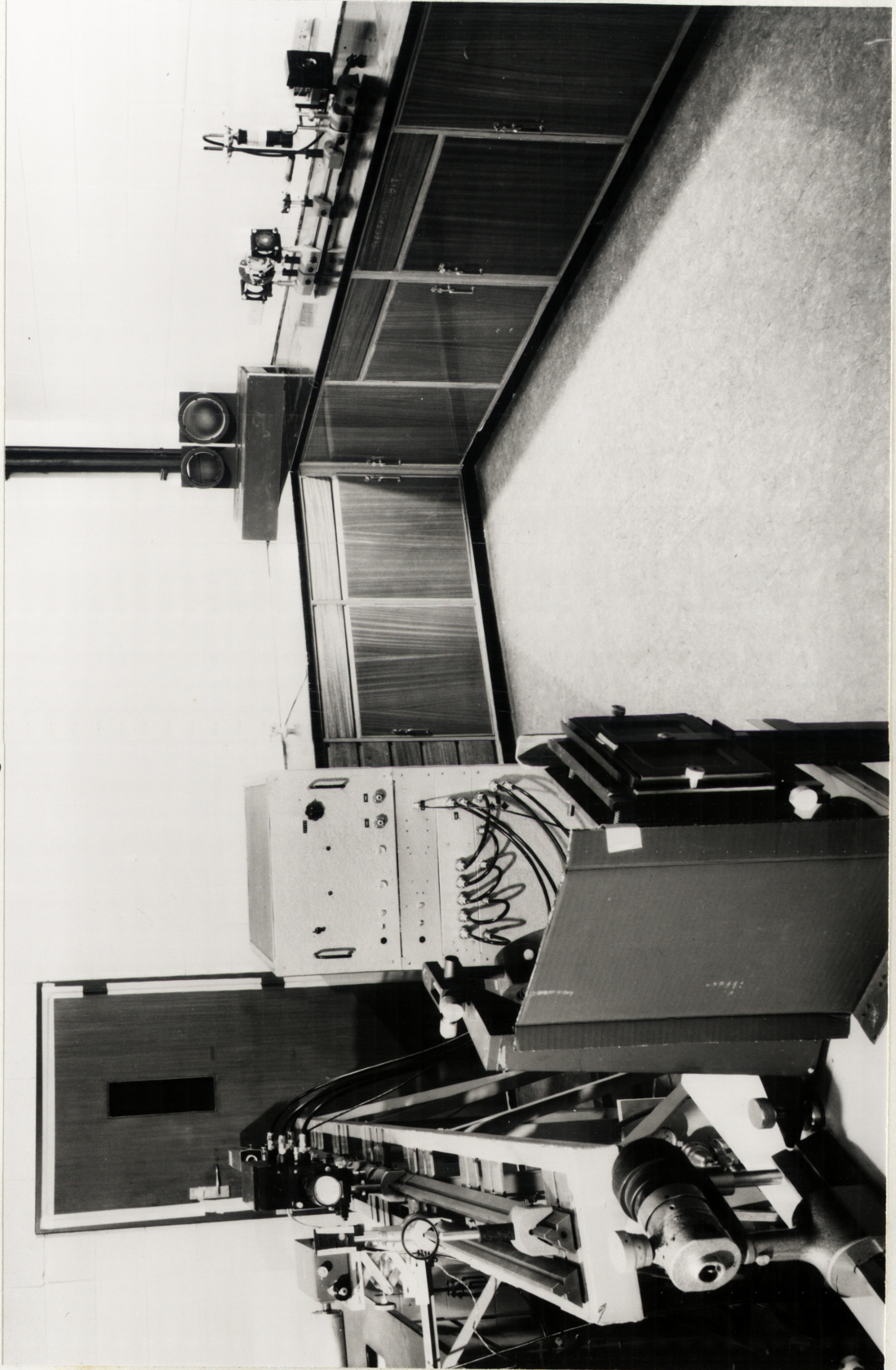
Instead of the image converter camera, a rotating mirror streak camera was used for time resolved spectroscopy. Basically, the camera consists of a stainless steel mirror rotated about a horizontal axis by a special high speed air turbine, capable of 20000 rpm. By placing a slit 100 μm wide at right angles to the spectrograph slit, a time resolution of 0.3 μsec is obtained when the streak camera is adjusted to give a streak speed of 150 $\mu\text{sec/in}$ on the photographic plate. Synchronization with the mirror position is provided by a photodiode which picks up light passing through an off-centre hole drilled through the turbine axis. In the experiments to be described later, the pulse from the photodiode was used to trigger the laser, thus ensuring that the event fell into the acceptable time "window" of the camera. The electrical connections and their operation are illustrated by table 5.2 and fig. 5.7.1. Type I-Z plates were used in a modified Polaroid roll film camera back.

Fig. 5.6.1



Plan of the laboratory illustrating the arrangement of the optical bench and the spectrograph.

Fig. 5.6.2

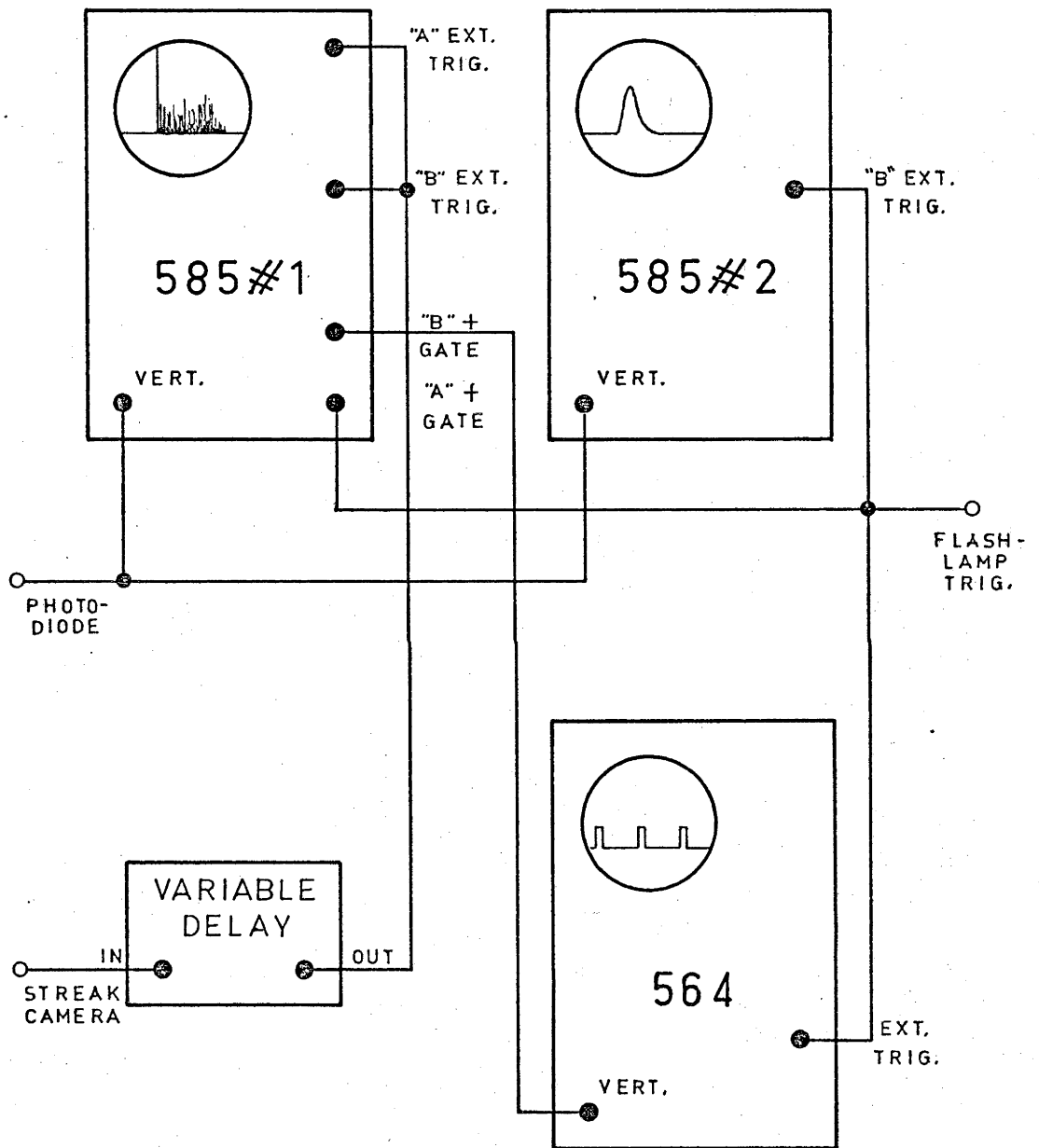


Photograph of the laboratory showing the optical bench and the spectrograph.

Table 5.2. Oscilloscope Control Settings

Type 564	Horizontal Scale; 2 msec/cm.
Type 585, No. 1	Mode: "A", single shot. "A" Sweep: External Trigger, Positive D.C.; Horizontal Scale; 100 μ sec/cm. "B" Sweep: External Trigger, Positive, D.C. Sweep Width adjusted so that "B" gate = 1 msec; Horizontal Scale; 100 μ sec/cm.
Type 585, No. 2	Mode: "A" delayed by "B". "A" Sweep: Internal Trigger, Positive, A.C. Horizontal Scale; 50 nsec/cm. "B" Sweep: External Trigger, Positive, D.C. Horizontal Scale; 100 μ sec/cm.

Fig. 5.7.1



Electrical connections between the streak camera and the oscilloscopes.

§6. TIME RESOLVED SPECTROSCOPY

6.1. Introduction

This section deals with experiments designed to investigate how the wavelength of the laser emission varies with time. By studying different glasses in two different cavity configurations, both when the laser is operated normally and when it is Q-spoiled, the importance of these various factors on the spiking behaviour can be assessed. In addition, by observing the bandwidth and wavelength structure of adjacent spikes, it is possible to investigate the nature of the fluorescent line. The special procedures used in the experiments and the scope of the investigation are described in the first two subsections, and the results are presented and discussed in the last two.

6.2. Infra-Red Plate Processing

One of the more troublesome aspects of the experiment was the processing of the infra-red-sensitive plates. These plates (type I-Z) are supplied by Eastman Kodak in minimum quantities of four boxes of 36. Their lifetime is estimated to be three months if refrigerated, but we have found plates to be usable for up to 18 months if kept under deep-freeze conditions and dessicated to prevent condensation.

Before use, the plates must be hypersensitized. A modified procedure given by Pope and Kirby (1967) was followed and it is described here briefly. The plates are sensitized in a dilute solution of ammonia, neutralised in an acetic acid-alcohol solution, dehydrated in 90% methyl alcohol, and dried in a cold air blast.

All baths are kept at 5° C. Several failures indicated the importance of keeping the plates cool at all times, so the following method was adopted. A cold room was available which could be set at 1° C. The solution trays were put in a recirculating water bath which was heated to 5° C, and the plates were dried in the air blast from the cold room heat exchanger fan. Plates thus sensitized were kept in the cold room until immediately before use, and returned there after exposure if processing could not begin immediately. Even with these precautions, they deteriorated noticeably if not processed within one hour after sensitizing. Fresh developer was used at all times, and developer temperature was adjusted so that average temperature was 20° C during processing.

6.3. Experiments

Since the majority of the experiments used a thin film to produce Q-spoiling, a short description will be given of the preparation of the films and the behaviour of the laser when this method of Q-spoiling is used. The film consists of a thin layer of gold sputtered on to glass microscope slides. The densities used varied from 0.2 to 0.8 (at 1 μm) and were measured by comparison of photocurrent from a HPA4201 photodiode when the slides were inserted and then removed from a collimated beam of 1 μm radiation. The density variation from one area of a slide to another was generally less than 20% and, providing no mirror damage occurred, reproducibility of laser energy output from shot to shot using different areas of the same slide was also within 20%. When the pulse output is observed on an oscilloscope, it is seen to consist of one or

more Q-spoiled pulses followed by normal spiked lasing. The laser shot vapourises the gold film, producing an extremely bright plasma. Time resolved photographs of this plasma indicate that the light output falls by at least three orders of magnitude in the 10 μ sec following the Q-spoiled pulse, and by an order of magnitude in the first 500 nsec. Switching is therefore virtually over by the end of the first Q-spoiled pulse and any pulses following are produced in a static situation as far as the cavity losses are concerned. Thus one is able to study the transient output of the laser after a high inversion has been produced.

Experiments were performed with both types of laser glass (Schott LG-56 and Kodak Nd-11) in order to assess the effect of different glass hosts, and also in two types of resonant cavities, a Fabry-Perot cavity and a ring cavity. In a ring cavity, waves travelling in both directions are amplified by the medium, the modes being such that self-consistency is established when the wave has travelled once around the closed path. If stationary conditions exist, then two waves travelling in opposite directions with the same mode number will set up a standing wave in the cavity. However, as discussed in §9, this situation will bring about an uneven gain distribution in the active medium, which should result in sufficient non-linearity to slightly alter the frequencies of these two waves so that a standing wave no longer results. This is in contrast to a Fabry-Perot cavity, in which the waves travelling in opposite directions are not independent, and standing waves must arise. A study of the two cavities should aid in the assessment of the importance of mode interaction on the spiking behaviour of the Nd^{3+} laser.

Finally, a comparison was made between different methods of Q-spoiling. Streak photographs were taken of the output when a Pockel's Effect shutter was inserted in the laser cavity rather than the gold film. This shutter was modified electrically so that rather than opening and then closing 50 nsec later, it remained open for several hundred μ sec, thus behaving in a similar manner to the thin film switches.

6.4. Results

Photographic reproductions of representative time-resolved spectra are given in figs. 6.4.1 - 6.4.9. On all plates time increases from left to right, and wavelength from top to bottom. No attempt was made to maintain a consistent scale in the reproductions because different streak speeds were used on different plates. However, the approximate streak speed scalings are indicated on the figure captions and comparison can be made by noting that the fine structure in wavelength is in all cases due to the Fabry-Perot etalon formed by the 1/8 in. thick sapphire flats on which the dielectric mirrors were coated ($\Delta\lambda = 1.78 \text{ \AA}$). A study of the plates indicated that the pulses can be classified into five major types based on the correlation of the pulse time as a function of wavelength. These are described below. For ease of interpretation, sketches illustrating the essential features of the different types are given in fig. 6.4.10.

Type I - No Correlation with Wavelength

Each mode appears to start oscillating independently of other adjacent modes, with a random start time relative to previous

Fig. 6.4.1

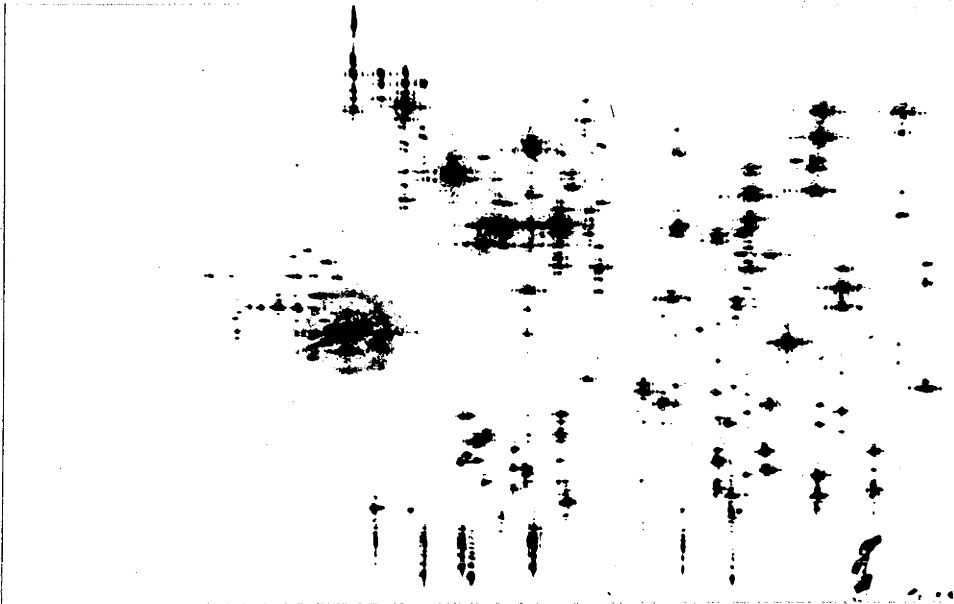


Plate #1-1 of 15-2-69: time scale - 49 $\mu\text{sec}/\text{in}$; wavelength scale - 26 $\text{\AA}/\text{in}$; Kodak ND-11 glass rod in 60 cm Fabry-Perot cavity, Q-spoiled with gold film, $D = 0.63$; $E_{\text{in}} = 900 \text{ J}$ ($5.6 \times$ threshold); $E_{\text{out}} = 1.5 \text{ J}$.

Fig. 6.4.2

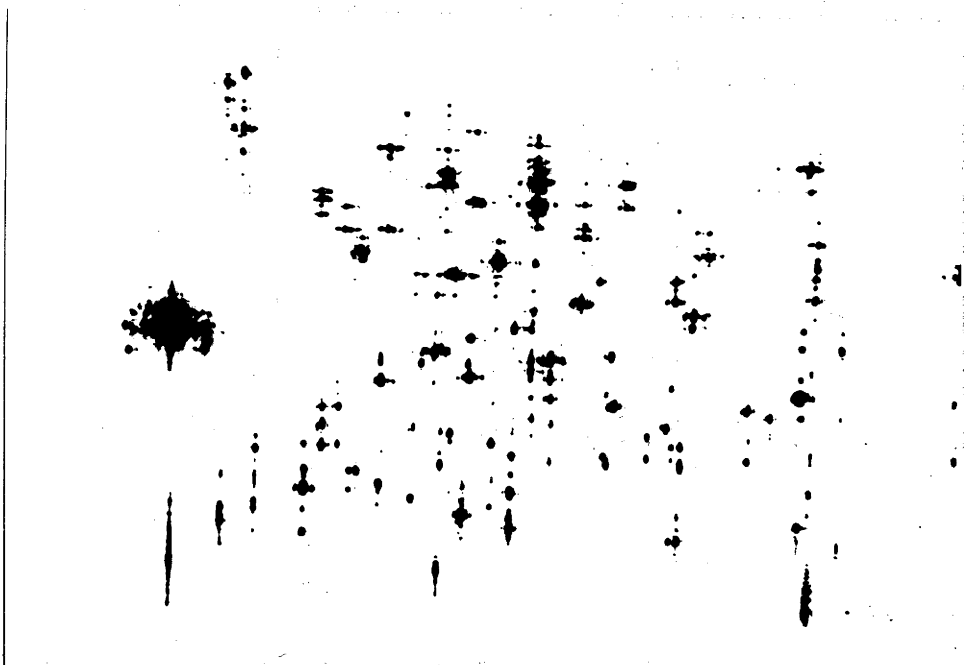


Plate #1-2 of 15-2-69: same parameters as fig. 6.4.1.

Fig. 6.4.3

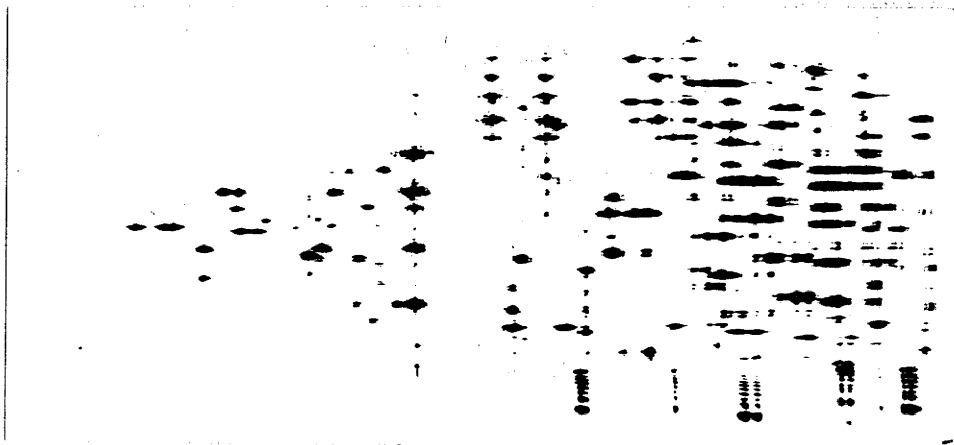


Plate #2-4 of 16-3-69: time scale - 59 $\mu\text{sec}/\text{in}$; wavelength scale - 32 $\text{\AA}/\text{in}$; Kodak ND-11 glass rod in 251 cm ring cavity, Q-spoiled with gold film, $D = 0.50$; $E_{\text{in}} = 1200 \text{ J}$ ($3.75 \times$ threshold); $E_{\text{out}} = 1.0 \text{ J}$.

Fig. 6.4.4

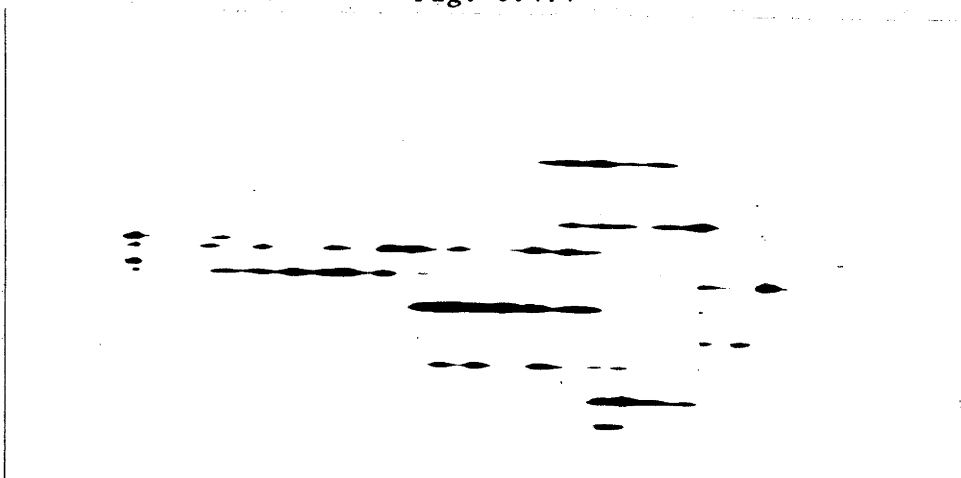


Plate #1-1 of 5-4-69: time scale - 39 $\mu\text{sec}/\text{in}$; wavelength scale - 21 $\text{\AA}/\text{in}$; Kodak ND-11 glass rod in 251 cm ring cavity, Q-spoiled with gold film, $D = 0.59$; $E_{\text{in}} = 1000 \text{ J}$ ($3.1 \times$ threshold); $E_{\text{out}} = 0.3 \text{ J}$.

Fig. 6.4.5

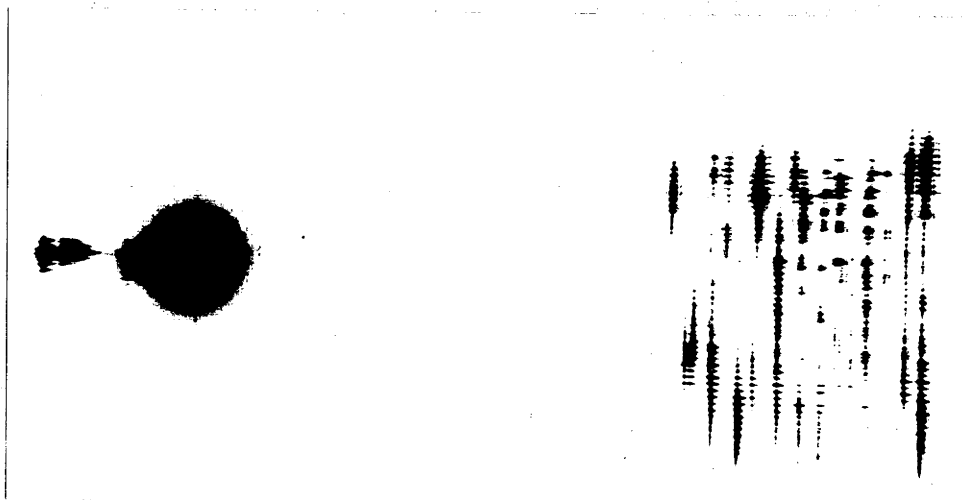


Plate #2-4 of 6-4-69: time scale - 38 $\mu\text{sec}/\text{in}$; wavelength scale - 31 $\text{\AA}/\text{in}$; Kodak ND-11 glass rod in 251 cm ring cavity, Q-spoiled with gold film, $D = 0.3$, on 0.038 mm thick mica plate; $E_{\text{in}} = 1400 \text{ J}$ ($4.37 \times$ threshold); $E_{\text{out}} = 1.2 \text{ J}$.

Fig. 6.4.6

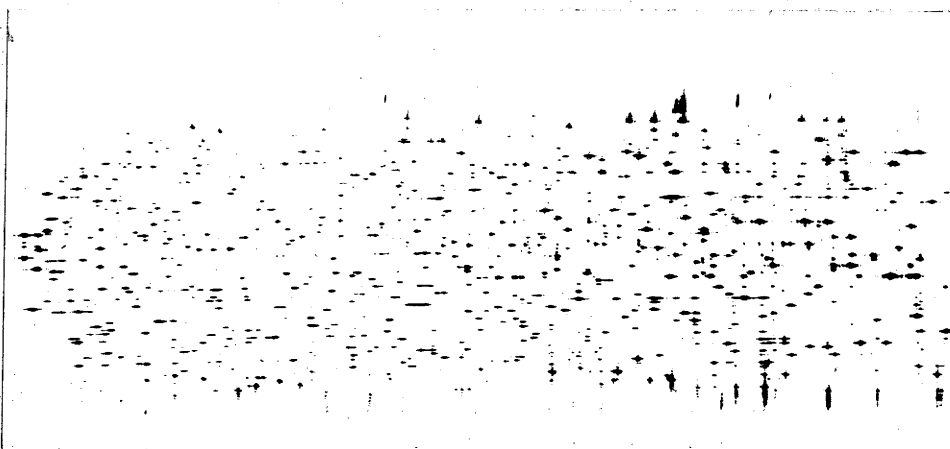


Plate #3-6 of 19-9-69: time scale - 86 $\mu\text{sec}/\text{in}$; wavelength scale - 46 $\text{\AA}/\text{in}$; Kodak ND-11 glass rod in 100 cm Fabry-Perot cavity with open Pockel's cell; $E_{\text{in}} = 1000 \text{ J}$ ($3.7 \times$ threshold); $E_{\text{out}} = 1.1 \text{ J}$.

Fig. 6.4.7

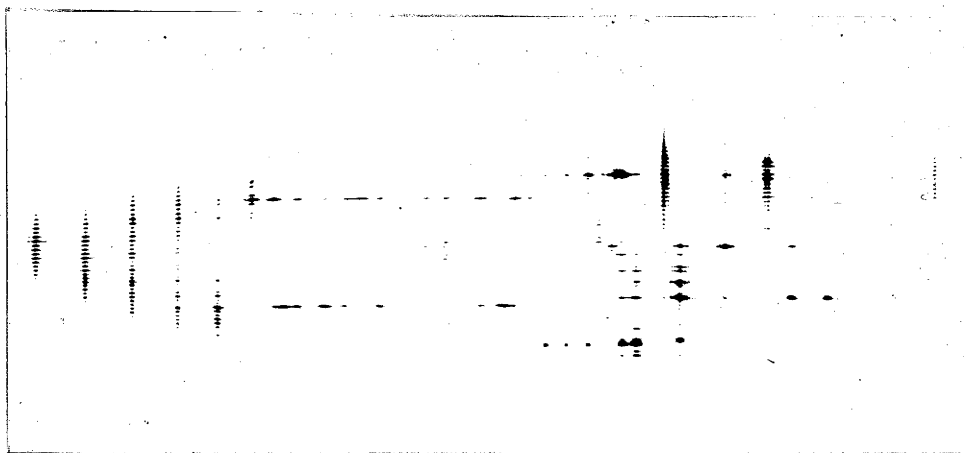


Plate #1-1 of 16-8-69: time scale - 96 $\mu\text{sec}/\text{in}$; wavelength scale - 52 $\text{\AA}/\text{in}$; Schott LG-56 glass rod in 251 cm ring cavity; $E_{\text{in}} = 800 \text{ J}$ ($1.95 \times$ threshold); $E_{\text{out}} = 1.0 \text{ J}$.

Fig. 6.4.8

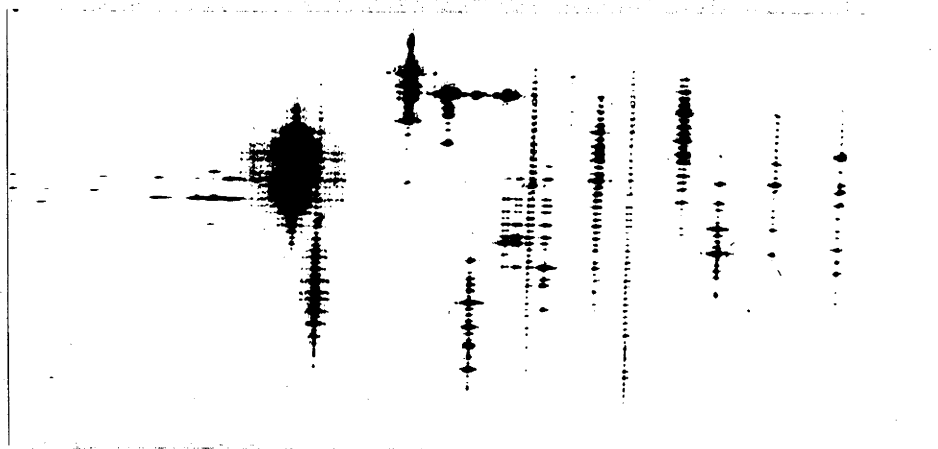


Plate #4-8 of 20-8-69: time scale - 51 $\mu\text{sec}/\text{in}$; wavelength scale - 27 $\text{\AA}/\text{in}$; Schott LG-56 glass rod in 251 cm ring cavity, Q-spoiled with gold film, $D = 0.24$; $E_{\text{in}} = 1400 \text{ J}$ ($3.4 \times$ threshold); $E_{\text{out}} = 0.24 \text{ J}$.

Fig. 6.4.9

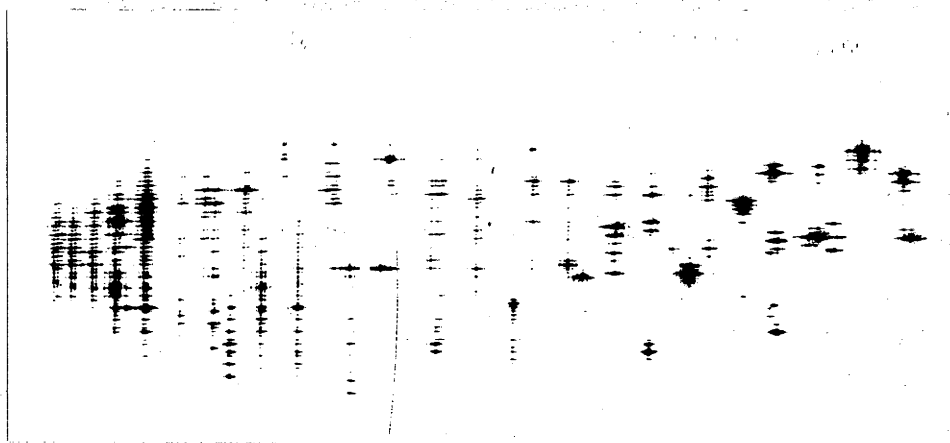


Plate #1-1 of 10-6-69: time scale - 79 $\mu\text{sec}/\text{in}$; wavelength scale - 42.5 $\text{\AA}/\text{in}$; Schott LG-56 glass rod in a 100 cm Fabry-Perot cavity with a Pockel's cell, Q-spoiled 100 μsec after the pump pulse begins, $E_{\text{in}} = 1200 \text{ J}$ ($4.0 \times \text{threshold}$); $E_{\text{out}} = 0.55 \text{ J}$.

pulses, and continues in a series of pulses for tens of microseconds. There is little or no relationship between pulses of adjacent modes. A good example of such behaviour is seen in fig. 6.4.6. This behaviour is typical of the normal laser and is similar to the results of Vanukov, Issayenko and Lubimov (1964).

Type II - Short Term Correlation of Adjacent Modes

This behaviour is usually associated with spectrally localized Q-spoiling. There is intense pulsing of several adjacent modes up to 10 \AA wide. Sometimes two such groups are correlated, with many missing modes in between. Correlation lasts only for the duration of the single pulse. See figs. 6.4.1 and 6.4.9.

Type III - Limited Correlation in Wavelength, extending over Hundreds of Microseconds

Each oscillating mode produces a train of pulses up to 200

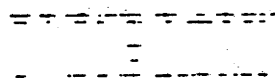
Fig. 6.4.10



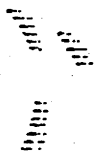
TYPE I



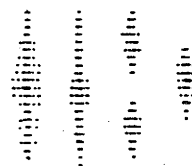
TYPE II



TYPE III



TYPE IV



TYPE V

Drawings illustrating the five pulse types.

usec long, with a period of 7 - 8 usec. Only two or three modes oscillate and may be up to 30 Å apart, while still exhibiting a high degree of correlation. See figs. 6.4.3, 6.4.4, 6.4.7 (especially).

Type IV - Dispersion in Time

Correlation lasts only for the duration of a single pulse, but extends over many Ångstroms, dispersed in time. That is, each mode starts oscillating at a progressively later time as wavelength is increased (or decreased). The dispersion is usually in the direction of the peak of the fluorescent line. Fig. 6.4.6 shows some indication of this type of pulse at the edges of the oscillation linewidth.

Type V - Correlation over the Entire Oscillating Linewidth

All the modes in a 30 - 40 Å wide band pulse simultaneously with a quasi-regular period of 7 - 8 usec (or some multiple) with a correlation time of 50 - 100 usec. See figs. 6.4.5, 6.4.7, 6.4.8, 6.4.9.

6.5. Discussion

6.5.1. Cross-Relaxation Rate

Figs. 6.4.1 and 6.4.2 are exceptionally good examples of hole burning in the peak of the fluorescent line and can be explained in no other way than by assuming that cross relaxation is slow compared to the length of the Q-spoiled pulse. Indeed, the oscillations in the lineshape take nearly 200 usec to die down, and give an estimate of the time for cross relaxation to re-establish

equilibrium. It should be noted that even without appreciable cross relaxation, the intense pulse has managed to deplete the central 15 \AA of the fluorescent linewidth. Cavity photons have been able to induce emission in ions with preferred emission frequencies displaced from the photon frequencies by tens of Angstroms by interacting with the wings of the stimulated emission cross section.

6.5.2. Q-Spoiled Pulse Spectral Width

A comparison of the streak plates according to method of Q-spoiling immediately suggests that there are systematic differences in the spectral widths of the Q-spoiled pulses. No streak photos were taken when a saturable dye absorber was used as Q-spoiler, because it invariably oscillated over a very narrow spectral range, typically one or two modes. By comparison, Q-spoiling with the Pockel's cell produced pulses whose width was in some cases greater than the acceptance range of the streak camera, i.e., greater than 80 \AA . When Q-spoiling is attempted with thin films, the pulse may be quite narrow spectrally, may consist of several narrow peaks across the fluorescent peak, or may consist of a single broad peak similar to the results obtained with the Pockel's Cell shutter, but rather narrower spectrally. The results of the dye and electronic shutter agree with those obtained by others (McFarland, Hoskins and Soffer 1965, Michon 1966). Sooy (1965) has suggested that this effect can be explained by the difference in time which the two systems allow for oscillations to build up. The argument is that longer times for oscillating modes

to build up allow greater selectivity between modes. In the case of the electronic shutter, this build-up time is the 10 nsec it takes for the shutter to open fully. On the other hand, dye solutions are always partially open ($D \sim 0.2$), and there is thus several tens of microseconds for oscillations to build up. The results of the high speed photography of the destruction of the thin films indicate that the speed of shutter opening for the films lies somewhere in between that of the dye shutter and the electronic shutter. However, this is not a valid approach. In fact, the dye shutter can switch from minimum transmission to maximum in a few psec. The real difference between the dye and electronic shutters lies in the minimum transmission. Dye shutters have densities of $\sim 0.2 - 0.5$, whereas the equivalent density of a good electronic shutter is $\sim 4 - 6$. The thin films used here ranged from $0.2 - 0.8$ in density and thus clearly fall into the same class as the dye shutters.

There are two reasons why the thin films do not behave in the same manner as the dye shutter. Sooy's discussion was based on considerations for ruby, which is homogeneously broadened. In this case, mode competition is very important since all modes are competing for the same population inversion. However, in an inhomogeneously broadened laser, coupling is only through population inversions that have overlapping homogeneously broadened lines and thus should be much weaker, assuming that cross relaxation is slow compared to the development of the Q-spoiled pulse. In fact, further consideration of the plates of the thin film Q-spoiling show that those exhibiting wide band Q-spoiling are associated with

the ring laser, and to a lesser extent, with the Schott glass rod. See table 6.1. (Since the transition from the broad band to narrow band Q-spoiled pulses is rather arbitrary, a pulse was assumed to be broad band if it belonged to two or more Type V pulses.) If the transition is inhomogeneously broadened, one would expect the oscillating linewidth to broaden with increasing population inversion, and this is just where broadening is more pronounced, since the threshold in the ring laser is considerably higher than in the Fabry-Perot cavity. It is due partly to the addition of an extra mirror, but mainly because the cavity length is four times longer (251 cm as compared to 60 cm). This situation also occurs in our case with the electronic shutter, because of higher cavity loss and because the timing of the shutter is delayed until late in the pumping pulse (minimum 100 μ sec). The implication is that the effects discussed by Sooy are not of major importance in a laser which is inhomogeneously broadened with slow cross relaxation, but one then has to explain the line narrowing observed with the dye solution. Our suggestion is that in a system involving a thick absorber such as a dye cell, preferred modes grow because of spatial hole burning at the maxima of the standing waves set up in the dye cell. For the dyes used with Nd^{3+} lasers this process could happen quite rapidly, and the preferred wave would experience considerably lower losses than all others. The homogeneity of the absorption line of the dye is thus the determining factor rather than the fluorescent line of the laser. There is good evidence that this does happen in such dye solutions, although Harrison, Key, Little, Magyar and Katzenstein (1968) attribute the diffrac-

Table 6.1. Breakdown of Streak Photographs into Wide and Narrow Band Pulses

GLASS TYPE	CAVITY TYPE	BAND WIDTH	
		NARROW	WIDE
Kodak	Fabry-Perot	10	0
	Ring	17	5
Schott	Ring	8	8

tion effects observed through the phase grating thus formed in the liquid (observed in a cross-beam experiment) to thermal inhomogeneities set up by the uneven absorption rather than arising directly from changes in the absorption.

6.5.3. Pulse Period

A large number of microdensitometer traces were made of the plates, with scans both in the time and in the wavelength direction, and although no reproductions will be presented here, the results will be given and can be compared with the figures of the streak photos themselves.

The most obvious periodicity is that associated with the giant Type V pulses. They all have peak powers of such magnitude as to class them as multiple Q-spoiled pulses, and multiple exposure photographs of a superposed train of them on the oscilloscope show that the peak output power is decaying monotonically. The inter-pulse period is between 7 and 8 μ sec, and sometimes

pulses appear which are a sub-multiple or multiple of this period, i.e., 3.5, 10.5 or 14 μsec .

There is even a limited periodicity observed in a single mode of Type I pulses. In this case the period is shorter, about 4 μsec , and less regular, and the peak power is not necessarily monotonically decreasing. All these pulses appear to have their origin in the gross dynamics of the inversion populations, and are damped out after 5 - 10 cycles. Further evidence that the pulses are due to inversion dynamics can be found in the Type III pulse trains observed in fig. 6.4.7. It is impossible for the coupling between these two pulse trains, separated by some 30 \AA , to be due to mode coupling through the interaction of non-linear susceptibilities. The computer solutions of the rate equations, discussed in §8, give similar results.

Careful inspection of the streak plates, however, shows that many pulses also possess a fine structure with a period of about 0.3 μsec (the limit of resolution of the streak photos), but which can be as long as 1.9 μsec . These are rapidly damped. Such oscillations do not appear in the computer solutions and it is difficult to imagine what sort of mechanism could be responsible for them. It is certainly not the quantum statistical properties discussed by Fleck (1970), as those fluctuations have periods in the sub-nanosecond range. Perhaps it is due to a beating effect between the 25 - 30 cavity modes associated with each resolvable sapphire etalon mode.

6.5.4. Comparison between Glasses

As might be expected from similar glasses, there are only minor differences in the gross features of the lasing pulses. The most obvious is the difference in the mean wavelength of the lasing line. In the Kodak glass, it is centred at $1.060\ \mu\text{m}$, whereas the Schott glass has its peak at $1.058\ \mu\text{m}$. In addition, the Schott glass was found to have a threshold 30% higher than the Kodak rod. This is due to a variation in the behaviour of the Nd^{3+} ions, since the optical quality of all the rods was checked on a Mach-Zender interferometer and found to be comparable. There appears to be a tendency for the Schott rod to produce regular Type V pulsations more easily than the Kodak rod. Certainly there are no instances with the Kodak rods of the behaviour shown in fig. 6.4.7, where the laser output both begins and ends with highly regular spiking. It is particularly noticeable on the oscillograms of the photodiode output. Some of this behaviour can be attributed to the higher threshold as mentioned in §6.5.2, but it is also possible that cross relaxation plays a less important part in the dynamics of the Schott rod, or that the homogeneous linewidth is narrower than in the Kodak rod.

57. TUNABLE NARROW BAND LASER

7.1. Introduction

If the laser can be forced to oscillate within a linewidth narrow compared to the natural linewidth, two aspects of laser operation can be investigated. In the first place, narrowing the spectral output limits the number of longitudinal modes which can participate to several hundred or less, thus giving an estimate of the effect of large scale mode interaction on the oscillations.

Secondly, forcing oscillation at one frequency and measuring the output gives an estimate of the amount of stored energy in the active medium available for oscillation at different wavelengths. If the medium possesses fast cross relaxation mechanisms, one should expect little difference in output whether the laser is constrained to oscillate at one wavelength or is free to oscillate over the entire width of the line.

In the sections which follow, a description is first given of the method used to force the laser to oscillate over a narrow bandwidth, and the alignment procedure. The results are then presented and discussed.

7.2. Method

Several authors (Wright, Carmichael and Brown 1965, Hercher 1965, Snitzer 1966, Magyar 1967) have discussed interferometric methods of achieving single mode operation, but these suffer from disadvantages which are important in an experiment of this type. They generally require precise optical flats and spacers in an arrangement which must be accurately aligned, and

they are tunable (if at all) only over a range over several Ångstroms. For these reasons, it was decided to attempt to use a diffraction grating as a frequency selective mirror in the cavity. Such an arrangement allows continuous tuning across the entire width of the transition but does not possess sufficient selectivity to force single mode oscillation.

The aluminised surface of the replica grating would be easily damaged by the high power density found in a laser cavity. Some experience with gold-plated optical flats used as mirrors in the cavity indicated that there was no possibility of successful operation unless the power density could be reduced significantly. A telescope can be used to expand the laser beam to fill the entire area of a grating and thus reduce the power density considerably, with the added advantage of decreasing the linewidth over which the laser oscillates. This is because the linewidth is determined by the acceptable angular divergence of the beam in the cavity which will maintain oscillations. The telescope magnifies any angular divergence of the beam leaving the grating and thus greatly increases the sensitivity of the cavity to the dispersive power of the grating.

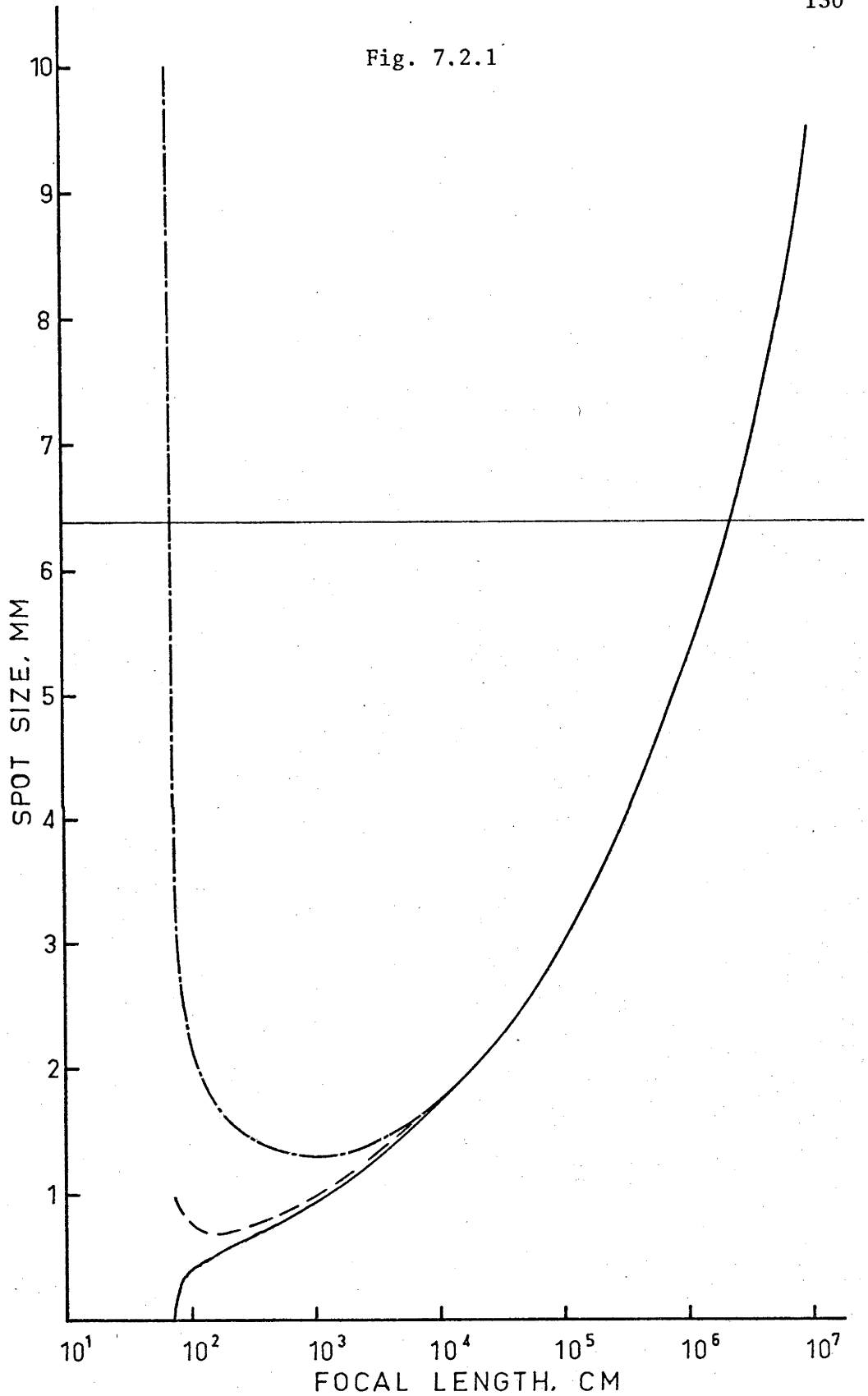
The arrangement used consisted of a 1 in. square grating, 600 lines/mm, blazed at $1 \mu\text{m}$, and a 4:1 beam expander constructed by C.S.I.R.O. Division of Physics, National Standards Laboratory and based on a design of a Galilean telescope by Gelles (1968).

One of the main problems with such an arrangement is to ensure proper adjustment of the telescope. If the spacing between lenses is not correct, the telescope behaves as a diverging or con-

verging lens and transforms the cavity into either a long radius or an unstable arrangement. This has three deleterious effects. Firstly, the angular acceptance of the system increases with a loss in frequency selectivity of the grating. Secondly, there is the possibility of a divergent beam being focused on the grating or the exit mirror, with disastrous consequences. Thirdly, the transverse mode structure of such a system may be significantly different from the Fabry-Perot modes, and studies of the effects of the number of modes on laser spiking would be difficult to interpret.

An investigation of the variation of beam profile for long radius resonators suggested the following considerations. One can consider the cavity to consist of a plane mirror (the output mirror) plus a second mirror of variable focal length. Cavity losses will be lowest for the TEM_{00} mode, and these increase as the focal length of the second mirror increases, until the plane mirror configuration is reached. Any further change in radius of curvature will drastically increase losses in the beam, because negative curvature produces an unstable resonator configuration. Fig. 7.2.1 is a graph of the size ($1/e$) of the TEM_{00} mode, (a) at the plane mirror, (b) 72 cm from the plane mirror, and (c) 250 cm from the plane mirror, as a function of the focal length of the second mirror in the cavity. A line is drawn to indicate the diffraction-limited spot size of the 1/4 in. diameter laser rod. Thus, a careful comparison of beam spot size with and without the telescope will ensure that the resonator is very close to a plane parallel configuration, and monitoring of the threshold as adjustments are made on the telescope will indicate if the curvature has become negative.

Fig. 7.2.1



Spot size ($1/e$) of the TEM_{00} mode for a 60 cm cavity with one plane mirror and one curved mirror, as a function of the focal length of the curved mirror; at the plane mirror (solid line), 72 cm from the plane mirror (broken line), and 250 cm from the plane mirror (broken and dotted line).

7.3. Procedure

The initial adjustment of the telescope was carried out using a 1 in. diameter, 100% reflecting plane mirror rather than the diffraction grating. The arrangement was first centred and aligned using a He-Ne laser and the beam expander adjusted for a compromise between useful beam output and possibly converging optics, as described above. Photographs were taken of the visible output produced by allowing the beam to impinge on a sheet of Kodak I.R. phosphor at various distances from the output mirror, to determine if a beam waist occurred. Adjustment was deemed satisfactory when no waists could be found and when the beam profile was similar to that obtained without the telescope.

The grating was then substituted for the 100% mirror. It had previously been approximately aligned using a lens and slits mounted on the optical bench and the 5350.57 Å thallium line in second order. The centre of the laser line could be set to ± 1 Å by comparing the output of the laser at the focal plane of the spectrograph (in second order) using the Kodak phosphor and fiducial marks established from argon spectral lines. With the laser tuning grating in first order at 1.06 μm , the linewidth was found to be about 15 Å and it was therefore decided to use the grating in second order to give a narrower linewidth.

Measurements of the grating reflectivity for various orders using a He-Ne laser indicated that the grating was blazed in second order at the -2 position relative to the first order blaze and this was confirmed by threshold measurements with the laser. A check on the spectrograph grating indicated the same conditions and

henceforth it also was used in the -2 position. With the grating in second order, linewidth was always less than 5 \AA and usually was $\approx 3 \text{ \AA}$.

A series of measurements was then taken at various wavelengths and different output energies in order to yield curves from which threshold and slope efficiency could be obtained for each wavelength.

7.4. Results and Discussion

Fig. 7.4.1 is a reproduction of a sweep camera plate of the laser output with the telescope inserted and the 100% mirror used instead of the grating. A careful examination of this plate and the oscillograms of the output when the grating was used to tune the laser indicates that there is no apparent change in the spiking output due to the telescope or to the number of modes having been reduced by a factor of 10 or more to less than 500.

Figs. 7.4.2, 7.4.3, 7.4.4 and 7.4.5 are the graphs of the slope efficiency and the square root of the slope efficiency versus wavelength for a Kodak laser rod and the Schott glass rod. A graph of the reciprocal of the threshold versus wavelength is superposed on each of these for comparison, and all are normalized to unit area.

We note from eqn. (4.2.20) that the reciprocal of the threshold is proportional to the lineshape function $g(\nu)$. In addition, with no cross relaxation, the slope efficiency should be roughly proportional to the square of the lineshape [eqn. (4.3.20)], and with very fast cross relaxation, there should be little depend-

Fig. 7.4.1

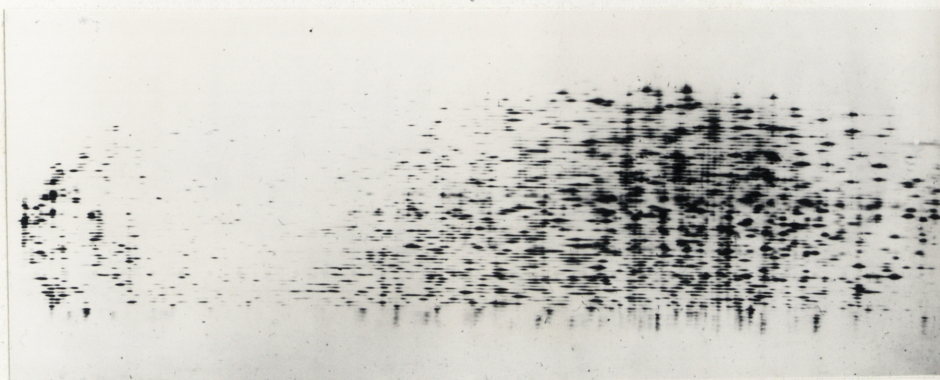
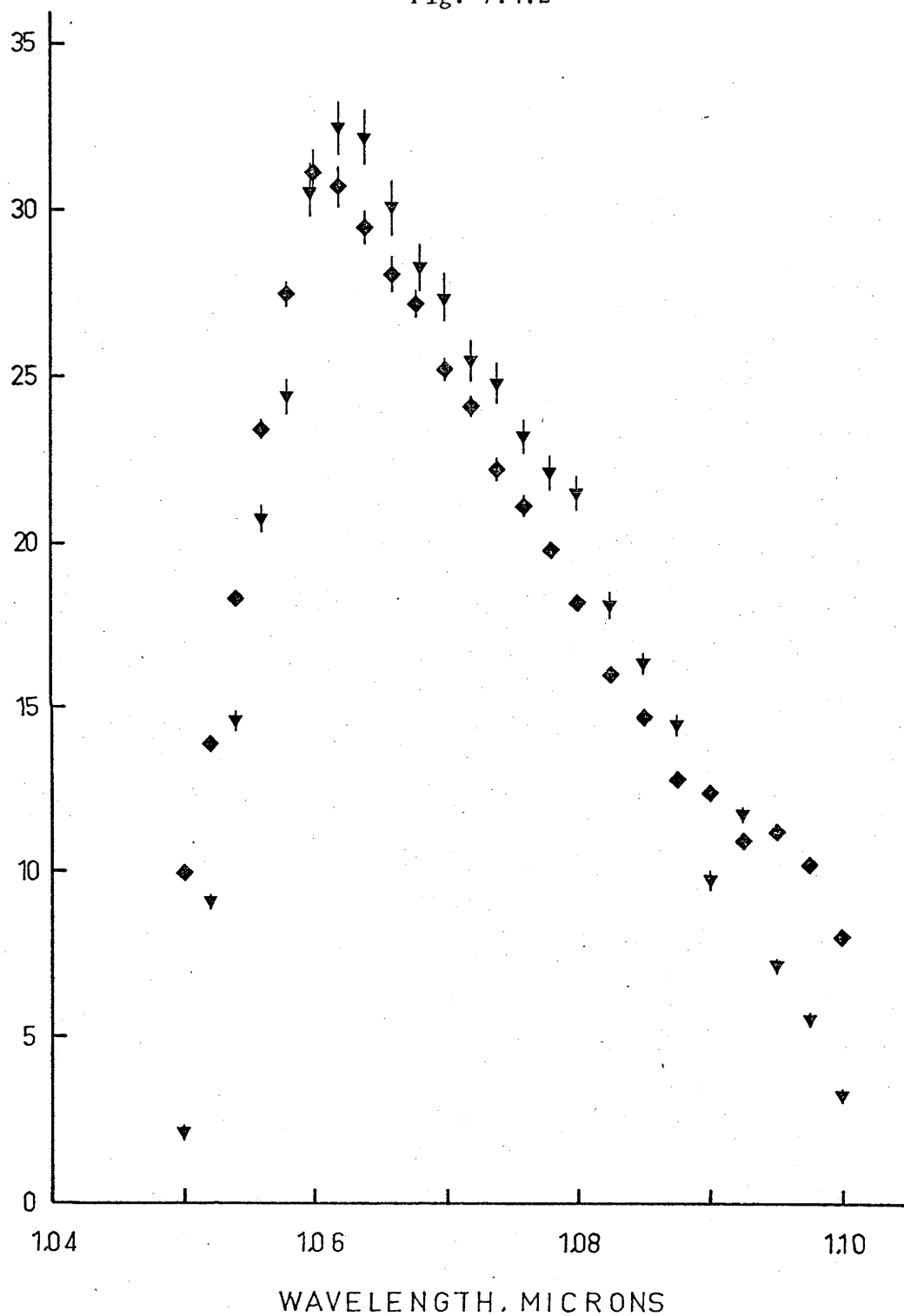


Plate #1-1 of 15-10-69: time scale - 101 $\mu\text{sec/in}$; wavelength scale - 54 \AA/in ; Kodak Nd-11 glass rod in 60 cm Fabry-Perot cavity with grating and telescope; $E_{\text{in}} = 800 \text{ J}$; $E_{\text{out}} = 1.15 \text{ J}$.

ence of slope efficiency upon the wavelength [eqn. (4.3.17)].

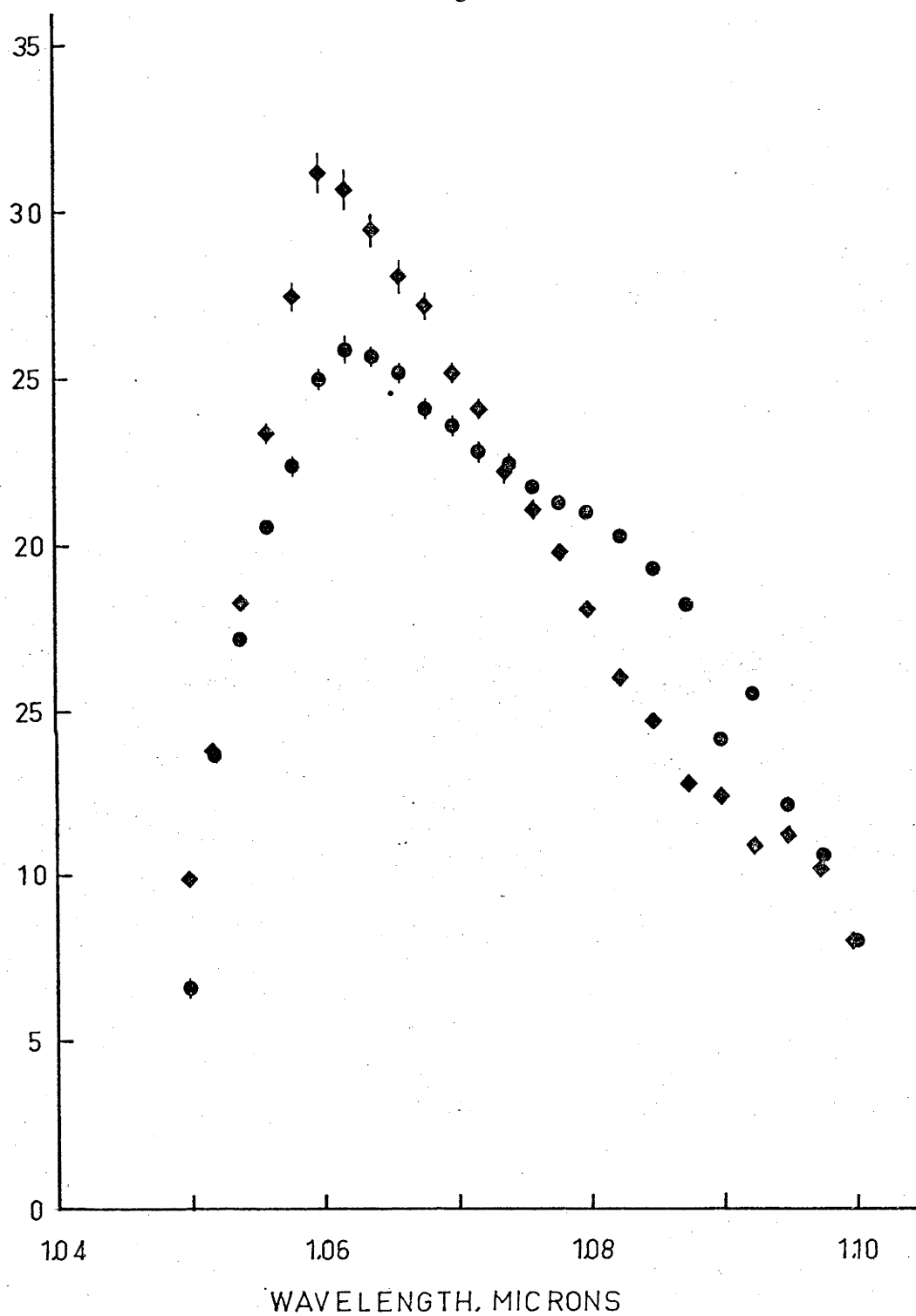
The gross discrepancies between theoretical prediction and experimental results illustrate a number of important shortcomings of the theory. Consider the graphs for the Kodak rod. There is an indication of a slight flattening at the peak of the slope efficiency curve compared to the reciprocal of the threshold. This is attributed to cross relaxation taking place over populations which have centre frequencies near the peak, but it is limited to relaxation between ions with an energy defect less than $\sim 45 \text{ cm}^{-1}$. However, if one remembers from §2.6 that the splitting of the ${}^4\text{F}_{3/2}$ level means that the degeneracy of the ${}^4\text{I}_{11/2}$ level must also be completely removed, then the fluorescent line must be

Fig. 7.4.2



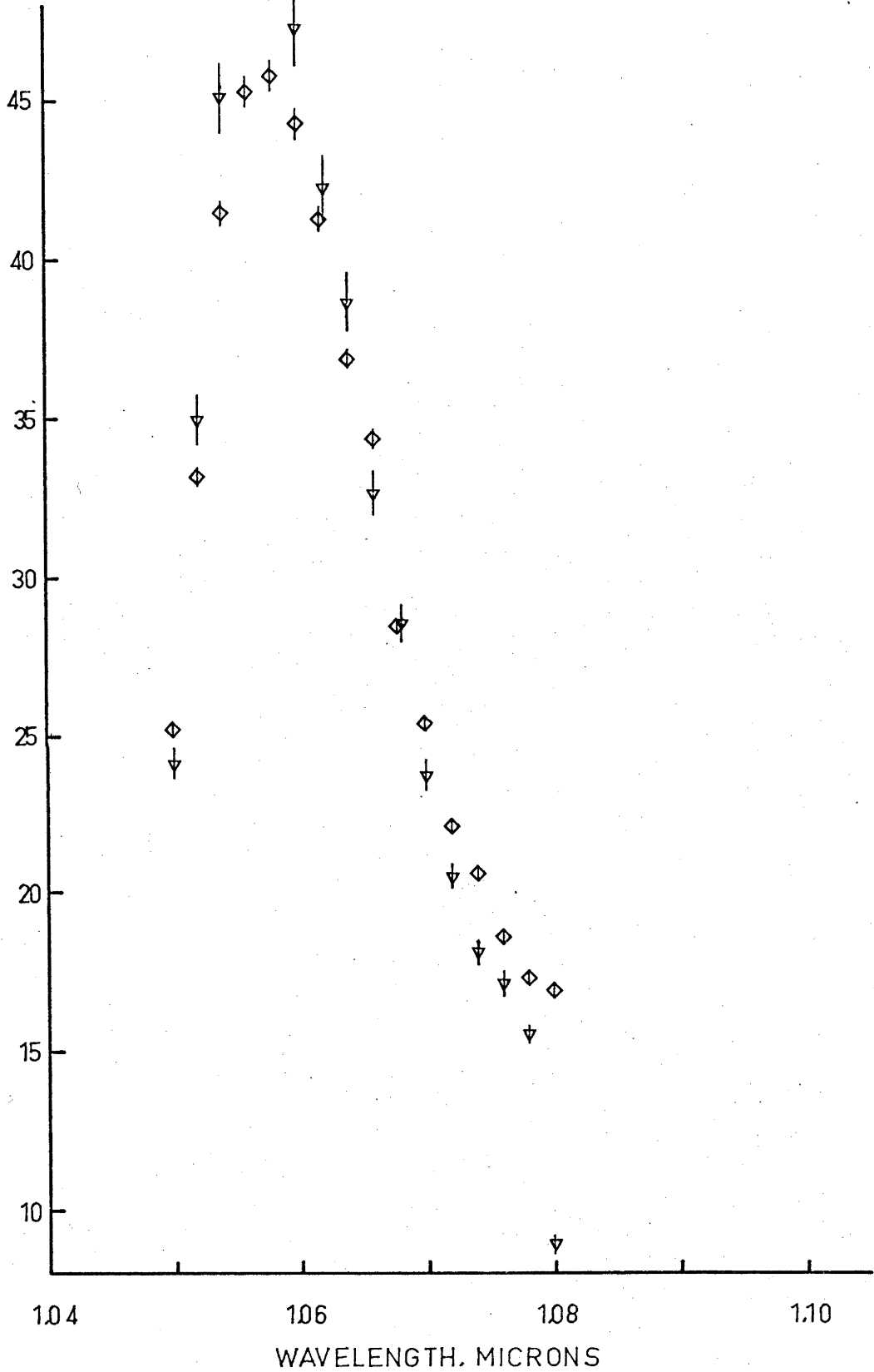
Normalized slope efficiency (triangles) and reciprocal of the threshold (squares) as a function of wavelength for Kodak ND-11 glass.

Fig. 7.4.3

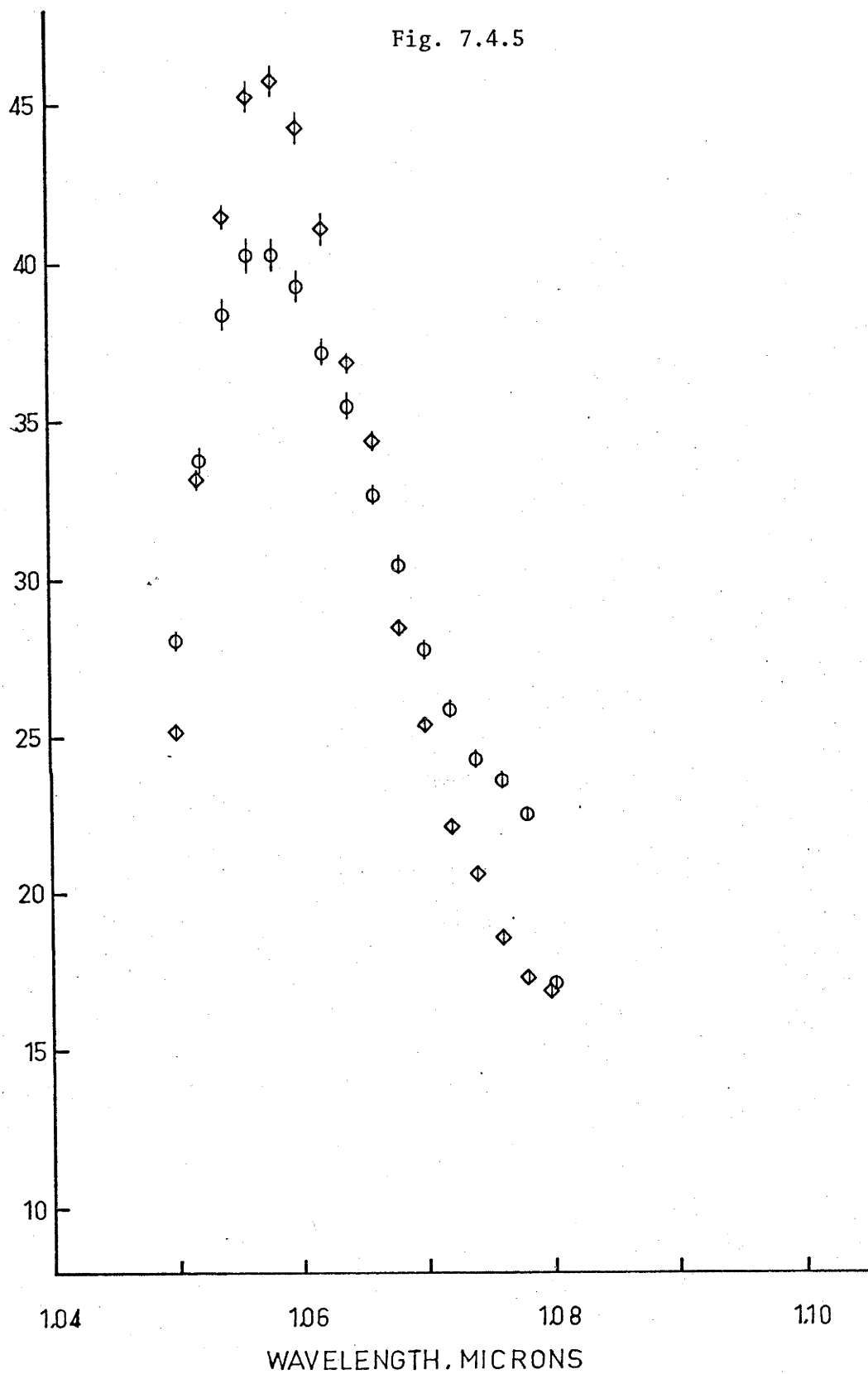


Normalized square root of slope efficiency (circles) and reciprocal of the threshold (squares) as a function of wavelength for Kodak ND-11 glass.

Fig. 7.4.4



Normalized slope efficiency (triangles) and reciprocal of the threshold (squares) as a function of wavelength for Schott LG-56 glass.



Normalized square root of slope efficiency (circles) and reciprocal of the threshold (squares) as a function of wavelength for Schott LG-56 glass.

a composite of the twelve possible transitions between the two split metastable sublevels and the six terminal state sublevels. The broadening of the efficiency peak is then seen as a manifestation of cross relaxation between inhomogeneous ions in one ${}^4F_{3/2}$ level (probably the lower) as observed in its major transition. If the other transitions could be resolved, they also would be seen to be broadened. Even if only a portion of the fluorescent line is not coupled through cross relaxation, the shape of the slope efficiency curve for that part should be proportional to the square of the lineshape function. This is not the case, and it further illustrates defects in the theory. By relating the lineshape function to the fluorescent lineshape the tacit assumption has been made that the peak stimulated emission cross section is not a function of centre frequency, and that the lineshape is due to different number densities of ions with different centre frequencies. In fact, the fluorescent lineshape is due to a superposition of the transitions to different sublevels of the ${}^4I_{11/2}$ level, and each has a different stimulated emission cross section. The lineshape arises from different transition probabilities rather than number densities.

It is true that all the transitions making up the fluorescent line have their source in the same two sublevels and, in this sense, reduction in the inversion by lasing at one wavelength will reduce the fluorescence in the other transitions which have the same ${}^4F_{3/2}$ sublevel as a source. This is the reason why Michon (1966) and Boyden and Clark (1966) were able to conclude that the line exhibited very fast cross relaxation. In Michon's experiment, a Brewster angle rod was Q-spoiled with a rotating

prism and the change in fluorescence was observed by looking down the end of the rod. This Q-spoiled pulse was 20 Å wide and would thus completely deplete the inversion through the major transition whether or not there was any cross relaxation. In addition, by monitoring fluorescence through the end of the rod one observes a combination of super-radiance and scattered laser energy. Boyden and Clark monitored the fluorescence of a rod used as an amplifier for a Q-spoiled pulse produced by a $\text{Nd}^{3+}:\text{CaWO}_4$ rod, which lases at 1.06524 μm with a 10 Å bandwidth (DeShazer and Maunder 1968). When one also considers the wing depletion effect mentioned in §6.5.1, it is easy to see that any cross relaxation is unlikely to be detected in this experiment. The experiments of Belan, Gregoryants and Zhabotinski (1969) are difficult to interpret because too few details are given but, for it to be successful, the Q-spoiled pulse must have been narrow band, either through the use of filters or by the optical arrangements. In any case, their value of 10^4 sec^{-1} for the cross-relaxation rate is the same as indicated by our streak photos (§6.5.1) and is consistent with the small flattening observed in the experiments described in this section. In fact, such a slow rate means that the relaxation time constant is of the same order as the pump pulse length used in our experiments, with the result that any flattening of the slope efficiency peak due to cross relaxation will be considerably attenuated.

§8. COMPUTER SIMULATION OF LASER RATE EQUATIONS

8.1. Introduction

One of the main problems in the understanding of the behaviour of solid state lasers has been to explain the existence of pulsations, often highly irregular, in the output. In glass, three types of pulsations have been described. The first is the type observed in all our experiments and is the most common. The output consists of a series of spikes random in time and amplitude with a half width of ~ 1 μ sec and a peak power of 2 - 5 kW, and generally has a narrow angular divergence. This random spiking is characteristic of glass rods of high optical quality, especially where steps have been taken to suppress trapped internal modes (so-called "whispering modes"), e.g., by giving the rod surface a ground-glass finish. The second and third types occur if clad rods or fibres are used. In these cases, the output may consist of periodic pulse trains whose amplitude follows the shape of the pump pulse (limit cycle operation), or it may exhibit ringing at the beginning and thereafter follow the shape of the pump pulse (damped oscillations). See Snitzer (1964). Attempts to relate the observed spiking to theory have been largely unsuccessful. Makhov (1962) and Sinnett (1962) have shown that the rate equations for a two level system with a homogeneously broadened line and a single oscillating mode do not admit random spiking or limit cycle solutions. Limit cycle behaviour can be introduced by the addition of a term involving some power of the inversion, but there is no physical basis for it. Korobkin and Uspenskii (1963) were able to demonstrate limit cycle operation in a similar system by introduc-

ing a frequency shift term between the polarization of the medium and the electric field of the stimulated emission and have attempted to relate this to the behaviour of ruby, which is adequately described by a two level system with homogeneous broadening. In fact, ruby can be made to show limit cycle behaviour if care is taken to force oscillation in a single longitudinal mode. It appears that in ruby, the major cause of irregular spiking is due to "mode hopping". This effect is due to spatial inhomogeneities in the inversion as a result of the standing waves of a Fabry-Perot resonator. As one mode depletes the cavity volume available to it, another mode soon has sufficient gain to break into oscillation and replaces the previous one. Fleck and Kidder (1964) have considered the case of an arbitrary number of oscillating modes in a homogeneously broadened two level system, using a density matrix formalism. They include terms which couple the various modes through non-linear susceptibilities and are able to arrive at limit cycle and irregular spiking behaviour in computer simulations for the case of two coupled modes. The non-linear behaviour of the medium is due in part to spatial inhomogeneities introduced by the Fabry-Perot resonator, as previously discussed, and in part to radial inhomogeneities in the pumping rate. Moreover, the assumption of pumping inhomogeneities appears to be essential for limit cycle or irregular spiking behaviour, and it is through the coupling of off-axis modes that this is accomplished. However, it is difficult to believe that off-axis modes are excited to any great extent in Fabry-Perot cavities with laser rods of high optical quality. This is especially true if the cavities are long. Another conclusion

which certainly contradicts experimental evidence is that irregular spiking is observed for "moderate" pumping inhomogeneities, whereas the spiking becomes regular for "severe" pumping inhomogeneities.

Nd^{3+} can be realistically approximated by a three level scheme with inhomogeneously broadened lines, but a two level approximation is not likely to be a valid description of the population when periods as short as a single spike are concerned. It is possible that absorption by the terminal level could lead to limit cycle or irregular behaviour, as could the cross relaxation interaction, and it was thought desirable to investigate these possibilities. However, the investigation of the stability of the coupled equations (4.2.13) - (4.2.17) by analytical methods is a formidable if not impossible problem and recourse to computer simulation of the equations was adopted.

8.2. Computer Simulation

8.2.1. Numerical Integrator

Early solutions of the rate equations were obtained from an analog computer and were subsequently found to be in error (see Makhov 1962), indicating that great care should be taken to make certain that the numerical integration method used is stable at all times. The requirement that stability and truncation error be monitored for each step means that some form of predictor-corrector method must be used and that change of step size should be accomplished without an undue amount of re-computation. The routine finally chosen is based on a method of Nordsieck (1962), who originally developed it for a fixed point binary machine, and modified

for floating point use by R.H. Hudson (C.S.I.R.O.) and I.R. Simpson (A.N.U.). It has a number of advantages which make it suitable as a general integrator. Because the stored constants are the coefficients of a truncated Taylor expansion of the approximation polynomial, rather than the coefficients of the polynomial itself, changes in step size are particularly simple and fast. Stability and truncation error are continuously monitored and the step size adjusted automatically (within prescribed limits) to satisfy the tests. In addition, the integrator is self starting. Tests were made with our program using both single and double precision arithmetic to see if round-off errors could be significant, but with no appreciable differences even after thousands of iterations. Since the integrator had previously been tested exhaustively by Nordsieck himself and by Simpson, it was considered that it should behave satisfactorily.

8.2.2. Method of Computation

Equations (4.2.13) - (4.2.15) (three level approximation) and (4.2.16), (4.2.17) (two level approximation) could be investigated by the same program by making minor changes to several of the subroutines, and the discussion below on the three level approximation applies as well to the two level approximation. The three derivatives as a function of frequency were approximated by $3N$ simultaneous differential equations, where $N_{\max} = 20$ is a practical upper limit above which computer time becomes excessive. The definite integrals in the equations are evaluated by a modified Simpson's rule. The problem is somewhat simplified by considering

both $g(\nu)$ and $\sigma(\nu, \nu')$ to be symmetric functions, and storing only one half of the function values. This quantization of the equations as a function of frequency simulates very closely the actual case of a Fabry-Perot cavity with its discontinuous mode structure, but such a coarse grid means that the quadratures involving $\sigma(\nu, \nu')$ are rather poor approximations to the definite integrals, since $\sigma(\nu, \nu')$ is a rapidly varying function of frequency. However $\sigma(\nu, \nu')$ is not a function of time and one should expect the quadrature estimates to be in error by the same proportion for all frequencies and thus have no effect on the general behaviour of the system. Provision was made in the program to investigate the effect of a variety of lineshapes but, due to computer time limitations, the investigation was restricted to the case where $g(\nu)$ was a Gaussian with full width at half maximum of 133.5 cm^{-1} (150 \AA), centred at $1.06 \text{ }\mu\text{m}$, and $\sigma(\nu, \nu')$ was a Lorentzian with full width at half maximum of 8.9 cm^{-1} (10 \AA). The peak absorption cross section was assumed to be 10^{-20} cm^2 and the ion number density $1.66 \times 10^{20} \text{ ions/cm}^3$. Following calculations of Cabezas and Treat (1966), a pump rate of 100 sec^{-1} was used. The cavity parameters were chosen to approximate those used in our experiments, namely, a cavity length of 50 cm and a laser rod $6 \frac{1}{2} \text{ in.}$ long with a 75% output mirror. The fluorescent decay time constant was assumed to be $360 \text{ }\mu\text{sec}$, and simulation runs were made for cross relaxation rates of 0 , 10^4 sec^{-1} and 10^6 sec^{-1} .

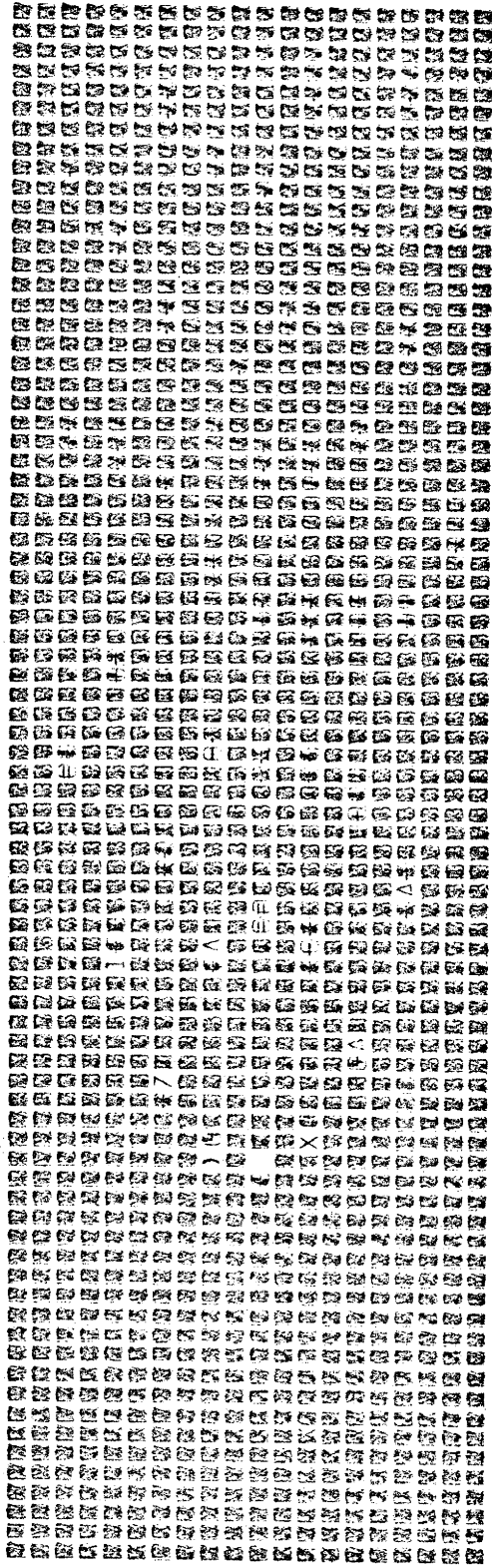
Some mention should be made of the method of introducing initial conditions, and the values used. By referring to eqns. (4.2.13) - (4.2.15), one can see that if the photon flux density is

initially zero, and the term in β (the fluorescence contribution) is also set to zero, no stimulated emission takes place and the normalized inversion density rises to its equilibrium value of $W_p / (A_3 + W_p)$. The term in β is a forcing term for the system and represents fluorescent photons emitted into the cavity modes. The fraction coupled into the modes of the cavity will be approximately equal to the solid angle subtended by the rod cross section and the cavity length. Thus, considering a single excited ion, whether or not it emits a photon into the cavity modes is a random experiment of two outcomes. This leads to a Poisson distribution when large numbers are involved. In the computer simulation, all variables and their derivatives were initially set to zero and the pump light introduced as a step function. An inversion then starts to build up and the fluorescence is used to prime the stimulated emission through the term β in such a manner that $\beta n(\nu)$ is a Poisson variable with an expectation equal to the mean number of photons which are emitted into the cavity. The Poisson distribution is generated by a method described by Hufnagel and Kerr (1969) from a normal random variable.

8.3. Results and Discussion

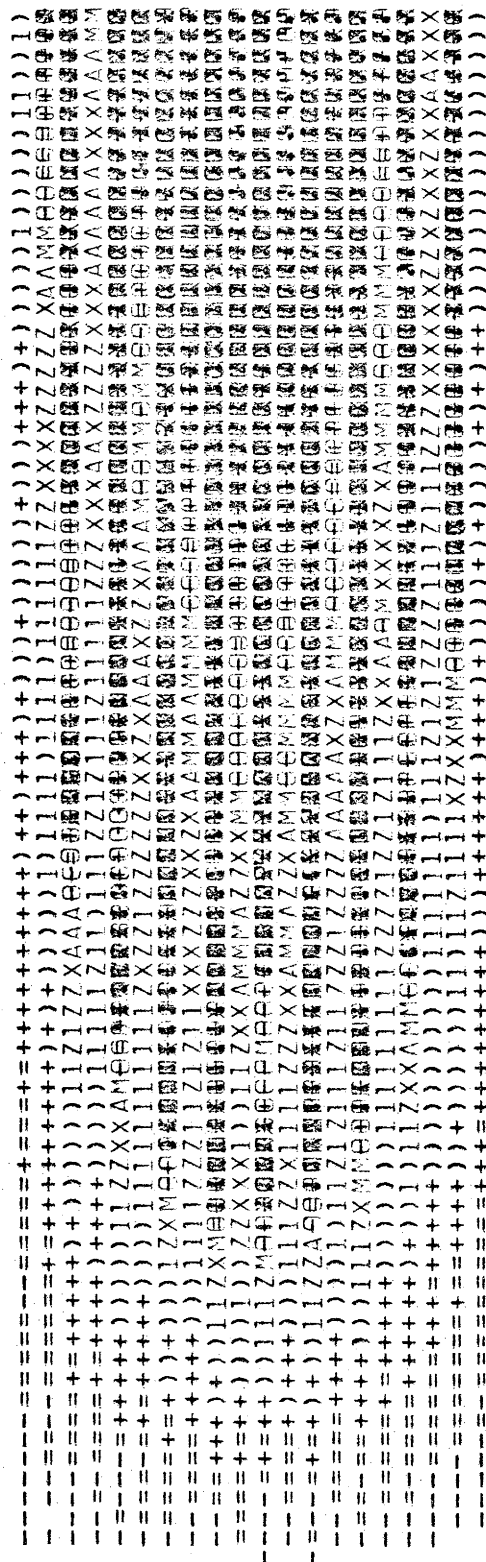
Figures 8.3.1 - 8.3.6 are density plots of $\phi(\nu, t)$ and $\log_{10} \phi(\nu, t)$ for cross relaxation rates of 0, 10^4 and 10^6 sec^{-1} , plotted on the computer's line printer using a routine supplied by MacLeod (1970). Fig. 8.3.7 is a representative plot of the graphs of $\phi(\nu, t)$ versus t for four adjacent wavelengths. A normalized photon density of 10^{-7} corresponds to a peak power output of 5 kW

Fig. 8.3.1



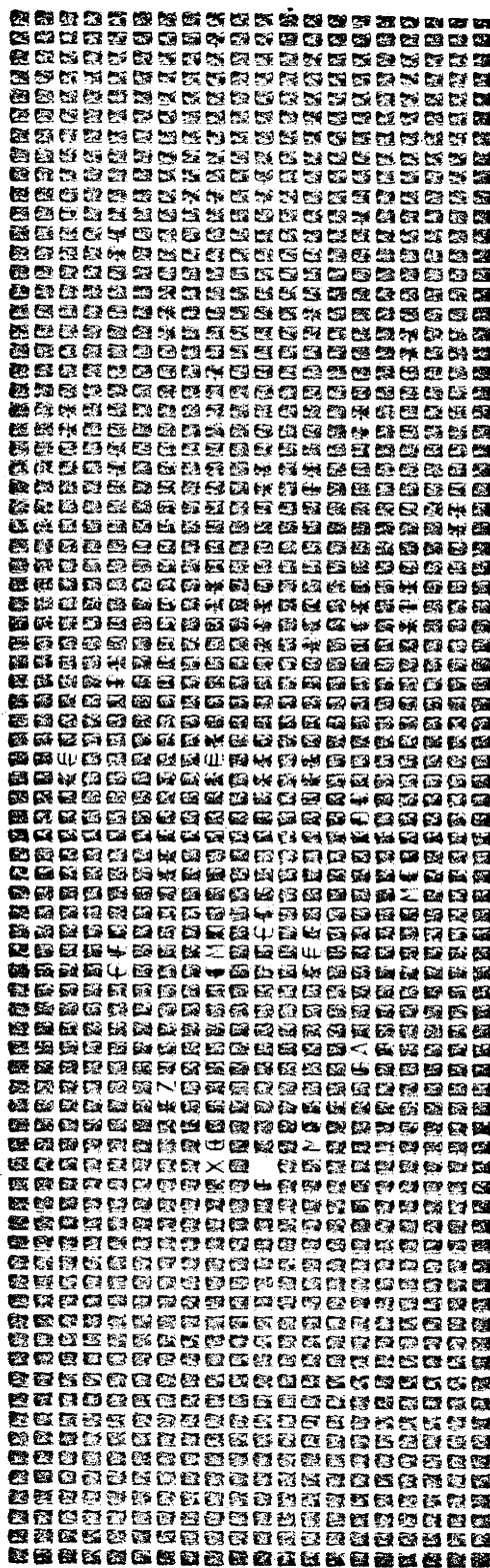
Density plot of $\phi(v, t)$ for cross-relaxation rate = 0.

Fig. 8.3.2



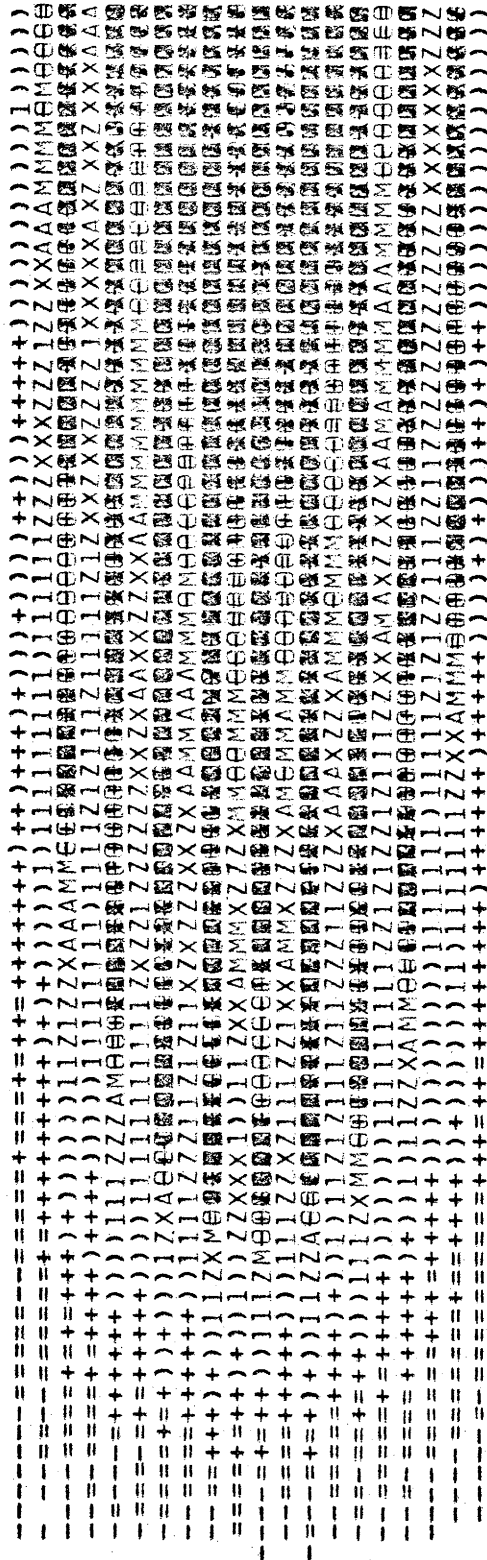
Density plot of $\log_{10}[\phi(v,t)]$ for cross-relaxation rate = 0.

Fig. 8.3.3



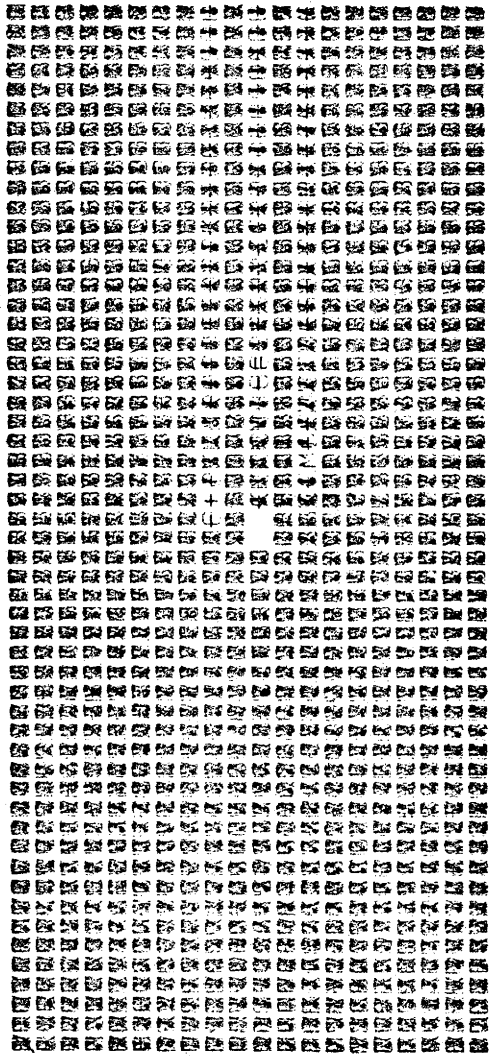
Density plot of $\phi(\nu, t)$ for cross-relaxation rate = 10^4 sec^{-1} .

Fig. 8.3.4



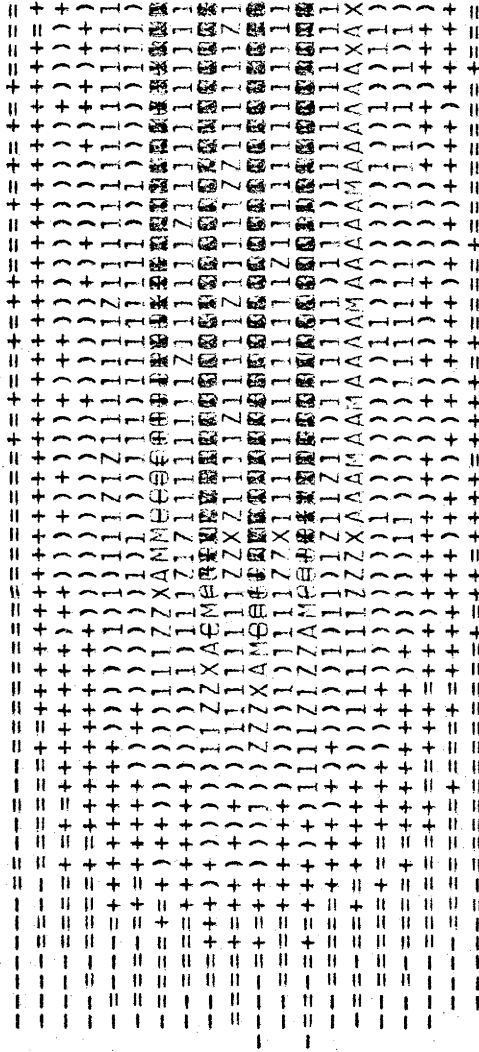
Density plot of $\log_{10}[\phi(v,t)]$ for cross-relaxation rate = 10^4 sec^{-1} .

Fig. 8.3.5



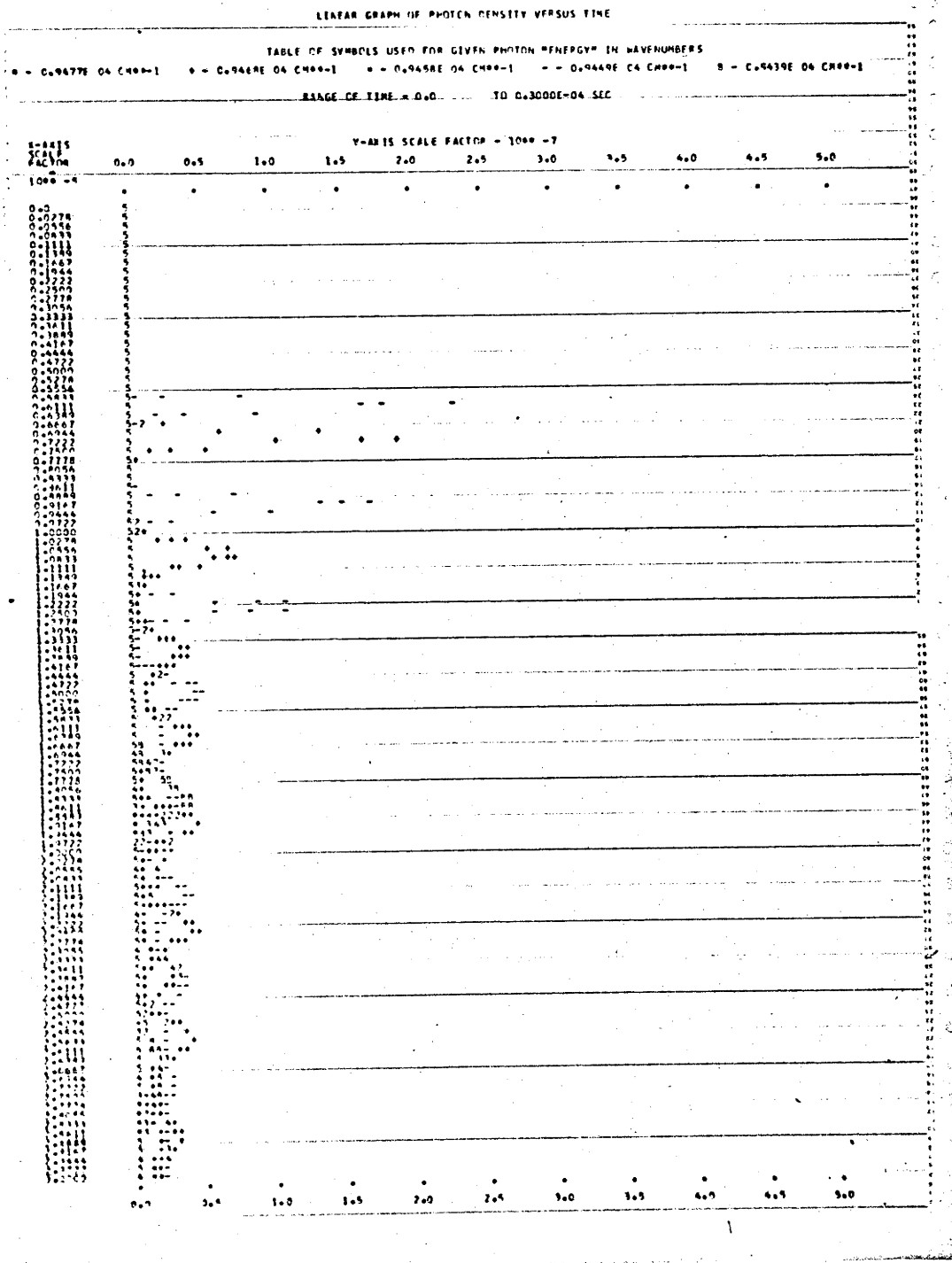
Density plot of $\phi(\nu, t)$ for cross-relaxation rate = 10^6 sec^{-1} .

Fig. 8.3.6



Density plot of $\log_{10}[\phi(v,t)]$ for cross-relaxation rate = 10^6 sec^{-1} .

Fig. 8.3.7



Graph of photon density versus time for cross-relaxation rate = 0:
 * - $0.9477 \times 10^4 \text{ cm}^{-1}$; + - $0.9468 \times 10^4 \text{ cm}^{-1}$; = - $0.9458 \times 10^4 \text{ cm}^{-1}$;
 - - $0.9499 \times 10^4 \text{ cm}^{-1}$; B - $0.9439 \times 10^4 \text{ cm}^{-1}$.

using a 1/4 in. diameter laser rod and a 75% reflectivity output mirror.

All the solutions are seen to correspond to transient oscillations and thus the equations do not admit limit cycle or random spiking solutions. In addition, careful appraisal of equivalent runs for the three level and the two level approximations fails to disclose any appreciable differences. One is thus forced to the conclusion that inhomogeneous broadening, with or without cross relaxation, fails to provide the necessary instability for spiking to occur. This is also true of absorption of the cavity photons by the terminal level which has been considered in the three level approximation. The results are still of interest, however. Whatever the mechanism responsible for the random continuous spiking, it appears to be generally agreed that its effect is to shock excite these transient oscillations, or to somehow modify them so as to make them unstable. There appear to be no other mechanisms which give the same order of magnitude of pulse train period. Several aspects of the model solution should apply to a real laser. This is true because the population dynamics are adequately described before the oscillations are damped out. First of all, even with very rapid cross relaxation, lasing can take place over much of the central portion of the linewidth. This is in agreement with the results of Peressini and Linford (1968), who considered the steady state solutions of the rate equations [eqns. (4.3.1) and (4.3.2)] to arrive at a criterion for oscillation linewidth. In addition, some evidence can be seen in our solutions of the spectral peaking observed by them. The

initial transient spiking observed in our solutions occurs over a much broader band than their results, but this can be related to the slower cross-relaxation rates we investigated.

Secondly, the computer solutions correctly simulate the random behaviour of the spiking of different modes observed in a real laser. Compare fig. 8.3.2 with fig. 6.4.6, which is a streak spectrogram of a normally oscillating laser. In the simulation, each mode begins oscillations when threshold is reached, nearly independent of adjacent oscillating modes. Nearest neighbour modes are inhibited from spiking, and as the cross relaxation rate increases, fewer modes begin spiking. There appears to be more correlation between the spiking of the modes as they are coupled to a common power source and sink.

Thirdly, it is clear that the simplistic model of the noise driving source used here, while providing a suitable random starting flux, does not have sufficient variance (even with the help of the inhomogeneous broadening) to cause the instability needed for random spiking. The observed pulsations seem to require a model in which the population inversion is depleted sufficiently for the stimulated emission to become the same order of magnitude as the background fluorescence into a given mode. Fluctuations then introduce uncertainty into the starting time of the next pulse. In other words, if the rate equations can be made to exhibit limit cycle behaviour, a suitable random driving source would provide the observed random spiking. While it is true that the simulations were investigated only for a few parameter variations, spiking is a quite general phenomenon in solid state lasers

and thus appears to be relatively parameter independent. If certain gross features of the dynamics, such as the existence of inhomogeneities, cannot cause the rate equations to become unstable, then another approach must be used in the description of laser dynamics.

§9. DISCUSSION AND CONCLUSIONS

9.1. Line Broadening and Energy Transport within the Line

First of all, consider the group theoretical results of §2. These results show that if the metastable ${}^4F_{3/2}$ level is split into two sublevels, then the degeneracy of the terminal level (${}^4I_{11/2}$) and the ground level (${}^4I_{9/2}$) is completely removed. All experimental evidence to date indicates that the metastable level is split in glass (See, for example, Maurer 1963 and Snitzer and Young 1968.). This means that the fluorescent line must be considered a composite of the twelve lines arising from the splitting of both the metastable and the terminal level. However, just as the cascade process from the pumping bands to the metastable level is mediated by coupling of excess energy to the lattice, so also is the transition between the two sublevels of the metastable state, as illustrated in the results of Maurer (1963). He shows that the number densities of the excited ions in the two sublevels are given by the Boltzmann distribution for the temperature of the glass host. Judging by the cascade process, energy transfer between the host structure and the ions is very fast compared to any other relaxation processes. An excited ion thus spends part of its time in each of the two sublevels and therefore both form a common energy source for the laser action. Each of the twelve lines is inhomogeneously broadened as is shown conclusively by the experiments described in §6. It is unfortunate that streak photographs of the glass fluorescence could not have been made at the same time as the streak plates of fig. 6.4.1 and 6.4.2, which illustrate so well hole burning in the population inversion. This is because all

the lines have a common source and hole burning will occur in each one. Even with such heavy overlapping, some evidence should be visible of this effect in the fluorescence. An attempt was made to observe the fluorescence from the side of the laser rod in the single frequency experiments, but the $1 \mu\text{m}$ radiation from the flash-lamp could not be sufficiently suppressed.

Secondly, now that the origin of the lineshape is understood, an estimate of the width of the inhomogeneously broadened line can be made. We first note that even at room temperature, only about 14% of the excited ions are in the upper sublevel of the metastable state at any one time, and thus the major portion of fluorescence and stimulated emission is due to the six possible transitions from the lower sublevel, assuming that each sublevel of the metastable state has comparable transition probabilities to the terminal levels. The peak in the fluorescent line is thus seen to be due to the major transition from the lower sublevel of the metastable state, and the 20 - 80 Å wide Q-spoiled pulses are seen as belonging to that transition. This is so because the stimulated emission cross section is highest for this particular transition. Therefore, the width of the Q-spoiled pulse is taken to be equal to the half-width of the inhomogeneously broadened transition. This proposal is further strengthened by Michon's (1966) observations, which agree with ours, that the line width is quite independent of energy output. In addition, the peak flattening observed in the experiment described in §7 for the Kodak glass, attributed to cross relaxation, is nearly the same width as the Q-spoiled pulse. In this manner, one obtains a value for the half width of the inhom-

geneous broadening of the Kodak glass of $65 \pm 5 \text{ cm}^{-1}$, and of the Schott glass of $70 \pm 5 \text{ cm}^{-1}$.

Thirdly, the hole burning effect sometimes displayed when Q-spoiling with thin films can be used to obtain an estimate of the cross relaxation rate of the glass. The cross relaxation rate is certainly less than the reciprocal of the time taken for the hole to fill in as indicated by the convergence of oscillation in the streak photographs. On this basis, and using figs. 6.4.1 and 6.4.2 for the Kodak glass, and figs. 6.4.7, 6.4.9 and others for the Schott glass, one obtains $W_c \leq 1.5 \times 10^4 \text{ sec}^{-1}$ for the Kodak glass, and $W_c \leq 3.8 \times 10^3 \text{ sec}^{-1}$ for the Schott glass. However, the measurements of slope efficiency described in §7 should be quite sensitive to cross relaxation rate, and only a weak response is shown for the Kodak glass, and no detectable one for the Schott glass. The problem is that the theory is based on an assumption of steady state, which means that the pump pulse should be long compared to the cross relaxation rate and this is not the case. Judging by the poor response to this test, it is likely that the cross relaxation rates are considerably less than the above values, a more likely value for the Schott glass being the reciprocal of the pump pulse width, i.e., $W_c \leq 2 \times 10^3 \text{ sec}^{-1}$.

As discussed in §7, these results disagree with those of Michon (1966) and Boyden and Clark (1966), for the reasons given. They did not take into consideration the special nature of the fluorescent line structure and thus used probe pulses so wide and so intense as to deplete completely the entire inhomogeneous line through the saturation of the major transition. Only by using

pulses whose spectral width is less than $1 - 2 \text{ \AA}$ could they have been successful in observing hole burning. In fact, rather than exhibiting fast cross relaxation, the glasses they used should exhibit slower rates than the glasses studied here. This is based on the fact that the glasses used by both investigators have longer fluorescent lifetimes than our glasses. Cross relaxation depends on suitable energy transfer mechanisms between ions, and these same mechanisms allow concentration quenching (Snitzer and Young 1968) to compete with the cross relaxation and shorten the measured lifetime of the fluorescence. Thus, in general, the longer the lifetime of the fluorescence of a glass, the smaller will be the cross relaxation.

9.2. Spiking Behaviour

The problem of the irregular continuous spiking found in many solid state lasers is still far from being solved, and our contribution is largely a negative one, i.e., in the sense of what does not produce the pulsations. There are two aspects. One must first find the source of instability which will allow limit cycle behaviour (regular pulsing) and secondly an interrupting mechanism which produces the random spiking. It may be that one mechanism fulfils both requirements. The computer solutions show that inhomogeneous broadening with or without cross relaxation cannot provide the instability necessary to cause continuous spiking in the rate equations. In addition, the three level approximation allows one to consider the effect of cavity photon absorption by the terminal level in conjunction with the effects discussed above. The trans-

ient pulses produced in the simulation of the rate equations are in many ways (shape, period, peak power) similar to the spikes observed in real lasers, and it is thought that the real spikes are produced by random starting and cut-off of these oscillations. In some materials, such as ruby, the irregular pulsations can be shown to arise from spatial hole burning due to the Fabry-Perot resonator, and subsequent mode hopping as the other modes use the inversion in volumes inaccessible to the previous modes. On the basis of our results, this does not appear to be the case with Nd^{3+} in glass. It is true that the cavity modes are not resolved and hopping could occur in adjacent cavity modes, but this is certainly not the case on the large scale of the modes arising from the sapphire flats. The ring resonator configuration minimizes spatial inhomogeneities, since any tendency for two counter-rotating modes to form a standing wave would cause frequency "pulling" of one mode to use the higher inversion thus obtainable. In addition, for reasons we have not been able to fathom, one Kodak rod (#1) consistently produced over 90% of its total power in the C.W. direction. No differences in spiking were noticed with this rod when compared with the other three, which produced output energy evenly split in the two directions. With this rod at least, there should be very little if any spatial inhomogeneities and, if mode hopping was effective, regular pulse trains should have been produced as in experiments with ruby. Snitzer (1964) in his early work with clad rods and fibres, was able to produce regular pulsations as well as damped regular oscillations similar to our computer solutions, but these appeared only when observing all wavelengths simultaneously. Such regular-

ity failed to show up when the output of a narrow frequency band was observed. In this case, there are so many modes, and they are so scrambled, that one is really dealing with a super-radiant laser. We conclude that if mode interaction is the source of irregular spiking in Nd^{3+} in glass, it is a more general interaction which is not dependent either on the number of modes or the mode structure to any great extent.

Three other observations from the streak photographs are clearly separate problems to that discussed above, although the first, the existence of micro-pulsations within a spike, may possibly have its source in the same instabilities that drive the macro-spikes. Our observations indicate that it is most often associated with Q-spoiled pulses or large normal spikes, and that it is probably coupled somehow to inversion dynamics, since it is correlated completely with frequency when it appears in a Type V pulse. We venture three possible suggestions as to their source. The suggestion given in §6.5.3 that the fluctuations may be due to mode beating is unlikely because it does not account for the correlation in Type V pulses unless very stringent requirements are placed on the allowed modes, and because it would take some very strange modes to give such low beat frequencies. Another unlikely possibility is that the micro-pulsations are due to ultrasonic oscillations being excited in one of the optical components of the cavity. If the micro-pulsations had been observed only with thin film Q-spoiling, then a quite plausible explanation would be that the exploding plasma of the thin film had shock excited the glass slide, which has the correct thickness for ultrasonic oscillations

at this frequency. However, the micro-pulsations are also observed in Q-spoiling with a Pockel's effect shutter, and in this case there appears to be no other suitable driving source or resonant structure. The final suggestion is that the pulsations are due to oscillations set up in the inversion population by the time lag between photon emission and the recycling of an ion to the metastable state by the pump source. In our approximation, the cascade from the pump bands to the metastable level is assumed to be infinitely fast, but it is possible that this time together with the lifetime of the terminal level could introduce sufficient phase delay to cause oscillations. The effect would be quite weak, since the maximum possible inversion density is only $\sim 10^{-2}$.

A second observation from the streak photographs is the character of the giant Type V pulsations. Clearly they behave exactly like the damped pulsations in the computer solutions, and there is no doubt they are correctly described by the rate equations. Their remarkable coherence across a 50 \AA band is simply a result of all the modes being started simultaneously by the sudden lowering of threshold in a Q-spoiling experiment. The re-appearance of these pulses towards the end of the laser pulse in such examples as fig. 6.4.7 is attributed to the synchronizing effect of a sudden peak in the pumping rate at the end of the pumping pulse.

The third observation concerns the Type IV pulse train of fig. 6.4.7. The existence of a Type IV pulse train implies a common energy source, if inversion dynamics are to provide the coupling. There is no problem where the pulse trains are several \AA apart, as they share the same homogeneous line. In the

case of fig. 6.4.7, the separation is 25 \AA and for these trains to share a common source, they must be a result of transitions to different sublevels of the terminal level.

9.3. Implications of Results

It is evident from the type of experiments previously performed to determine the cross relaxation rate (Michon 1966, Boyden and Clark 1966) and the subsequent wide acceptance of the results (for instance, Cabezas and Treat 1966, Peressinni and Linford 1968) that there is general confusion as to the nature of inhomogeneous broadening in electronic transitions as opposed to Zeeman transitions. We believe that the review and analysis in §2 and §3 indicates the proper approach, and that our experimental results support it. The confusion of lines with a common source which constitutes the fluorescent line means that for many experiments and applications inhomogeneity and cross relaxation cannot be used as labels to describe the behaviour of the experiment. One is usually concerned with inhomogeneity in connection with amplifiers, either with extracting the maximum energy from an active medium for pulse amplification, or with the linear amplification of small signals. In the former case, unless the pulse spectral width is exceedingly narrow and the pulse is just beginning to drive the amplifier into the saturation region, then essentially all the energy stored in the medium is available for amplification and the amplifier will behave as if the entire linewidth was homogeneously broadened. Amplification in the linear region is another thing altogether. Narrow band signals can be expected to burn holes in

the fluorescent line, and care must be taken to avoid the resulting saturation. In short, for small signal amplification, the line appears to be inhomogeneously broadened and all the effects such as saturation at low gain, hole burning, etc., will be observed. However, when operated well into the saturation region, or with wide band signals, the energy of the entire line is available for amplification and the line appears to be homogeneously broadened.

APPENDIX I

Complete Character Tables for "Double" Groups

The "double" groups are formed by adding a fictitious operator, Q , such that $Q^2 = E$. The additional representations so formed are given under the dotted line in the tables and are those used with the half-integer values of J . Because of the artificial nature of Q , many of the elements have the same character and are thus grouped together in the same column. In addition, most of the more complex groups are obtained by allowing a single new symmetry operation on a simpler group. These new groups will have twice as many classes and twice as many representations as the subgroups from which they are formed. Only the characters of the additional elements formed by the new symmetry operations will be indicated, by listing the elements of the new operations, enclosed in double lines, below the tables of the simple groups. The values of the special symbols used in the character tables are listed below:

$$i = \sqrt{-1} , \quad \alpha = \exp(\pi i/4) , \quad \beta = \exp(\pi i/6) ,$$

$$\epsilon = \exp(2\pi i/3) , \quad \omega = \exp(\pi i/3) , \quad \alpha^* = \exp(-\pi i/4) , \text{ etc.}$$

A. Triclinic (C_1, S_2), Monoclinic (C_{1h}, C_2, C_{2h}), Orthorhombic (C_{2v}, D_2, D_{2h})

C_1	E	Q
A	1	1
A'	1	-1

S_2			E	i	Q	Qi
	C_2		E	C_2	Q	QC_2
		C_{1h}	E	σ_h	Q	$Q\sigma_h$
A_g	A	A^e	1	1	1	1
A_u	B	A^o	1	-1	1	-1
E'	E'	E'	1	1	-1	-1
			1	-1	-1	1

C_{2h}			E	QC_2	$Q\sigma_h$	Qi	Q
				C_2	σ_h	i	
	C_{2v}		E	QC_2	$Q\sigma^y$	$Q\sigma^x$	Q
				C_2	σ^y	σ^x	
		D_2	E	QC_2^z	QC_2^y	QC_2^x	Q
				C_2^z	C_2^y	C_2^x	
A_g	A_1	A	1	1	1	1	1
B_g	B_2	B_3	1	-1	-1	1	1
A_u	A_2	B_1	1	1	-1	-1	1
B_u	B_1	B_2	1	-1	1	-1	1
E'	E'	E'	2	0	0	0	-2
D_{2h}				Qi	$Q\sigma_h$	$Q\sigma^x$	$Q\sigma^y$
				i	σ_h	σ^x	σ^y
							Q

$D_{2h} = D_2 \times S_2$. D_{2h} has representations of type g and u, depending on whether $\chi(i) = \chi(S_2) = \pm 1$.

B. Rhombohedral (Trigonal) ($C_3, S_6, C_{3V}, D_3, D_{3d}$), Hexagonal($C_6, C_{3h}, C_{6h}, C_{6V}, D_6, D_{3h}, D_{6h}$)

C_3	E	C_3	C_3^2	Q	QC_3	QC_3^2
A	1	1	1	1	1	1
E	1	ϵ	ϵ^*	1	ϵ	ϵ^*
	1	ϵ^*	ϵ	1	ϵ^*	ϵ
A'	1	-1	1	-1	1	-1
E'	1	ω	$-\omega^*$	-1	$-\omega$	ω^*
	1	ω^*	$-\omega$	-1	$-\omega^*$	ω
$C_{3h} \rightarrow$	σ_h	S_3	S_3^2	$Q\sigma_h$	QS_3	QS_3^2
$S_6 \rightarrow$	S_2	S_6^5	S_6	Qi	QS_6^5	QS_6

$$C_{3h} = C_3 \times \sigma_h$$

$$S_6 = C_3 \times S_2$$

A' doubles to E' in C_{3h} and

S_6 . In C_{3h} , A becomes A^e

or A^o , depending on whether

$\chi(\sigma_h) = \pm 1$. Similarly, in

S_6 , A becomes A_g or A_u as

$\chi(i) = \pm 1$.

C_{3v}		E	QC_3^2	QC_3	$3\sigma(i)$	Q	$3Q\sigma(i)$	
			C_3	C_3^2				
	D_3	E	QC_3^2	QC_3	$3C_2(i)$	Q	$3Q_2(i)$	
			C_3	C_3^2				
A_1	A_1	1	1	1	1	1	1	
A_2	A_2	1	1	1	-1	1	-1	
E	E	2	-1	-1	0	2	0	
E'_1	E'_1	}	1	-1	1	1	-1	-1
			1	-1	1	-1	-1	1
E'_2	E'_2	2	1	-1	0	-2	0	
D_{3d}	\rightarrow	i	QS_6^5	QS_6	$3\sigma(i)$	Qi	$3Q\sigma(i)$	
			S_6^5	S_6				

$D_{3d} = D_3 \times S_2.$

D_{3d} has representations of type g and u, depending on whether $\chi(i) = \pm 1.$

C_6	E	C_6	C_3	C_2	C_3^2	C_6^5	Q	QC_6	QC_3	QC_2	QC_3^2	QC_6^5
A	1	1	1	1	1	1	1	1	1	1	1	1
B	1	-1	1	-1	1	-1	1	-1	1	-1	1	-1
E_1	1	ω	$-\omega^*$	-1	$-\omega$	ω^*	1	ω	$-\omega^*$	-1	$-\omega$	ω^*
	1	ω^*	$-\omega$	-1	$-\omega^*$	ω	1	ω^*	$-\omega$	-1	$-\omega^*$	ω
E_2	1	$-\omega$	$-\omega^*$	1	$-\omega$	$-\omega^*$	1	$-\omega$	$-\omega^*$	1	$-\omega$	$-\omega^*$
	1	$-\omega^*$	$-\omega$	1	$-\omega^*$	$-\omega$	1	$-\omega^*$	$-\omega$	1	$-\omega^*$	$-\omega$
E_1'	1	ι	-1	-1	1	ι	-1	-1	1	ι	-1	-1
	1	-1	-1	ι	1	-1	-1	ι	1	-1	-1	ι
E_2'	1	β	ω	ι	$-\omega^*$	$-\beta^*$	-1	$-\beta$	$-\omega$	-1	ω^*	β^*
	1	β^*	ω^*	-1	$-\omega$	$-\beta$	-1	$-\beta^*$	$-\omega^*$	ι	ω	β
E_3'	1	$-\beta$	ω	-1	$-\omega^*$	β^*	-1	β	$-\omega$	ι	ω^*	$-\beta^*$
	1	$-\beta^*$	ω^*	ι	$-\omega$	β	-1	β^*	$-\omega^*$	-1	ω	β
$C_{6h} \rightarrow$	i	S_3^2	S_6^5	σ_h	S_6	S_3	Qi	QS_3^2	QS_6^5	$Q\sigma_h$	QS_6	QS_3

$C_{6h} = C_6 \times S_2$. C_{6h} has representations of type g and u, depending on whether $\chi(i) = \pm 1$.

			D_6, C_{6v}, D_{3h}								
D_3			E	QC_3^2	QC_2	QC_6^5	$3QC_2^{(i)}$	$3QC_2^{(ii)}$	Q	C_3^2	C_6^5
			C_3	C_2	C_6	$3C_2^{(i)}$	$3C_2^{(ii)}$	QC_3	QC_6		
	C_{6v}		E	QC_3^2	QC_2	QC_6^5	$3Q\sigma^{(i)}$	$3Q\sigma^{(ii)}$	Q	C_3^2	C_6^5
		D_{3h}	E	QC_3^2	$Q\sigma_h$	QS_3^2	$3QC_2^{(i)}$	$3Q\sigma^{(ii)}$	Q	C_3^2	S_3^2
			C_3	σ_h	S_3	$3C_2^{(i)}$	$3\sigma^{(ii)}$	QC_3	QS_3		
A_1	A_1	A_1^e	1	1	1	1	1	1	1	1	1
A_2	A_2	A_2^e	1	1	1	1	-1	-1	1	1	1
B_1	B_2	A_1^o	1	1	-1	-1	1	-1	1	1	-1
B_2	B_1	A_2^o	1	1	-1	-1	-1	1	1	1	-1
E_1	E_1	E^o	2	-1	-2	1	0	0	2	-1	1
E_2	E_2	E^e	2	-1	2	-1	0	0	2	-1	-1
E_1'	E_1'	E_1'	2	1	0	$\sqrt{3}$	0	0	-2	-1	$-\sqrt{3}$
E_2'	E_2'	E_2'	2	1	0	$-\sqrt{3}$	0	0	-2	-1	$\sqrt{3}$
E_3'	E_3'	E_3'	2	-2	0	0	0	0	-2	2	0
D_{6h}	\rightarrow	i	QS_3	$Q\sigma_h$	QS_6	$Q\sigma^{(ii)}$	$Q\sigma^{(i)}$	Qi	S_3^2	S_6^5	
			S_3^2	σ_h	S_6^5	$\sigma^{(ii)}$	$\sigma^{(i)}$		QS_3	QS_6	

$D_{6h} = D_6 \times S_2$. D_{6h} has representations of type g and u, depending on whether $\chi(i) = \pm 1$.

C. Tetragonal Point Groups ($C_4, S_4, C_{4h}, C_{4v}, D_4, D_{2d}, D_{4h}$)

C_4	E	C_4	C_2	C_4^3	Q	QC_4	QC_2	QC_4^3
S_4	E	S_4	C_2	S_4^3	Q	QS_4	QC_2	QS_4^3
A	1	1	1	1	1	1	1	1
B	1	-1	1	-1	1	-1	1	-1
E	1	i	-1	-i	1	i	-1	-i
	1	-i	-1	i	1	-i	-1	i
E_1'	1	α	i	$-\alpha^*$	-1	$-\alpha$	-i	α^*
	1	α^*	-i	$-\alpha$	-1	$-\alpha^*$	i	α
E_2'	1	$-\alpha$	i	α^*	-1	α	-i	$-\alpha^*$
	1	$-\alpha^*$	-i	α	-1	α^*	i	$-\alpha$
$C_{4h} \rightarrow$	i	S_4^3	σ_h	S_4	iQ	QS_4^3	$Q\sigma_h$	QS_4

$C_{4h} = C_4 \times S_2$. C_{4h} has representations of type g and u, depending on whether $\chi(i) = \pm 1$.

C_{4v}	E	QC_4^3 C_4	QC_2 C_2	$2Q\sigma^{(i)}$ $2\sigma^{(i)}$	$2Q\sigma^{(ii)}$ $2\sigma^{(ii)}$	Q	C_4^3 QC_4
D_4	E	QC_4^3 C_4	QC_2 C_2	$2QC_2^{(i)}$ $2C_2^{(i)}$	$2QC_2^{(ii)}$ $2C_2^{(ii)}$	Q	C_4^3 QC_4
D_{2v}	E	QS_4^3 S_4	QC_2 C_2	$2QC_2^{(i)}$ $2C_2^{(i)}$	$2Q\sigma^{(ii)}$ $2\sigma^{(ii)}$	Q	S_4^3 QS_4
A_1		1	1	1	1	1	1
A_2		1	1	-1	-1	1	1
B_1		1	-1	1	-1	1	-1
B_2		1	-1	1	-1	1	-1
E		2	0	-2	0	0	0
E_1'		2	$\sqrt{2}$	0	0	0	-2
E_2'		2	$-\sqrt{2}$	0	0	0	$\sqrt{2}$
$D_{4h} \rightarrow$	i	QS_4^3 S_4	$Q\sigma_h$ σ_h	$2Q\sigma^{(i)}$ $2\sigma^{(i)}$	$2Q\sigma^{(ii)}$ $2\sigma^{(ii)}$	Qi	S_4^3 QS_4

$D_{4h} = D_4 \times S_2$. D_{4h} has representations of type g and u, depending on whether $\chi(i) = \pm 1$.

D. The Cubic Groups (T, T_h, T_d, O, O_h)

T	E	$4C_3$	$4C_3^2$	$3QC_2^{(i)}$ $3C_2^{(i)}$	Q	$4QC_3$	$4QC_3^2$
A	1	1	1	1	1	1	1
E	1	ϵ	ϵ^*	1	1	ϵ	ϵ^*
	1	ϵ^*	ϵ	1	1	ϵ^*	ϵ
F	3	0	0	-1	3	0	0
E'	2	1	-1	0	-2	-1	1
G'	2	ϵ	$-\epsilon^*$	0	-2	$-\epsilon$	ϵ^*
	2	ϵ^*	$-\epsilon$	0	-2	$-\epsilon^*$	ϵ
$T_h \rightarrow$	i	$4S_6^5$	$4S_6$	$3Q\sigma^{(i)}$ $3\sigma^{(i)}$	Qi	$4QS_6^5$	$4QS_6$

$T_h = T \times S_2$. T_h has representations of type g and u, depending on whether $\chi(i) = \pm 1$.

O	E	$4QC_3^2$	$3QC_4^3$	$3QC_4^2$	$6QC_2^{(ii)}$	Q	$4C_3^2$	$3C_4^3$
		$4C_3$	$3C_4$	$3C_4^2$	$6C_2^{(ii)}$		$4QC_3$	$3QC_4^3$
T_d	E	$4QC_3^2$	$3QS_4$	$3QS_4^2$	$6Q\sigma^{(ii)}$	Q	$4C_3^2$	$3S_4$
		$4C_3$	$3S_4^3$	$3S_4^2$	$6\sigma^{(ii)}$		$4QC_3$	$3QS_4^3$
A_1	1	1	1	1	1	1	1	1
A_2	1	1	-1	1	-1	1	1	-1
E	2	-1	0	2	0	2	-1	0
F_1	3	0	1	-1	-1	3	0	1
F_2	3	0	-1	-1	1	3	0	-1
E'_1	2	1	$\sqrt{2}$	0	0	-2	-1	$-\sqrt{2}$
E'_2	2	1	$-\sqrt{2}$	0	0	-2	-1	$\sqrt{2}$
G'	4	-1	0	0	0	-4	1	0
$O_h \rightarrow$	i	$4QS_6$	$3QS_4$	$3QS_4^2$	$6Q\sigma^{(ii)}$	Qi	$4S_6$	$3S_4$
		$4S_6^5$	$3S_4^3$	$3S_4^2$	$6\sigma^{(ii)}$		$4QS_6^5$	$3QS_4^3$

$O_h = O \times S_2$. O_h has representations of type g and u, depending on whether $\chi(i) = \pm 1$.

APPENDIX II

Tables of Spectral Lines Used for Calibration

In the following tables are listed the spectral lines used in calibrating the spectrograph. They are grouped according to the order of the infra-red spectral lines being observed as they appear on the plate, in increasing order of wavelength.

$\lambda(\text{actual})$ is the true wavelength in air of the observed spectral line, and $\lambda(\text{Equiv.})$ is the wavelength of the position it occupies on an infra-red plate for the infra-red order being observed.

All wavelengths are given in Ångstroms. The values for the wavelengths of the spectral lines are taken from the Handbook of Chemistry and Physics, 40th Edition, 1958, Charles D. Hodgman, ed. (Cleveland: Chemical Rubber Publishing Co.), with the exception of the infra-red spectral lines of argon, which are from Rao, Humphreys and Rank (1966).

A. FIRST ORDER INFRA-RED

i. Thallium

$\lambda(\text{actual})$	order	$\lambda(\text{Equiv.})$
3519.24	3	10557.72
3529.43	3	10588.29
5350.46 *	2	10700.92

* used only for locating the proper order visually, since the plates are not sensitive in this region.

ii. Argon

λ (actual)	order	λ (Equiv.)	λ (actual)	order	λ (Equiv.)
10470.05	1	-----	3554.31	3	10662.93
3491.54	3	10474.62	3555.97	3	10667.91
10478.04	1	-----	10673.56	1	-----
10506.12	}	-----	10681.77	1	-----
10506.50		-----	10683.40	1	-----
3506.46	3	10519.38	3563.26	3	10689.78
10529.32	1	-----	3564.27	3	10692.81
3514.39	3	10543.17	10700.98	1	-----
3545.58	3	10636.74	3567.66	3	10702.98
3545.84	3	10637.52	10712.77	1	-----

B. SECOND ORDER INFRA-RED

i. Argon - Actinic Lines

λ (actual)	order	λ (Equiv.)	λ (actual)	order	λ (Equiv.)
10470.05	2	-----	4266.29	4	10665.73
10478.04	2	-----	4266.53	4	10666.33
10506.12	}	-----	10673.56	2	-----
10506.50		-----	4272.17	4	10680.43
10529.32	2	-----	10681.77	2	-----
7067.22	3	10600.83	10683.40	2	-----
4251.18	4	10627.95	10700.98	2	-----
4259.36	4	10648.40	10712.77	2	-----

ii. Argon - Lines Used for Visual Calibration

λ (actual)	order	λ (Equiv.)	λ (actual)	order	λ (Equiv.)
4190.71	5	10476.78	5410.47	4	10820.94
4200.67	5	10501.68	4333.56	5	10833.90
7030.26	3	10545.39	4335.34	5	10838.35
7067.22	3	10600.83	5421.35	4	10842.70
4259.36	5	10648.40	4348.11	5	10870.28
4266.29	5	10665.73	5451.65	4	10903.30
4272.17	5	10680.43	7272.94	3	10909.40
7147.04	3	10720.56	5473.44	4	10946.88
5373.49	4	10746.98	5495.87	4	10991.74
4300.10	5	10750.25	5506.11	4	11012.22

REFERENCES

- Abragam, A., and Proctor, W.G., 1958, *Phys. Rev.*, 109, 1441.
- Allemand, Charley D., 1968, *J. Opt. Soc. Amer.*, 58, 159.
- Bates, T., 1962, Modern Aspects of the Vitreous State, v.2, edited by J.D. Mackenzie (London: Butterworths), p. 195.
- Belan, V.R., Grigoryants, V.V., and Zhabotinski, M.E., 1969, *Opto-Electronics*, 1, 33.
- Birgeneau, R.J., 1968, *Appl. Phys. Lett.*, 13, 193.
- Bloembergen, N., Purcell, E.M., and Pound, R.V., 1948, *Phys. Rev.*, 73, 679.
- Bloembergen, N., Shapiro, S., Pershan, P.S., and Artman, J.O., 1959, *Phys. Rev.*, 114, 445.
- Boyden, J.H., and Clark, G.L., 1966, *IEEE J. Quantum Electronics*, QE-2, No. 4, lvii.
- Brandewie, R.A., and Telk, C.L., 1967, *J. Opt. Soc. Amer.*, 57, 1221.
- Brown, M.R., Shand, W.A., and Whiting, J.S.S., 1965, *Brit. J. Appl. Phys.*, 16, 619.
- Brown, M.R., Whiting, J.S.S., and Shand, W.A., 1965, *J. Chem. Phys.*, 43, 1.
- Cabezas, Amado Y., and Treat, Richard P., 1966, *J. Appl. Phys.*, 37, 3556; Erratum, 1966, *J. Appl. Phys.*, 37, 4598.
- Carnall, W.T., Fields, P.R., and Wybourne, B.G., 1965, *J. Chem. Phys.*, 42, 3797.
- Casimir, H.B.G., and Du Pré, F.K., 1938, *Physica*, V, 507.
- Chandler, C., 1949, Practical Spectroscopy, (Glasgow: University Press).
- Chandler, Graham G., 1968, *J. Opt. Soc. Amer.*, 58, 895.

- DeMaria, A.J., Stetser, D.A., and Glenn, W.H., 1967, *Science*, 156, 1557.
- DeShazer, L.G., and Komai, L.G., 1965, *J. Opt. Soc. Amer.*, 55, 940.
- DeShazer, L.G., and Maunder, E.A., 1968, *IEEE J. Quantum Electronics*, QE-4, 642.
- Dicke, Robert H., and Wittke, James P., 1960, Introduction to Quantum Mechanics, (Reading, Mass: Addison-Wesley).
- Dieke, G.H., and Crosswhite, H.M., 1963, *Appl. Optics*, 2, 675.
- Dustan, D., 1970, *IEEE J. Quantum Electronics*, QE-6, 3.
- Edwards, J.G., 1966, *Nature*, 212, 752.
- Edwards, J.G., 1969, *Opto-Electronics*, 1, 1.
- Emmett, J.L., Schawlow, A.L., and Weinberg, E.H., 1964, *J. Appl. Phys.*, 35, 2601.
- Fain, V.M., and Khanin, Ya. I., 1969, Quantum Electronics, v. 1, (London: Pergamon).
- Fleck, J.A. Jr., and Kidder, R.E., 1964, *J. Appl. Phys.*, 35, 2825; Erratum 1965, *J. Appl. Phys.*, 36, 2327.
- Fleck, J.A. Jr., 1970, *Phys. Rev. B*, 1, 84.
- Gelles, Rubin, 1968, *Appl. Optics*, 7, 375.
- Gradshteyn, I.S., and Ryzhik, I.M., 1965, Tables of Integrals, Series, and Products, (New York: Academic Press).
- Harrison, R.G., Key, P., Little, V.I., Magyar, G., and Katzenstein, J., 1968, *Appl. Phys. Lett.*, 13, 253.
- Hass, G., 1955, *J. Opt. Soc. Amer.*, 45, 945.
- Hercher, M., 1965, *Appl. Phys. Lett.*, 7, 39.
- Hillenkamp, Franz, 1969, *Appl. Optics*, 8, 351.
- Hugnagel, Robert E., and Kerr, Edwin L., 1969, *Proc. IEEE*, 57, 2088.

- Kisliuk, P., Krupke, W.F., and Gruber, J.B., 1964, *J. Chem. Phys.*, 40, 3606.
- Kittel, C., 1958, Elementary Statistical Physics, (New York: Wiley).
- Knox, Robert S., and Gold, Albert, 1964, Symmetry in the Solid State, (New York: Benjamin).
- Korobkin, V.V., and Uspenskii, A.V., 1963, *JETP*, 45, 1003 (English translation: 1964, *Soviet Physics JETP*, 18, 693).
- Kronig, R. De L., and Bouwkamp, C.J., 1938, *Physica*, V, 521.
- Landau, L.D., and Lifshitz, E.M., 1958, Quantum Mechanics, (London: Pergamon).
- Lengyel, Bela A., 1966, Introduction to Laser Physics, (New York: Wiley and Sons).
- McFarland, B.B., Hoskins, R.H., and Soffer, B.H., 1965, *Nature*, 207, 1180.
- Mackenzie, J.D., 1960a, Modern Aspects of the Vitreous State, v. 1, edited by J.D. Mackenzie (London: Butterworths), p. 1.
- Mackenzie, J.D., 1960b, Modern Aspects of the Vitreous State, v. 1, edited by J.D. Mackenzie (London: Butterworths), p. 188.
- MacLeod, I.D.G., 1970, *IEEE Trans. on Computers*, C-19, 160.
- McWeeny, R., 1963, SYMMETRY an Introduction to Group Theory and its Applications, (London: Pergamon).
- Magyar, G., 1967, *Rev. Scient. Instr.*, 38, 517.
- Makhov, George, 1962, *J. Appl. Phys.*, 33, 202.
- Mauer, Paul, 1964, *Appl. Optics*, 3, 433.
- Maurer, R.D., 1963, *Appl. Optics*, 2, 87.
- Michon, Maurice, 1966, *IEEE J. Quantum Electronics*, QE-2, 612:
see also Michon, M., Ernest, J., Dumanchin, R., Hanus, J.,
and Raynaud, S., 1965, *Phys. Lett.*, 19, 217; Michon, M.,

- Ernest, J., Hanus, J., and Auffret, R., 1965, Phys. Lett., 19, 219.
- Mozzi, R.L., and Warren, B.E., 1969, J. Appl. Cryst., 2, 164.
- Nordsieck, Arnold, 1962, Math. Computation, 16, 22.
- Peressini, E.R., and Linford, G.J., 1968, IEEE J. Quantum Electronics, QE-4, 657.
- Perlman, David E., 1967, Rev. Scient. Instr., 38, 68.
- Pettit, Joseph M., 1959, Electronic Switching, Timing, and Pulse Circuits, (New York: McGraw-Hill).
- Pope, Thomas P., and Kirby, Thomas B., 1967, J. Opt. Soc. Amer., 57, 951.
- Porter, John F., 1965, IEEE J. Quantum Electronics, QE-1, 113.
- Purcell, E.M., and Pound, R.V., 1951, Phys. Rev., 81, 279.
- Rao, K.N., Humphreys, C.J., and Rank, D.H., 1966, Wavelength Standards in the Infrared, (New York: Academic).
- Sinnett, D.M., 1962, J. Appl. Phys., 33, 1578.
- Snitzer, Elias, 1961, Phys. Rev. Lett., 7, 444.
- Snitzer, Elias, 1964, Quantum Electronics III, edited by P. Grivet and N. Bloembergen (New York: Columbia University Press), p. 999.
- Snitzer, Elias, 1966, Appl. Optics, 5, 121.
- Snitzer, E., and Young, C.G., 1968, Advances in Lasers II, edited by Albert K. Levine (New York: Dekker), p. 198.
- Sooy, W.R., 1965, Appl. Phys. Lett., 7, 36.
- Stetser, D.A., and DeMaria, A.J., 1966, Appl. Phys. Lett., 9, 118.
- Tang, C.L., Statz, H., and deMars, G., 1963, J. Appl. Phys., 34 2289.

Urbach, Frantz, Perlman, Ronald, and Hemmendinger, Henry, 1946,

J. Opt. Soc. Amer., 36, 372.

Vanukov, M.P., Issayenko, V.I., and Lubimov, V.V., 1964, Quantum

Electronics III, edited by P. Grivet and N. Bloembergen (New York: Columbia University Press), p. 1477.

Van Vleck, J.H., 1948, Phys. Rev., 74, 1168.

Vuylsteke, Arthur A., 1960, Elements of Maser Theory, (New York:

Van Nostrand).

Waller, I., 1932, Zeit. für Physik, 79, 370.

Wright, J.K., Carmichael, C.H.H., and Brown, B.V., 1965, Phys.

Lett., 16, 264.

Young, C.G., 1969, Proc. IEEE, 57, 1267.